# Atg8 licenses adipokine nuclear exit

Michelle E. Poling[1, #], Camille E. Sullivan[1, #], Ava E. Brent[1#], Terry L. Hafer[1, 2] and Akhila Rajan[1, 2, *].

[1] Basic Sciences Division, Fred Hutch, Seattle, WA 98109, USA.

[2] Graduate Program in Molecular and Cellular Biology, University of Washington, Seattle, USA.

[#]equal contribution. * corresponding author: akhila@fredhutch.org

Adipocytes release adipokines to function as a systemic 'adipometer' and signal satiety. For organisms to function effectively, adipocytes must switch adeptly between adipokine release and retention. We investigated how Unpaired2 (Upd2), a *Drosophila* ortholog of the human adipokine Leptin, is retained during fasting. Unexpectedly, we find that fasting induces Upd2 nuclear accumulation; and that Upd2 nuclear retention is regulated by Atg8. Atg8 is a ubiquitin like protein which conjugates to a lipid moiety. In fed cells, Atg8 localizes both to the nucleus and the cytoplasm. On fasting Atg8 lipidation levels increase, and the nuclear pool of Atg8 is depleted. We find that Atg8 lipidation is the rate limiting step in Upd2 nuclear exit. Illustrating the physiological significance of Atg8-mediated adipokine nuclear retention, we show that this mechanism promotes starvation resilience and post-fasting hunger. Our findings uncover a new facet of Atg8 biology in regulating context-dependent nuclear export and protein localization.

## Introduction

Organisms constantly evaluate their basal nutritional reserves to decide on whether to allocate resources to expensive functions that enhance fitness or to conserve energy. Adipokines, secreted by fat cells provide an accurate assessment of nutrient-reserve information. Leptin in mammals (Ahima et al., 1996) and its functional ortholog in fruit-flies, Unpaired2 (Upd2) (Rajan and Perrimon, 2012), are primary adipokines that are released in proportion to fat stores (Hickey et al., 1996; Kolaczynski et al., 1996a; Kolaczynski et al., 1996b). They impinge on brain circuits that control energy expenditure, appetite and overall metabolism (Brent and Rajan, 2020; Farooqi and O'Rahilly, 2009; Rajan and Perrimon, 2012). In surplus nutrient states, adipokines convey a permissive signal, indicating that energy resources can be devoted to costly activities like immunity and reproduction. During periods of scarcity, their circulation is reduced, signaling an energy deficit, and enabling organisms to conserve energy.

Starvation-induced reduction in Leptin/Upd2 levels is crucial for an organism's neuroendocrine response to reduced energy reserves; this has been well-documented in humans (Kolaczynski et al., 1996a; Kolaczynski et al., 1996b), mice (Ahima et al., 1996; Flier and Maratos-Flier, 2017) and flies (Rajan et al., 2017; Rajan and Perrimon, 2012). Specifically, Leptin injections, during fasting, dysregulates neuroendocrine physiology, and decreases survival capacity in mice (Ahima et al., 1996). Based on this study (Ahima et al., 1996), Flier and colleagues have proposed that "*the primary physiologic role of Leptin is to provide a signal of energy deficit to the CNS*" (Flier, 2019; Flier and Maratos-Flier, 2017). Similarly, flies with reduced levels of Upd2 display increased starvation survival (Rajan and Perrimon, 2012), suggesting that reduced Upd2 levels enable flies to develop resilience to starvation.

Despite the central requirement for adipocytes to retain adipokines during starvation in order to allow organismal adaptation to nutrient deprivation, how fasting induces adipokine retention remains to be fully characterized. Importantly, hyperleptinemia, i.e., high levels of circulating leptin, has been identified as a primary cause of 'leptin resistance'- a state wherein Leptin is unable to effectively signal satiety state to the brain (Knight et al., 2010), resulting in dysfunctional feeding behavior and decreased energy expenditure. Hence, understanding how adipokine retention is regulated in fat cells will provide mechanistic insights that can be applied to intervene in hyperleptinemia-induced adipokine signaling resistance.

We previously showed that in *Drosophila* cells, both Upd2 and human Leptin adopt a unconventional secretion route for release into circulation (Rajan et al., 2017). We also showed that during nutrient deprivation, increased circulating levels of the starvation hormone Glucagon impinges on fat cells to inhibit adipokine release via this route, ultimately enabling fat cells to retain adipokines (Rajan et al., 2017). This mechanistic insight is consistent with the idea of using glucagon like peptides (GLPs) to treat obesity and sensitize Leptin signaling (Baggio and Drucker, 2020). While our work (Rajan et al., 2017) provided clues on how systemic signals, including glucagon, impinge on fat cells to regulate adipokine retention, what cell intrinsic mechanisms mediate fasting induced adipokine retention remained an open question, and a central focus of our investigations.

A primary mechanism by which organisms adapt to metabolic stress is the nutrient scavenging pathway called autophagy (Kaushik et al., 2010; Singh and Cuervo, 2011). In adipocytes, autophagy controls lipid metabolism by a process known as lipophagy (Singh et al., 2009a; Singh et al., 2009b). A central player in the autophagy pathway is a ubiquitin-like protein family member (Shpilka et al., 2011) called LC3/GABARAP in mammals, and Atg8 in flies and yeast (Kirisako et al., 1999). Atg8 is widely distributed in the nucleus (Drake et al., 2010) and during starvation, it translocates to the cytoplasm (Huang et al., 2015) where its gets conjugated to the lipid moiety phosphatidylethanolamine (PE) (Ichimura et al., 2000). Lipidated Atg8 regulates fusion of autophagosomes to lysosomes, resulting in cargo degradation (Nakatogawa et al., 2007). It is now widely recognized that many core autophagy proteins, including Atg8, play central roles in non-degradative cellular activities (Galluzzi and Green, 2019). These include, but are not limited to: LC3-associated phagocytosis (LAP) (Cunha et al., 2018), viral replication (Reggiori et al., 2010), extracellular vesicle secretion (LDELS) (Leidal and Debnath, 2020a), and LC3 associated endocytosis (LANDO) (Heckmann et al., 2019). These non-degradative roles for Atg8 have been documented in the cytosol. But what remains unclear is whether Atg8/LC3 proteins localized to the nucleus (Drake et al., 2010) play a specific role other than to provide a pool of Atg8 available for lipidation (Huang et al., 2015), and to help cells cope with oncogenic stress by degrading the nuclear lamina (Dou et al., 2015).

While investigating cell intrinsic mechanisms which regulate acute adipokine retention, we unexpectedly found a direct, non-degradative role for Atg8 in licensing adipokine nuclear exit in fed cells and promoting adipokine retention during fasting. Furthermore, we found that this mechanism is central to systemic energy balance as it provides a resilience mechanism for flies

during fasting and sensitizes adipokine signaling post-fasting. Given, the deep conservation of autophagy machinery between flies and mammals (Neufeld and Baehrecke, 2008; Zirin and Perrimon, 2010), and also the processes governing energy homeostasis, particularly lipid biology, between flies and mammals (Baker and Thummel, 2007; King-Jones and Thummel, 2005; Musselman and Kuhnlein, 2018; Teleman et al., 2012; Tennessen et al., 2014; Welte and Gould, 2017), we believe that our findings in the *Drosophila* model, regarding Atg8's role in licensing adipokine release, will be of relevance more broadly.

## Results

### Fasting induces Upd2 nuclear accumulation:

To explore whether cells have intrinsic mechanisms to retain adipokines during fasting, we probed whether cells retain Upd2/Leptin on amino-acid (AA) deprivation. Note, we chose the AA-starvation regime, because it provided the most consistent results, as opposed to serum starvation or culturing cells in buffers including PBS and EBSS. Upd2, a JAK/STAT pathway agonist, is secreted into media of cultured *Drosophila* S2R+ cells (Hombria et al., 2005). In previous work, a quantitative assay (ELISA) for Upd2 release was established in the *Drosophila* S2R+ cell culture system (Rajan et al., 2017). For these experiments a C-terminal GFP-tagged version of Upd2 (*Upd2::GFP*) is transiently transfected into S2R+ cells (Rajan et al., 2017). *Upd2::GFP* can rescue *upd2Δ* mutants (Rajan and Perrimon, 2012), strongly suggesting that GFP tagged version of Upd2 likely recapitulates the function of untagged wild-type (WT) Upd2. Using this previously established quantitative secretion assay (see methods) we asked whether culturing S2R+ cells in amino acid (AA)-free media affected Upd2::GFP release (hereafter referred to as Upd2-WT). We observed a -76% reduction ($p<0.001$) in Upd2 secretion within 6 hours of AA-starvation. Furthermore, 20 hours post-starvation, Upd2 secretion decreased by -96% ($p=0.0004$) (Figure 1A). These results suggest that *Drosophila* S2R+ cells sense a fasted state and acutely retain a significant portion of the adipokine Upd2 (~76%) within a brief period of AA deprivation (6 hours).

Fasting induced transcriptional (Goldstein and Hager, 2015) and translational (Shu et al., 2020) controls, are likely to work in concordance with acute mechanisms to retain already transcribed and translated adipokines. Acute adipokine retention mechanisms possibly include a "brake" on the trafficking machinery involved in Upd2 release, and/or degradation of adipokine primed for release. To begin to explore these acute mechanisms, we documented Upd2's

cellular localization during a fasting time-course (imaging fixed cells - every 2-4 hours on AA-fasting). When cells are cultured in complete medium ('Fed' state), Upd2 exhibits a punctate cytoplasmic localization, with diffuse and faint nuclear localization (Figure 1Ba). Within 4-8 hours of AA fasting, increased Upd2 nuclear accumulation is observable (Figure 1Bb- Starved (Stv), 8hr). Upd2 nuclear accumulation is detected even at 16 hours of AA-starvation (Figure 1Bc- Stv, 16hr). We also noted that Upd2, at time points assayed (4-24hr), exhibits a punctate cytoplasmic localization (Figure 1Bb, Bc). While it is possible that this cytoplasmic pool of Upd2 is retained or degraded, we did not further define or characterize the fasting-induced acute adipokine retention mechanisms in the cytoplasm (See Discussion).

Instead, intrigued by fasting-induced Upd2 nuclear accumulation, we sought to define and characterize it. To this end, we performed independent fasting-time series experiments with 50-100 cells per time-point (these were blinded experiments-see methods) and quantified the ratio of Upd2 nuclear intensity versus the whole cell at each time point (Figure 1B'). Across such independent experiments, we observed a similar dynamic in Upd2 nuclear accumulation. No significant increase in Upd2 nuclear accumulation was observable at 2 hours of AA-fasting. However, within 4 hours we observed, on average, a +25% increase (p=9.9E-7) in Upd2 nuclear accumulation. This upward trend in Upd2 nuclear accumulation peaks at 8-12 hours post-AA starvation with a 30-50% increase in Upd2 nuclear accumulation (p= 1.2E-8). At 16 hours, Upd2 nuclear accumulation while higher than fed state (+17%; p=5.1E-3), was lower than the peak at 8-12 hours (Figure 1B').

Next, we asked whether refeeding restores Upd2 release. On performing a quantitative ELISA for Upd2-WT in cells from three different nutrient states--fed, starved, and re-fed--we observed that by 5 hours after refeeding (Figure 1C), the amount of Upd2-WT released into the media was 104% higher than the starved state (p=1.2E-6). This indicates that cells can toggle between retention and release within a 5-hour period; strikingly, this mirrors the temporal dynamics of adipokine retention (Figure 1A). Next, we examined the correlation between refeeding and Upd2 nuclear accumulation. As observed previously (Figure 1B, B'), within 8 hours of starvation, significantly higher Upd2 nuclear accumulation can be seen (+43%; p=6.8E-14; Figure 1Db, D'). Within 4 hours of refeeding, Upd2 nuclear accumulation is about +14% higher (p=0.0001) than fed cells (Figure 1Dc, D'). By 6 hours after refeeding, Upd2 nuclear accumulation is reduced and closer to the 'original' fed levels (+6%; p=0.07/ns; see Figure 1Dd, D'); this correlates with Upd2 release within 5-hours on refeeding. Taken together these

observations indicate that fasting-induced nuclear accumulation is an acute adipokine retention mechanism, and that refeeding reverses Upd2 nuclear accumulation within a similar timeframe (4-6 hours). For the rest of this study, we focused on understanding the mechanisms that regulate the early phase (4-8 hours) of acute adipokine Upd2 nuclear accumulation.

**Atg8 regulates nucleocytoplasmic localization of Upd2:**

We then sought to identify mechanisms that link nutrient state to adipokine nuclear retention. AA-starvation triggers autophagy, a nutrient scavenging pathway (Mortimore et al., 1983), of which Atg8/LC3, a ubiquitin-like protein, is a primary component (Kirisako et al., 1999). In fasted cells, Atg8 undergoes a ubiquitin-like conjugation to a lipid moiety phosphatidylethanolamine (PE) (Ichimura et al., 2000). Subsequent to its lipidation Atg8 regulates fusion of autophagosomes to lysosomes, resulting in cargo degradation (Nakatogawa et al., 2007). It is now widely recognized that many core autophagy proteins, including Atg8, play central roles in non-degradative cellular activities (Galluzzi and Green, 2019). For instance, Atg8 is well-documented for its involvement in the unconventional secretion of a wide variety of cargoes including, but not limited to, yeast Acb1, mammalian interleukins and RNA binding proteins (Bruns et al., 2011; Dupont et al., 2011; Duran et al., 2010; Leidal et al., 2020; Zhang et al., 2015).

In a previous study, our lab demonstrated that the adipokine Upd2 and its human ortholog Leptin (hLeptin), adopts an unconventional secretory route (Rajan et al., 2017). Given Atg8's role in AA-deprivation triggered nutrient-scavenging (Kirisako et al., 1999), and its documented role in unconventional secretion (Dupont et al., 2011; Duran et al., 2010; Leidal et al., 2020; Zhang et al., 2015), we specifically examined the effect of removing Atg8 on Upd2 release. In fed *Drosophila* S2R+ cells, dsRNA mediated knockdown of Atg8 (Atg8-KD) results in an -85% reduction ($p=0.048$) in Upd2 secretion (Figure 2A), phenocopying the effect of fasting on Upd2 release. Moreover, this observation, that Atg8 is required for Upd2 release, is consistent with both Atg8's role in unconventional secretion (Cadwell and Debnath, 2018; Leidal and Debnath, 2020a) and our prior report that Upd2 is a cargo of the unconventional secretion pathway (Rajan et al., 2017).

To better understand this reduced secretion phenotype, we examined cellular localization of Upd2 following *Atg8-KD* (Figure 2Bb) compared to a control dsRNA (*LacZ-KD*) (Figure 2Ba). While punctate cytoplasmic Upd2 is still present, nuclear Upd2 accumulation is clear in *Atg8-KD*

cells by confocal microscopy. On quantifying, *Atg8-KD* resulted in a +34% (p=0.0035) to +60% (p=3.9E-5) increase in Upd2 nuclear accumulation (Figure 2B'). Collectively, these observations are consistent with Atg8 reduction, even in fed cells, correlating with increased Upd2 nuclear accumulation.

As Atg8 itself is degraded by autophagy (Mizushima and Yoshimori, 2007), we considered that in *Atg8-KD*, reduced Atg8 levels perhaps signify a nutrient scavenging state; hence an increase in Upd2 nuclear accumulation could be a 'passive' outcome. An alternate, but not mutually exclusive, hypothesis is that Atg8 plays an 'active'/ direct role that ultimately results in fasting-induced adipokine localization. This latter hypothesis is consistent with the idea that Upd2 might interact in a complex with Atg8, directly or via adapter molecules. To test this, we co-transfected Myc::Atg8-WT and Upd2-WT::GFP and performed GFP and Myc pull downs, we found that Upd2-WT co-immunoprecipitates (Co-IPs) with Atg8-WT (Figure 2C, lane 1).

Next, we wanted to test whether Upd2's interaction with Atg8 is reliant on a short linear protein domain known as the AIM (Atg8-interacting motif), which contains the consensus sequence W/F/Y-X-X-L/I/V, and is present in *bona fide* Atg8 interaction proteins (Noda et al., 2010). On analyzing protein sequences, we found that Upd2 has AIM-like sequences (Figure. 2D). Mutating Upd2's AIM (using an established approach of mutating W and L to A (Noda et al., 2008);here after referred to as Upd2-AIM$^-$) impaired the interaction between Upd2 and Atg8, as assayed by a co-immunoprecipitation experiment (Figure 2C, lane 2). Upd2 is usually found at very low levels in the lysate of S2R+ cells because of its constitutively secreted (see GFP-IP lane 1 in Figure 2C). We noted that Upd2-AIM$^-$ levels appeared higher than Upd2-WT in lysate (GFP-IP lane 2 in Figure 2C). Despite being present at a higher level it does not effectively complex with Atg8 (RFP-IP lane 2 in Figure 2C). Furthermore, the higher levels of Upd2-AIM$^-$ in the lysate is suggestive of a defect in release of Upd2-AIM$^-$.

To test whether Upd2-AIM$^-$ impairs Upd2 release, we performed a quantitative ELISA and found that single amino acid point mutations of the AIM motif of Upd2 (W and L to A) reduced secretion by -96% (p=4.29E-05) (Figure 2D). This reduction in Upd2-AIM- release phenocopies *Atg8-KD* (Figure 2A) and fasting-induced states (Figure 1A). Hence, we examined whether Upd2-AIM$^-$ exhibits increased nuclear accumulation as occurs in an *Atg8-KD* (Figure 2Eb). We observed a significant increase in Upd2 nuclear localization (Figure 1E). Specifically, Upd2-AIM- (Figure 1Eb, b') exhibited a diffuse but highly enriched Upd2 nuclear localization (+72%; p=1.7E-11 compared to control Figure 1E'). Furthermore, as evidenced by both confocal (Figure 1Eb)

and super-resolution images (Figure 1Eb'), Upd2-AIM- is contained within the nuclear lamina, and distinct cytosolic puncta are not readily detectable. The absence of punctate cytosolic localization of Upd2-AIM- contrasts with Upd2 localization following both *Atg8-KD* (Figure 2Bb) and fasting-induced Upd2 nuclear accumulation (Figure 1Bb, 1Db), and represents a stronger retention (-96% reduction in secretion and an increased nuclear accumulation +72%). Given that AIM- significantly impairs Upd2's association with Atg8, we reasoned that Upd2-AIM$^-$ represents an "Atg8-null" state for Upd2, while dsRNA knockdown of *Atg8*, reflects a hypomorphic state (see Discussion).

Altogether, these datasets suggest that when Atg8 levels are reduced (*Atg8-KD*) or when Upd2's interaction with Atg8 is significantly impaired (Upd2-AIM-), Upd2 is retained in the nucleus and is not readily available for secretion. Hence, our results are suggestive of Atg8 playing a central role in Upd2's nucleocytoplasmic localization.

**Nucleocytoplasmic shuttling of Upd2 is required for its subsequent release:**

Upd2 is a 47 kDa protein. Given the structural restraint of nuclear pore complexes (NPC) to only permit proteins <40kDA to pass through (Davis, 1995), Upd2 is likely to require active nucleocytoplasmic (NC) transport mechanisms that enable transit through the NPC (Kaffman and O'Shea, 1999). Hence, we sought to explore whether Upd2's NC localization is regulated by classical NC transport pathways. In such a pathway, cargoes >40kDa (but even some smaller cargoes such as histones) rely on their ability to interact with a set of soluble nuclear transport receptors- 'importins' and 'exportins'- also known as Karyopherins (Gorlich and Kutay, 1999; Mattaj and Englmeier, 1998).

First, we analyzed Upd2's sequence using a bioinformatic tool- classic NLS (cNLS) mapper- (Kosugi et al., 2008; Kosugi et al., 2009a; Kosugi et al., 2009b) to ask whether Upd2 has a predicted NLS. cNLS mapper predicted that Upd2 contains an NLS at residues 141-150 (GRVIKRKHLE) with a score of 10.5. According to cNLS mapper, a GUS-GFP reporter protein fused to an NLS with a score of 8, 9, or 10 is exclusively localized to the nucleus. Next, we asked whether Upd2 is predicted to contain an NES using another tool NetNES (la Cour et al., 2004). While NetNES predicted an NES like sequence for Upd2 residues 248-254 (LCEIELTI), residues 251 and 253 do not broach the threshold, thus making it difficult to say if this whole sequence is indeed an NES (see Discussion).

To clarify if Upd2 relies on a classical nuclear export factors, we genetically manipulated nuclear exportin CRM1 (Fukuda et al., 1997), also known as Embargoed (Emb) in flies (Fasken et al., 2000). We asked whether Emb knock-down (*Emb-KD*) affects Upd2 localization in a fed state. We found that transfection of fed S2R+ cells with *Emb dsRNA*, compared to control *LacZ dsRNA* (Figure 3Aa), recapitulated the increase in Upd2 nuclear accumulation (Figure 3Ab) that we had observed in either an AA-starved state (Figure 1Bb, Bc), or following *Atg8-KD* (2Bb). On quantifying (Figure 3A'), we observed that *Emb-KD*, using two independent dsRNAs, resulted in +18% ($p=0.0053$) and +16% ($p=0.024$) increase in Upd2 nuclear accumulation (levels akin to 16-hour starvation time point Figure 1B'). We also noted punctate Upd2 localization at the nuclear periphery (blue arrows in Figure 3Ab). We next analyzed the effect of reducing CRM1/Emb on Upd2's release from cells. We observed that, consistent with our previous findings on the inverse correlation between Upd2 nuclear accumulation and its release, that in *Emb-KD* cells, as assayed by ELISA, Upd2 release is reduced by -33 to -49%; $p<0.01$ (Figure 3B). Altogether, irrespective of whether Upd2 directly interacts with CRM1/Emb or via an adapter due to its "cryptic" NES (See Discussion), these data are indicative of CRM1/Emb export being involved in Upd2 nuclear exit. These observations support the hypothesis that manipulations which impede nuclear export Upd2 nuclear accumulation decreases its subsequent release.

Given the inverse correlation between Upd2's nuclear accumulation and its secretion, we wondered about the opposite condition., i.e., whether manipulations that impede nuclear import increase Upd2 release. In *Drosophila* there are at least four encoded *Importin-α* genes and at least eight *Importin-β* genes (Mason and Goldfarb, 2009). We were concerned that individual knock-down of these 12 genes may not produce a strong effect, should there be redundancy. Our goal was to blunt nuclear import in general and observe its effect on Upd2 release. Therefore, we adopted a pharmacological approach by using a small molecule Importin-β inhibitor, 2,4-diaminoquinazoline, commonly named Importazole (Soderholm et al., 2011). Heald and colleagues have shown that Importazole specifically blocks Importin-β-mediated nuclear import; it does so by impairing Importin-β's interaction with RanGTP, and importantly does not disrupt transportin-mediated nuclear import or CRM1-mediated nuclear export (Soderholm et al., 2011). This drug was established for blocking nuclear import using Xenopus egg extracts and cultured cells (Soderholm et al., 2011). Hence, to block Importin-β based nuclear import, we incubated *Drosophila* S2R+ cells for 6 hours with 40-100μM Importazole and assayed its effect on Upd2 release using the quantitative sandwich ELISA assay when compared to control

treatment (DMSO). Unlike what we predicted, we observed that 40μM Importazole reduced Upd2 secretion by -23% (p=0.15) and that 100μM Importazole reduced Upd2 secretion by -48% (p=0.01) (Figure 3B). We observed the similar reductions in Upd2 release with Importazole treatment, in three independent experiments, with 6 biological replicates per condition per experiment. We were surprised that Importin-β inhibition impaired Upd2 release and wondered whether it affected Upd2 nuclear entry. Therefore, we examined cells treated with Importazole and documented Upd2 NC localization by confocal imaging. As predicted, based on Upd2's NLS sequence, impeding Importin-β-based nuclear transport by treatment with Importazole, reduced Upd2 nuclear localization for both the 40μM Importazole (Figure 3Db) and 100μM Importazole (Figure 3Dc) compared to control DMSO treatment (Figure 3Da). Quantification of reduction in Upd2 nuclear accumulation (Figure 3D') showed a median of -30% reduction (p=0.0032). Significantly, Upd2 does not show an increase in fasting-induced nuclear accumulation (as observed in Figure 1B') when treated with Importazole during a starved state (see Figure 3D': -7% reduction in starved stated compared to fed in Importazole treatment p=0.54). We also noted that compared to control treatment (Figure 3Da), Upd2-WT in Importazole-treated cells (Figure 3Db and 3Dc), was hard to detect in distinct punctate localization. Instead, Upd2-WT in Importazole-treated cells appeared to 'fill' majority of the cytoplasmic compartment (Figure 3Da, 3Dc). Hence, increased Upd2 cytoplasmic accumulation correlates with reduced release. Taken together, these observations suggested to us that Upd2 uses an Importin-β based mechanism for its nuclear import.

It is possible that impairing NC shuttling broadly, including blocking nuclear import by pharmacological means, impacts Upd2 release in an indirect manner. Hence, we sought to precisely manipulate Upd2 so that it remains cytosolic and then assay how such a 'forced' cytosolic localization affects its release. In addition, we also wondered whether forced nuclear export, by appending a strong NES sequence, could 'override' the *Upd2-AIM-* nuclear accumulation phenotype. Studies in *Drosophila* models have shown that appending a particular NES sequence (LDELLELLRL) to the N-terminal of proteins that localize to the nucleus, reliably and actively shuttles those proteins out to the cytosol (Verboon et al., 2015), thus rendering nuclear proteins cytosolic. Hence, we added this strong nuclear export signal ($NES^+$: LDELLELLRL) in the N-terminal (See methods) of Upd2-WT (referred to here-in as *Upd2-NES+*) and Upd2-$AIM^-$( referred to here-in as *Upd2-NES+AIM-*). We then performed confocal imaging of cells transfected with: *Upd2-WT* (Figure 3Ea, Eb), *Upd2-AIM-* (Figure 3Ec, Ed), *Upd2-NES+*

(Figure 3Ee, Ef) and *Upd2-NES+AIM-* (Figure 3Eg, Eh). As previously documented in Figure 1, Upd2-WT in fed cells exhibits a punctate cytosolic localization (Figure 3Ea) and displays significant nuclear accumulation on AA-starvation (Figure 3Eb). Again, as reported in the prior section (Figure 2E), Upd2-AIM$^-$ is nuclear with almost no detectable punctate cytosolic expression in the fed or starved state (Figure 3Ec, Ed). Upd2-NES$^+$ is cytosolic in fed cells (Figure 3Ee) and continues to be cytosolic even in starved cells (Figure 3Ee, see 3E' for quantification). Moreover, like Upd2-WT localization in Importazole treated cells (Figure 3Db, Dc), Upd2-NES+ 'fills' the cytoplasm (Figure 3Ee), instead of exhibiting the punctate localization observed in Upd2-WT fed cells (Figure 3Ea). Like Upd2-NES$^+$, Upd2-NES$^+$AIM$^-$ is cytosolic in fed and starved cells (Figure 3Eg, Eh). Furthermore, the NES$^+$ appended to Upd2-AIM$^-$ overrides the Upd2-AIM$^-$ nuclear accumulation phenotype (Compare Figure 3Ec, Ed to Eg, Eh), indicating that by providing an ectopic active export mechanism, Upd2 can exit the nucleus. But again, just like Upd2-NES+ (Figure 3Ee, Ef), and Importazole treatment Figure 3Db, Dc, the cytosolic Upd2 appears more diffuse in Upd2-NES$^+$AIM$^-$ (Figure 3Ee, Ef). Hence, we asked if engineered nuclear export, which results in Upd2's nuclear export despite being AIM- is sufficient to promote Upd2 release. On performing quantitative ELISA on Upd2-NES$^+$ and Upd2-NES$^+$AIM$^-$, however we observed that both versions exhibit secretion defects (Figure 3F; -64% reduction p=0.0013), suggesting that forced nuclear export of Upd2 while can override the AIM- nuclear retention phenotype, it is unable to direct Upd2's release. This concurs with our observation that interfering with either Upd2's nuclear export (Figure 3B) or its nuclear import (Figure 3C), both affect Upd2 release.

In conclusion, these results suggest that Upd2 needs to be shuttled into the nucleus prior to being secreted. Also, these results are consistent with a model that after translation in the cytoplasm, Upd2 enters the nuclear environment in order to obtain 'licensing' for release.

**Upd2 nucleocytoplasmic shuttling licenses its release via Atg8-GRASP pathway:**

We surmised that Atg8 could potentially serve as Upd2's 'licensing' factor, by both enabling Upd2 nuclear exit, and then subsequently targeting Upd2 to an appropriate secretion route. To investigate this possibility, we asked whether, in fed cells, the Upd2 cytosolic puncta co-localized or associated with Atg8. First, we performed live imaging of fed cells transfected with Upd2::GFP and mCherry::Atg8 (Figure 4A and Figure S1, Movie S1), to gather preliminary information on the dynamics of the Upd2 puncta and Atg8. We observed that Atg8 and Upd2 co-localize in nuclear periphery (Figure 4A, see blue arrows in 0s, 90s and 135s. Similarly, we also observed

the two proteins co-localize in puncta at the cell periphery (Figure 4A, white arrows in 0s-180s). We found that this co-localization was not a stable one, i.e., a complete overlap changed into an association within 45 seconds (see blue arrows in nuclear periphery Figure 4A-135s vs. 180s). Altogether, these imaging datasets indicated that the Upd2 puncta in the cytosol were positive for Atg8, but that the co-localization of Atg8 to Upd2 punctum was dynamic and unstable, and suggesting that in fixed imaging we were likely to observe them overlap partially.

Once we obtained this baseline for dynamics of Atg8 and Upd2 co-localization, we wondered whether colocalization between Upd2 and Atg8 would be different for Upd2-NES+ compared to Upd2-WT. In fed cells co-transfected with Atg8 and either Upd2-WT (Figure 4Ba) or Upd2-NES+( Figure 4Bb), we examined and quantified the co-localization (see Methods) between these two proteins. In >10 cells per condition, we observed that Upd2-WT exhibited partial to complete (yellow arrows in Figure 4Ba) co-localization with Upd2 (quantified in B' : (0-90% co-localization) whereas Upd2-NES+ was almost mutually exclusive to Atg8 (Figure 4Bb, B'; note difference between Upd2-WT and NES+ is significant p=0.006) . This suggested to us that if Upd2 is forcibly shuttled out of the nucleus then, its ability to localize to Atg8 puncta in the cytosol is compromised. Significantly, this observation lends credence to the idea that Upd2 nuclear localization and subsequent exit is key to Upd2's ability to access Atg8 appropriately.

Since Upd2 release is impaired in both Upd2-NES+ (Figure 3F), and Upd2-AIM- (Figure 2A), we reasoned that Upd2's ability to interact with Atg8 is an important step both for its nuclear exit and subsequent secretion. Our lab previously reported that Upd2 uses a GRASP-secretion route (Rajan et al., 2017). Therefore, we examined the co-localization of GRASP with respect to Upd2-WT and Upd2-AIM-. Imaging fixed cells co-transfected with GRASP and Upd2-WT (Figure 4Ca) versus Upd2-AIM- (Figure 4Cb), showed that GRASP is largely a cytosolic protein and that Upd2-WT puncta co-localize with GRASP, whereas Upd2-AIM- renders Upd2 unable to access the cytosol. Consistent with this, we also observed that while Upd2-WT co-immunoprecipitates with GRASP (Figure 4D; Lane 2), despite being present in much lower amount in the lysate of the cells due to its higher secretion. By contrast, Upd2-AIM-, which is not secreted (Figure 2D), does not co-IP with GRASP (Figure 4D; Lane 2).

Taken together these observations (Figures 3,4) are consistent with a model that Upd2's nuclear entry provides Upd2 a 'venue' to have a productive interaction with Atg8 (note Upd2-NES+ co-localization with Atg8 is impaired: Figure 4B, B'). Atg8 then enables Upd2's nuclear exit and provides the context required for Upd2 to be targeted to the GRASP secretory route.

**Atg8's lipidation state is the rate-limiting step in Upd2 nuclear exit:**

The most well-characterized function of Atg8 is its degradative role in autophagy, where in undergoes a ubiquitin-like conjugation to a lipid moiety phosphatidylethanolamine (PE) (Ichimura et al., 2000) and enables the fusion of autophagosomes to lysosomes. Therefore, we asked whether Atg8's lipidation state has an impact on Upd2 nuclear exit.

First, we examined what effect, if any, autophagy induction and its subsequent induction of Atg8 lipidation, has on Upd2 nuclear retention. Torin1, is a highly potent and selective ATP-competitive mTOR inhibitor (Thoreen et al., 2009), and is one of the most widely used methods to pharmacologically activate autophagy (Galluzzi et al., 2017). Torin1 activated autophagy induces Atg8-lipidation (Stolz et al., 2017). We treated well-fed *Drosophila* S2R+ cells, cultured in complete media, with Torin1 (50-750nM; see Methods) and assayed its effect on Upd2 nuclear accumulation relative to control (DMSO) treatment (Figure 5A) in 50-150 cells per treatment in independent experiments (Figure 5A'). We observed a dose dependent effect on Upd2 retention (Figure 5Ab-d) in Torin1 treated cells, causing from a +20% (p=1.7E-8) increase with 50nM Torin1 (Figure 5Ab; 5A'), to a +75% (p=1.2E-27) increase with 750nM (Figure 5Ad; 5A'). This striking effect of Torin1 treatment (+75% increase) on Upd2 nuclear retention is consistent with the Upd2 nuclear retention observed during starvation (Figure 1B). Altogether, this suggested to us that induction of autophagy by Torin1 treatment, like AA-withdrawal, induced Upd2 nuclear accumulation.

Atg8-lipidation levels increase during autophagy induction. Atg8 is widely distributed in the nucleus (Drake et al., 2010). Whether this nuclear pool of Atg8 has any specific role remains to be fully understood. A study by Liu and colleagues (Huang et al., 2015), presented compelling evidence that the nuclear pool of Atg8 translocates to the cytosol on starvation, and is the primary source of lipidated Atg8 for autophagosome formation (Huang and Liu, 2015). However, it remains possible that Atg8 has a yet to be uncovered, non-degradative, functions in the nucleus via its actions on AIM/LIR containing proteins such as the adipokine Upd2. Therefore, going a step further, we considered the possibility that AA-starvation induced Atg8-lipidation may result in a depletion of the nuclear pool of Atg8 in *Drosophila* S2R+ cells, a state that would ensure Upd2 remains localized to the nucleus.

To test this directly, we examined the localization of 'normal' wild-type Atg8 (Atg8-WT) versus a lipidation-defective Atg8 [Atg8-PE$^-$; as done in prior studies which defined Atg8

lipidation, (Ichimura et al., 2000) we mutated the penultimate glycine, the lipidation acceptor amino acid of Atg8, to an alanine; see methods]. We transfected N-terminally mCherry tagged-*Atg8-WT* (Figure 5Ba, Bb) or *Atg8-PE-* (Figure 5Bc, Bd) into *Drosophila* S2R+ cells, and examined localization in fed and AA-starved states. We note that these experiments are all performed in WT S2R+ cells that do contain an endogenous Atg8 pool, however our goal was to document the distribution of mCherry-tagged versions of Atg8-WT and Atg8-PE- in the presence of endogenous Atg8. We observed that mCherry::Atg8-WT is distributed diffusely in the nucleus and the cytoplasm (Figure 5Ba) in fed cells, but during a short AA-starvation most of mCherry::Atg8-WT is localized to punctate structures in the cytoplasm (Figure 5Ba). This pattern of Atg8-WT localization in S2R+ cells concurs with what has been shown previously by Baehrecke and colleagues (Lin et al., 2017), indicating that our Atg8 transgenes and starvation regimes work as would be expected for this cell line (See also Figures S2A to see further tests of the *Atg8-WT* and *Atg8-PE-* transgenes in *Drosophila* fat).

Next, we examined the localization of lipidation-defective mcherry::Atg8-PE-. Unlike mCherry::Atg8-WT, which exhibits differential NC localization during starvation (Figures 5Ba, Bb; 5B'), mcherry::Atg8-PE$^-$ exhibited the same diffuse NC distribution in fed (Figure 5Bc) and starved states (Figure 5Bd). Importantly, as quantified in 80-125 cells per genotype per condition (Figure 5B'), lipidation-defective Atg8 showed no reduction in its nuclear localization during starvation (Figure 5B': Atg8 PE$^-$ fed vs. starved=+5%; p=0.1). Specifically, Atg8-PE$^-$ nuclear pool on starvation increases compared to Atg8-WT (in starved cells Atg8-WT vs. Atg8 PE$^-$= +34%; p=8.5E-10). These results strongly suggest that starvation, because it induces Atg8's lipidation and causes it to re-localize to punctate structures in the cytosol, depletes the Atg8 nuclear pool, while a lipidation-defective Atg8 molecule continues to be present in the nucleus even during starvation, at levels comparable to the fed state. We extended this observation to *Drosophila* adult fat cells (Figure S2B), in which we found that on starvation Atg8-WT localizes to punctate cytosolic structures (Figure S2Ba; white arrows) and is depleted from the nucleus (Figure S2Ba; blue arrows). Lipidation-defective Atg8 (Atg8-PE-), while present in the cytosol, continued to show strong nuclear enrichment, even on starvation (Figure S2Bb; blue arrows).

Thus far, our data show that events which induce Atg8-lipidation increase Upd2 nuclear accumulation, including AA-starvation (Figure 1B) and Torin1 treatment (Figure 5A). Hence, we hypothesized that lipidation-induced depletion of Atg8's nuclear pool is a rate-limiting step in Upd2's nuclear exit during starvation. To test this, we co-transfected Upd2-WT, with either

control (empty mCherry vector), mCherry::Atg8-WT (which can undergo lipidation and hence move into the cytosol on starvation; Figure 5Bb), or mCherry::Atg8-PE- (lipidation-defective Atg8 which remains in a nuclear pool even during starvation; Figure 5Bd). See schematic in the top panel of Figure 5C for experimental design. We then quantified (in 65-150 cells per condition) the ability of starvation to induce nuclear accumulation of Upd2, in the presence of these Atg8 transgenes. As documented in the prior section (Figure 1Ba), Upd2 is localized to cytosolic puncta in fed cells. Co-expression of either mCherry empty vector (Figure 5Ca), mCherry::Atg8-WT (Figure 5Cc), or mCherry::Atg8-PE- (Figure 5Ce) in fed cells results in normal Upd2-WT localization (Figure 1Ba). On starving for 8 hours, Upd2-WT exhibits significantly increased nuclear accumulation in mCherry control (Figure 5Cb, 5C', +59%; p=5.1E-6), and in mCherry::Atg8-WT (Figure 5Cd, 5C' , +25%; p=1.5E-7). Strikingly, when co-transfected with mCherry::Atg8-PE-, which continues to remain nuclear in starvation (Figure 5Bd, 5B'), Upd2-WT exhibits no increase in fasting-induced nuclear accumulation (Figures 5Cf, 5C'; 0.4%, p=0.95). Hence, providing cells a pool of lipidation-defective Atg8, that continues to be nuclear during starvation, interferes with fasting-induced Upd2 nuclear accumulation, and is sufficient to allow Upd2 to exit the nucleus during fasting. Consistent with this, co-IP experiments show that Upd2-WT can complex with Atg8 despite its lipidation-defective state (Figure S2C; lane 2). In sum, these observations support a model in which the nuclear pool of Atg8 licenses Upd2's nuclear exit, and during fasting, it is the depletion of the nuclear Atg8 pool due to lipidation that triggers Upd2 nuclear accumulation.

**Adipokine nuclear accumulation signals a systemic starvation state:**

We next wondered whether our studies of adipokine nuclear accumulation in *Drosophila* S2R+ cells, which are derived from macrophage like cells, are of any relevance to adult fat cells, the source tissue of adipokine signaling. We first examined whether fasting induces adipokine nuclear accumulation like we observed in *Drosophila* S2R+ cells, is visible in fat cells. To do this, we generated endogenous CRISPR engineered tag knock-ins into the Upd2 locus with two different tags (HA and GFP- See Methods) to follow Upd2's endogenous localization. Both these genomic tagged versions of Upd2 were able to rescue the fat storage defects (Figure S3 A, B) that have been reported for a upd2-deletion allele (*upd2Δ*) (Rajan and Perrimon, 2012). In addition to the genomic tagged Upd2 alleles, we also used flies that expressed an mCherry-tagged Upd2 cDNA transgene in fly fat (*Lpp-Gal4> UAS-Upd2::mCherry*). We acutely fasted flies with either tissue-specific expression of Upd2-WT::mCherry (Figures 6Ab, 6A'a) or the

endogenously tagged Upd2::HA (Figure 6A'b) and Upd2::GFP(Figure 6A'c) flies. In all these different over-expressed and endogenously tagged versions of Upd2, we observed that Upd2, which is usually barely detectable in fat cells, and especially their nuclei, exhibited a perceptible increase nuclear localization (Figure 6Ab) of Upd2 levels (Figure 6A'; +41-51% ($p<1.1E-6$)). This increase is comparable to the acute fasting induced Upd2 accumulation in S2R+ cells (Figure 1Bb), providing evidence for conservation of our findings in S2R+ cells.

To ask whether Atg8 controls adipokine accumulation in adult fly fat cells, we reasoned that examination of the Upd2-AIM- transgenes would provide the most clear answer, as *Atg8-KD* in fat tissue, even in clones can have numerous effects that might complicate interpretation. Furthermore, the AIM-mutation represents a "Atg8-null" situation for Upd2, and correlates strongly with *Atg8-KD* phenotype in S2R+ cells. To recap, the Upd2-AIM$^-$ mutation does not co-IP with Atg8 (Figure 2C) and displays strong nuclear accumulation (Figure 2Eb, E'). Hence, we examined the effect of the point-mutation to Upd2's AIM, on Upd2's localization in adult fly fat in a *upd2Δ* background (*upd2Δ; Lpp-Gal4> UAS-Upd2-AIM-*). We observed a striking increase in nuclear accumulation of the Upd2-AIM- transgene, even in adult fat cells from well-fed flies (Figure 6Bb), compared to Upd2-WT (Figure 6Ba) which, at the same imaging settings, was barely detectable. In addition, the Upd2-AIM- transgenes displayed similar nuclear accumulation even in a control background (*Lpp-Gal4> UAS-Upd2-AIM-*) where endogenous Upd2 is intact (Figure S5Ab). These results suggest that the mechanisms that we uncovered for Atg8's control of Upd2 nuclear exit in *Drosophila* S2R+ cells, are conserved in adult fly fat. Furthermore, they suggest that by examining the effect of Upd2-AIM- which accumulates in fly fat, we will be able to uncover whether Atg8-mediated regulation of Upd2's nuclear exit, and subsequent release, has an effect on systemic physiology.

In a starved state, insulin (Dilp2, Dilp5) accumulates in the fly insulin producing cells (IPCs) (Geminard et al., 2009). One of the primary functions of Upd2 in adult fly fat is to remotely signal to the brain to create a permissive environment for insulin release (Brent and Rajan, 2020; Rajan and Perrimon, 2012). As expected, based on a prior study (Rajan and Perrimon, 2012), compared to background control, *upd2Δ* flies have elevated levels of Dilp2 and Dilp5 fluorescence in the IPCs (Figure S4A), and expression of a Upd2-WT transgene (*upd2Δ; Lpp-Gal4>UAS-Upd2-WT*) rescues this defect (Figure S4A). Hence, we examined the effect of insulin release when *Upd2-AIM-* was expressed in fly fat (*upd2Δ; Lpp-Gal4> UAS-Upd2-AIM-)* and observed that *Upd2-AIM-* is unable to completely rescue the insulin accumulation phenotype of

*upd2Δ* flies (Figure 6C, C', S4B). This suggests that Upd2-AIM- is not able to be released and signal to the IPCs.

Having shown that the Upd2-AIM- variant of Upd2 is localized to the fat cell nucleus (7B), and unable to promote Insulin release when over-expressed in a *upd2Δ* mutant (7C, C'), we next wanted to characterize the effect of Upd2-AIM- on gene expression in fat tissue. Upd2 secretion from the fat tissue systemically signals Insulin release from IPCs (Brent and Rajan, 2020; Rajan and Perrimon, 2012). Circulating Drosophila Dilps are received by the fat tissue, where they regulate nutrient uptake and utilization, and promote triacylglyerol (TAG) storage of excess nutrients (DiAngelo and Birnbaum, 2009; Nassel et al., 2013). Additionally, within the fat tissue, stored fats are packaged into lipophorin/lipoprotein particles (LPPs)--complexes of protein and lipid assembled in fat cells—that re-enter circulation to provide essential lipids to tissues (Palm et al., 2012).

Because the Upd2-Insulin circuit communicates availability of stored energy, we expected that over-expression of Upd2-WT in fat would generate a gene expression profile reflecting TAG storage and active supply of nutrients to other tissues, while over-expression of Upd2-AIM- would not. To test our prediction, we performed qPCR on fat tissue from *upd2Δ* mutants in which either Upd2-WT or Upd2-AIM- was over-expressed in the fat and examined expression of genes involved in either de-novo lipid synthesis or LPP production. De-novo lipid synthesis genes included Sterol regulatory element binding protein (SREBP), a master-regulator of lipogenesis that activates transcription of lipogenic genes (Kunte et al., 2006; Porstmann et al., 2008), and Fatty acid synthase 1 (FASN1), required for de novo synthesis of FB-stored TAG (Garrido et al., 2015; Parvy et al., 2012). LPP production genes included Apolipophorin (Apolpp) and Microsomal triacylglycerol transfer protein (Mtp), both specifically expressed in fat cells. *Drosophila* Apolpp, a member of the ApoB family, is the main protein component of LPPs, and provides a scaffold for lipid assembly. Assembly of LPPs requires the activity of Mtp (Palm et al., 2012).As hypothesized, when compared to either control flies or *upd2Δ* flies expressing Luciferase (Luc) in the FB (*upd2Δ; Lpp-Gal4>UAS-Luc*), the Upd2-WT over-expressing flies (*upd2Δ; Lpp-Gal4>UAS-Upd2-WT*) showed increased expression of SREBP, FASN1, Apolpp, and Mtp (Figure 6D), supporting that Upd2-WT signals availability of excess nutrition for storage as well as Lpp packaging--even in a *upd2Δ* background. By contrast, in the *upd2Δ* flies expressing Upd2-AIM-, expression of SREBP, FASN1, ApoLpp, and Mtp was significantly lower compared to Upd2-WT (Figure 6D). Interestingly, expression of all four genes was reduced, even

compared to control (yw) or *upd2Δ* flies (*upd2Δ; Lpp-Gal4>UAS-Luc*), suggesting that Upd2-AIM- may actively repress pathways involved in lipogenesis and Lpp assembly. Fat specific Upd2-AIM- expression resulted in a similar gene expression profile for SREBP, FASN1, ApoLpp, and Mtp even in a WT background (Figure S5B). We also noted a slight increase in expression of SREBP, FASN1, Apolpp, and Mtp in the *upd2Δ* flies (*upd2Δ; Lpp-Gal4>UAS-Luc*) compared to yw, signifying that *upd2Δ* flies may compensate for their previously described diminished TAG stores by increasing de novo lipogeneis and Lpp assembly (Rajan and Perrimon, 2012).

Since over-expression of Upd2-WT promotes lipogenesis and Lpp assembly, and over-expression of Upd2-AIM- does not, we hypothesized either a cell-autonomous role for Upd2 within the FB, or a systemic role for Upd2 in Insulin release from the IPCs. To examine the latter possibility at the level of FB gene expression, we asked what effect over-expression of either Upd2-WT or Upd2-AIM- has on Insulin signaling within the FB of *upd2Δ* mutants. DILPs activate insulin receptor (InR) signaling by inhibiting the forkhead transcription factor, FOXO. FB expression levels of the FOXO target genes *InR*, *brummer* (*Bmm*), and *4ebp/Thor* can thus provide a readout of Insulin signaling (Eijkelenboom and Burgering, 2013). We found, as expected, that *upd2Δ* mutants (*upd2Δ*; *Lpp-Gal4>UAS-Luc*) showed increased expression of InR, Bmm, and 4ebp compared to yw controls, indicating that systemic Insulin signaling is reduced in the absence of Upd2 (Figure 6E). Moreover, we found that over-expression of Upd2-WT restored expression of all three FOXO targets to control levels, consistent with Upd2-WT's ability to promote Dilp release from *upd2Δ* mutant IPCs (Rajan and Perrimon, 2012). Following Upd2-AIM- over-expression, however, expression levels of InR, Bmm, and 4ebp remained high, underscoring that Upd2-AIM- cannot rescue Dilp release in *upd2Δ* mutants (Figure 6E). Interestingly, we observed that Bmm, which encodes a lipase required for the break-down of stored fats into fatty acids, and 4ebp, which has been shown to function as a metabolic brake during starvation (Gronke et al., 2005; Teleman et al., 2005), were expressed at higher levels in the *upd2Δ* flies with over-expressed Upd2-AIM-, compared to the *upd2Δ* flies expressing Luc—suggesting that the presence of Upd2-AIM- may signal a state of chronic starvation to the organism, it also implies that perhaps that the adipokine which is retained in the nucleus has a direct or indirect gene regulatory role (See Discussion).

**Atg8-mediated adipokine nuclear accumulation increases resilience to starvation and promotes post-fasting hunger:**

We wondered whether Atg8 controlled, fasting-induced adipokine nuclear accumulation (Figure 5C) affords an organism advantages during fasting. Consistent with this idea, we had documented in the prior section that expression of *Upd2-AIM-* signals a chronic starvation state, at least based on its gene expression profile (Figure 6E) and insulin accumulation phenotype (Figure 6C). Given that Upd2-AIM- phenocopies fasting-induced adipokine nuclear accumulation, we used it as a tool to ask what effect constitutive expression of *Upd2-AIM-* has on starvation survival. We subjected flies expressing fat-specific Upd2-WT (*upd2Δ; Lpp-Gal4>Upd2-WT)* and Upd2-AIM$^-$ (*upd2Δ*; *Lpp-Gal4>Upd2-AIM$^-$*), to a nutrient-deprivation regime (Starvation-1% sucrose agar diet), and assayed their survival (Figure 7A). At least, 90 flies were used per genotype and the experiments were repeated thrice (see methods). We observed that fat-specific over-expression of Upd2-WT causes starvation sensitivity (Figure 7A; -20 reduction in median survival; Mantel-Cox test: $\chi^2$= 5.28, p=0.026). This effect on survival of Upd2 overexpression in starved flies resembles the detrimental effects of artificial Leptin repletion in starved mice (Ahima et al., 1996). By contrast, nuclear retention of Upd2 (*upd2Δ; Lpp-Gal4> UAS-Upd2-AIM-*) caused flies to perform better in comparison to control (Figure 7A; Mantel-Cox test: $\chi^2$= 32.41, p<0.0001). Also, of note, Upd2-AIM- displays a resilience to starvation when constitutively expressed even in a background which has Upd2-WT expression (Figure S6A; compare *Lpp-Gal4>Upd2-AIM$^-$ vs. Upd2-WT and UAS-control*). Taken together, these results show that Atg8's control of Upd2 nuclear retention during starvation provides fruit flies an ability to withstand starvation.

Leptin is a satiety signal in mammals (Farooqi and O'Rahilly, 2009), therefore we reasoned that Upd2 overexpression could indicate a satiety state. Hence, we set out to test feeding behavior (see Methods) using a widely used (Deshpande et al., 2014) feeding behavior assay in flies, the FLIC assay (Ro et al., 2014). In the baseline state, i.e., flied fed *ad libitum,* overexpression of both Upd2-AIM- (*upd2Δ; Lpp-Gal4> UAS-Upd2-AIM-)* and Upd2-WT (*upd2Δ; Lpp-Gal4> UAS-Upd2-WT)* showed reduced feeding events (-50 to -80% ) compared to control transgene (Figure S6B). We next assayed hunger-driven feeding motivation (Figure 7B) and events (Figure 7C) by subjecting flies to an over-night starvation regime and measuring their feeding behavior in relation to their *ad libitum* fed siblings. We observed that flies expressing a control transgene in a *upd2Δ* background (*upd2Δ; Lpp-Gal4>UAS-Luc*) exhibited increased motivation to feed (Figure 7Ba; +197%; p=0.05) and increased feeding events (Figure 7Ca), and that this increase in hunger-driven feeding events for the control was consistent with what we

documented in a WT- background (*Lpp-Gal4>UAS-Luc*; Figure S6Ca; +76% p=0.02). Constitutive expression of Upd2-WT (*upd2Δ; Lpp-Gal4> UAS-Upd2-WT)*, in keeping with the idea that it acts as a satiety signal like Leptin, does not display any increase in hunger-driven feeding motivation following starvation ( Figure 7Bb; -28%; p=0.59) or events (Figure 7Cb; -10%; p=0.8). However, constitutive expression of Upd2-AIM-, despite showing reducing feeding events in an *ad libitum* state compared to control transgene (Figure S6B), displayed strong hunger-driven feeding motivation. Specifically, compared to its fed sibs, fat-specific Upd2-AIM-expressing flies (*upd2Δ; Lpp-Gal4> UAS-Upd2-AIM-)*, after an overnight fast, exhibit strong motivation to feed (Figure 7Bc; +471%; p=0.0031) and feeding events (Figure 7Cc; +502%' p=0.0014). Increased hunger-driven feeding events (Figure S6Cb; +867; p=0.0114) are observed even in a WT background (Figure S6Cb; *Lpp-Gal4>UAS-Upd2-AIM-*). Altogether, these results suggest that fasting-induced Upd2 nuclear accumulation, controlled by Atg8, sensitizes the hunger response, thus improving an organism's adaptation to nutrient scarcity.

**Discussion**

By exploring how cells retain adipokines during fasting, we identified a previously unknown, non-degradative role for Atg8 in licensing adipokine nuclear export in fed cells (see working model Figure 7D-top left panel). When interactions between Atg8 and the adipokine Upd2 are disrupted (AIM-), adipokine nuclear retention occurs, even in a fed state (see working model Figure 7D-middle panel). During fasting, Atg8 is lipidated and recruited to the cytosol; this depletes the nuclear Atg8 pool. A result of Atg8's reduced availability in the nucleus on fasting is adipokine nuclear retention (see model Figure 7D-top right panel). Thus, nuclear retention promotes organismal fitness by ensuring adipokine secretion does not occur during fasting. Furthermore, we illustrate that adipokine retention on fasting has beneficial effects, promoting resilience on fasting and driving post-fasting hunger response. Though this role of Atg8 in adipokine nuclear exit in fed cells, and adipokine retention in starved cells- which we collectively call 'licensing'- is an unexpected and novel finding, it is still very much fits within the continuum of the well-characterized role for Atg8 family of proteins in enabling cells to manage and survive nutrient stress (Kaushik et al., 2010; Singh and Cuervo, 2011). Thus, our findings broaden the central role Atg8 plays during systemic energy homeostasis by regulating adipokine release and retention.

Critically, our report provides a specific answer to an outstanding question: whether Atg8/LC3's localization in the nucleus has a role to play. Atg8 is widely distributed in the nucleus

(Drake et al., 2010). A recent study by Liu and colleagues (Huang et al., 2015), presented compelling evidence that the nuclear pool of Atg8, translocates to the cytosol on starvation and is primary the source of lipidated Atg8 for autophagosome formation (Huang and Liu, 2015). However, it remains possible that Atg8 has other, yet to be uncovered functions in the nucleus by acting on other proteins, in a non-degradative role. For instance, nuclear Atg8 is known to associate with lamin-associated domains (Dou et al., 2015) as well as act in repression of several genes in *Drosophila* fat (Jacomin et al., 2020). These findings support a growing body of evidence that most autophagy genes also function outside of their traditional autophagy context (Galluzzi and Green, 2019). By revealing Atg8's ability to serve as a context-dependent 'licensing factor' to promote adipokine Upd2's nuclear exit, we provide an important insight into a non-degradative role for nuclear Atg8.

More broadly, our findings indicate that Atg8 is likely to perform a context-dependent role in protein localization of other AIM/LIR bearing client proteins. Atg8 is a ubiquitin-like protein (Shpilka et al., 2011). Ubiquitin and ubiquitin-like proteins have been shown to function in cellular localization. (Jura et al., 2006; Nakagawa and Nakayama, 2015; Xu et al., 2010). Specifically, SUMO (small ubiquitin-like modifier) is conjugated to proteins and modulates protein localization (Melchior, 2000), in particular NC transport (Mahajan et al., 1997). Interestingly, SUMO conjugation is not essential for NC transport itself, but positions its target protein (RanGAP1) to the NPC, therefore increasing the efficiency of its translocation. Similarly, Atg8 might position adipokine Upd2, and other such 'client' proteins, to enable efficient export via the classical nuclear export pathway or may serve to direct its larger client proteins to other mechanisms of nuclear export such as nuclear budding (Speese et al., 2012).

In support of this possibility, we observed that *CRM1*/*Emb* plays a role in Upd2 nuclear export (Figure 3Ab). Our evidence comes from a *Emb-KD* test, which is a genetic approach, and leaves open the possibility that Upd2 may need an adapter protein to access Emb/CRM1 export pathway. This idea is consistent with our analysis that Upd2 has a strong predicted NLS(sequence GRVIKRKHLE with score 10.5: a GUS-GFP reporter protein fused to an NLS with a score of 8, 9, or 10 is exclusively localized to the nucleus) allowing it to enter the nucleus. However, Upd2's predicted NES is 248-254 (LCEIELTI) and the Glutamate residues in position 251 and 253 do not broach the threshold, making it difficult to say if this whole sequence is indeed an NES. Thus, perhaps Upd2 requires an adapter to access the CRM1 export pathway. This is reminiscent of a mechanism where-in a nuclear import importin-α requires a specific

nuclear export factor, CAS, to access the cytosol (Kutay et al., 1997). Whether Atg8 serves as such an adapter itself, or if Upd2's association with Atg8 changes its conformation allowing the cryptic NES to be exposed so that it can bind CRM1/Emb, and/or Atg8 enables Upd2 to associate with other proteins that then serve to link up Upd2 to a classical nuclear export pathway are all possibilities. Preliminary evidence that our lab gathered, using mass-spectrometry (MS) analysis of immunoprecipitated (IP) Atg8-WT, Upd2-WT and Upd2-AIM- indicate that while Atg8 and Upd2-WT, both pull-down Emb/CRM1 as a MS interactor, the Upd2-AIM- IP-MS interaction list does not contain Emb. This supports the idea that Atg8 may serve as an adapter to enable Upd2 access Emb/CRM1. However, the IP-MS interactors will need further biochemical validation that is being actively pursued. Importantly, despite having a putative NES, Atg8/LC3 itself does not seem to require CRM1 for its nuclear export (Drake et al., 2010). This is consistent with the idea that it can diffuse freely across the NPC barrier gives its size (<15kDa). In sum, how Atg8 interacts with the nuclear export machinery to enable context-dependent nuclear exit of adipokine Upd2, and whether other AIM/LIR containing proteins are regulated in such a fashion, will be developed in future work.

Another unexpected observation is that Upd2 requires both nuclear import, and then subsequent nuclear export, in order to be secreted (Figure 3). Impeding its nuclear entry by either pharmacological means, using Importazole (Figures 3C, D, D'), or using an ectopic NES to shuttle Upd2 out of the nucleus (Figures 3E, F), results in an abnormal cytosolic localization that is more diffuse, as opposed to its WT punctate localization (Compare Figure 3Ea to 3Ee), and results in a significant reduction in secretion. Furthermore, the ectopic nuclear export of Upd2 interferes with its ability to co-localize with Atg8 (Figure 4B). This is consistent with the idea that Upd2 requires the nuclear environment for a productive interaction with Atg8. We surmise that on entry into the nucleus, Upd2, via its AIM sequence, gains access to Atg8, which then routes it not only to a nuclear exit pathway, but to an appropriate secretory route (Schematic in Figure 7D, top left panel). Consistent with this, Upd2-AIM- mutant protein is unable to effectively complex with GRASP (Figure 4D) and our lab has previously shown that Upd2 uses a GRASP-mediated unconventional secretory route (Rajan et al., 2017). A tantalizing possibility is that Atg8 leads Upd2 through the outer nuclear envelope, which is continuous with the endoplasmic reticulum (ER) and, thus, with the cellular secretory route (Puddington et al., 1985; Rapoport et al., 1996). However, further characterization is needed to define precisely how Atg8 targets Upd2 to the correct cytosolic location for secretion. It will also be interesting to test

whether Atg8 enables Upd2 secretion via a mechanism akin to the one described by Debnath, Leidal and colleagues for RNA binding proteins, in which in a novel secretory process, called LDELS, the Atg8/LC3 conjugation pathway controls extracellular vesicle (EV) cargo loading and secretion (Leidal and Debnath, 2020a, b; Leidal et al., 2020).

A great deal is known about the role that Atg8 lipidation plays in autophagy (Geng and Klionsky, 2008). Our results (Figure 5B) are supportive of adipokine nuclear retention being an important additional result of fasting-induced lipidation and the resulting depletion of the Atg8 nuclear pool (7D, top panel). We show that the presence of lipidation-defective nuclear Atg8 is sufficient to promote Upd2 nuclear exit even in fasting (Figure 5Cf; see schematic model 7D bottom panel). Whether lipidation-defective Atg8 can produces a productive, bioactive secretion event, is still under investigation. It therefore remains possible that lipidation of Atg8, even in fed cells, may very well be an important requirement for productive Upd2 secretion and its subsequent access to the blood-brain barrier by following an LDELS like route (Leidal et al., 2020).

In addition, while in this study, we have focused our explorations on fasting-induced nuclear retention of Upd2, it will be equally important to ask whether the cytosolic pool of Upd2 in fasted cells undergoes degradation and, if so, whether Atg8 plays a role in such a process, similar to how Atg8 targets the nuclear lamina to degradation during oncogene induced stress (Dou et al., 2015). Consistent with this idea, preliminary findings from ongoing work, show that the cytosolic Upd2 puncta at a 24 hour AA-starvation co-localize with lysosomal markers. If indeed this observation holds-up, it would extend Atg8's function from licensing nuclear exit to a broader role in adipokine 'fate' regulation, wherein Atg8 is a bidirectional switch that promotes adipokine release during well-fed states, causes nuclear adipokine retention during acute fasting, but eventually degrades the adipokine during prolonged starvation.

From a physiological standpoint, the *Upd2-AIM-* mutation, provided us a unique opportunity to examine the systemic effect of Atg8's role in adipokine regulation. An *Atg8-KD* in adult fly fat, would result in defects that would be hard to tease apart due to the pleiotropic roles of Atg8, and Atg8 adult fat clonal analysis would not provide answers to its systemic effects on adipokine signaling. The Upd2-AIM- allele, which is impaired in its ability to interact with Atg8 (Figure 2C), not only phenocopies *Atg8-KD's* effects on Upd2 localization and secretion (Figure 2D), but displays an almost exclusive nuclear accumulation phenotype with barely detectable

cytosolic puncta (Figure 2Eb,b'), coupled with a -96% reduction in Upd2 secretion (Figure 2D). These observations suggest that a Upd2-AIM- mutation represents an "Atg8-null"-like state for Upd2. By expressing the *UAS-Upd2-AIM-* transgene in adult fly fat in an *upd2Δ* background, we were able to investigate how the Atg8-mediated adipokine nuclear licensing mechanism impacts an organism's ability to cope with nutrient deprivation. We identified that adipokine nuclear retention promotes resilience to nutrient stress and increased hunger-driven feeding behavior (Figures 7B, C S6C), despite having reduced basal feeding rate (Figure S6B). Thus, expression of *Upd2-AIM-* displays a dominant effect, even though it does not interfere with Upd2-WT localization (Figure S5C). These results suggest that nuclear accumulation of Upd2 not only prevents its release, but also affects gene regulation, reminiscent of SREBP, a master-regulator of lipogenesis that activates transcription of lipogenic genes (Kunte et al., 2006; Porstmann et al., 2008). This regulation of gene expression could occur either indirectly, through regulation of Insulin signaling, or directly via Upd2-dependent regulation of the nuclear landscape; thus, meriting further investigation.

In sum, we have uncovered an unexpected role for Atg8 in licensing the nuclear exit of a fly adipokine, Upd2, in fed cells, and in nuclear retention during fasting. This mechanism provides resilience during nutrient scarcity and sensitizes the post-fasting hunger response of an organism. Upd2 is a fly ortholog of human Leptin (Rajan and Perrimon, 2012) and Leptin, just like Upd2, must be retained during fasting in order to signal a starved state in mammals (Ahima et al., 1996; Flier, 2019; Flier and Maratos-Flier, 2017). Prior studies have shown that Leptin signaling and its regulation closely mirrors findings in the *Drosophila* model (Brent and Rajan, 2020; Rajan et al., 2017). A sequence analysis reveals that human Leptin has two AIM-like sequences, suggesting that it will be important to study the evolutionary conservation of Atg8's control of fasting-induced Leptin retention. Dysfunctional Leptin signaling- 'Leptin resistance' -is a leading cause of obesity. Our report that Atg8-mediated adipokine nuclear retention sensitizes an organism's hunger response, suggests a new mechanism to tackle adipokine resistance.

**Acknowledgments:** We are grateful to Gabor Juhasz for sharing Atg8 antibodies and to the late Suzanne Eaton for Lpp-Gal4 flies. We are grateful for advice from Scott Pletcher for establishing and running the FLIC assay. We thank Brooke Figureoa and Laura Holderbaum for excellent assistance with cell culture and immunoprecipitation experiments. Zach Goldberg for technical assistance with setting up the FLIC assay. We thank Susan Parkhurst for advice on

the NES sequences and Prashant Raghavan for critical input and discussions. **Funding:** This work is possible due to grants awarded to AR from NIDDK (DK101605), NIGMS (GM124593), and New Development funds from Fred Hutch. Genomic reagents from the DGRC which is funded by NIH grant 2P40OD010949 were used in this study. Stocks obtained from the Bloomington Drosophila Stock Center (NIH P40OD018537) and Transgenic RNAi Resource project (NIGMS R01 GM084947 and NIGMS P41 GM132087) were used in this study. **Author contributions:** Conceptualization: AR; Investigation: MEP, CES, AEB, AR; Formal analysis, Data Curation: MEP, CES, AB, AR; Visualization: MEP, CS, AR, AB, TH; Supervision: AR; Writing- original draft: AR; Writing- review and editing: AEB; Funding acquisition: AR. **Competing interests:** Authors declare no competing interests.

## RESOURCE AVAILABILITY

### Lead Contact

Requests for further information, reagents, and resources should be directed to and will be fulfilled by the Lead Contact, Akhila Rajan (akhila@fredhutch.org).

### Materials Availability

Drosophila strains generated in this study are available from the corresponding author, Akhila Rajan (akhila@fredhutch.org).

### Data and Code Availability

The datasets generated in this study are available from the corresponding author, Akhila Rajan (akhila@fredhutch.org).

## EXPERIMENTAL MODEL AND SUBJECT DETAILS

### Experimental Animals

### Drosophila melanogaster

Only males were used in experiments at an age of 5-10 days post-eclosion. Flies were cultured in a humidified incubator at 25ºC with a 12h light-12h dark cycle, and were fed a standard lab diet, containing per liter: 15 g yeast, 8.6 g soy flour, 63 g corn flour, 5g agar, 5g malt, 74 mL corn syrup. For acute starvation, adult male flies which were 7 days old, were subjected to 4-hour starvation on 0% sucrose in agar at 29ºC. For survival curves, flies were subjected to 1% sucrose in agar diet.

The following fly strains used in this study were from our previous work (Rajan et al., 2017; Rajan and Perrimon, 2012) and/or obtained from other investigators or the Bloomington *Drosophila* stock center (BDSC): upd2Δ3-62 (upd2Δ; (Hombria et al., 2005)), *Lpp-Gal4* (Brankatschk and Eaton, 2010), Atg8-Trojan-Gal4 ((Lee et al., 2018); BDSC 77836). The control UAS strain used for over-expression experiments is UAS-Luciferase (Rajan and Perrimon, 2012)

The following UAS lines were generated for this study: *UAS-Upd2::mCherry*, *UAS-Upd2-AIM-::mCherry, UAS-GFP::Atg8; UAS-GFP::Atg8-PE-*. To control for expression levels, all transgenes pertaining to the same gene were inserted at the same att site. Either attp40 or attP2.

Ability of UAS-GFP::Atg8 and UAS-GFP::Atg8-PE- to rescue loss of Atg8 function was tested by introducing Atg8 variant transgenes into the Atg8-Trojan-Gal4 line (Lee et al., 2018), in which insertion of the Trojan-Gal4 into the Atg8 locus generates a lethal allele.

**Cell lines**

*Drosophila* S2R+ cells were used for all cell culture related experiments. This cell line was chosen because previous studies have validated their applicability to study autophagy (Anding and Baehrecke, 2015; Lin et al., 2017; Shravage et al., 2013) and protein secretion (Bard et al., 2006). The cells were maintained in Schneider's medium (GIBCO), 10% heat-inactivated FBS (SIGMA) and 5% Pen-Strep (GIBCO) at 25˚C. For starvation, cells were incubated in Schneider's Insect Medium without Amino Acids (United States Biological, Cat# S0100-01.10) for indicated amount of time.

**METHOD DETAILS:**

**Cloning and Transgenic Flies**

All cloning was done using the Gateway® Technology. For Atg8, entry cDNA was PCR amplified from *Atg8* cDNA (clone LD05816 DGRC-Gold collection) and cloned into pENTR-D/TOPO using BP reaction (Gateway® BP Clonase II enzyme mix, Cat#11789-020, Invitrogen). pENTR-GRASP was previously described (Rajan et al., 2017). For *Drosophila* Upd2 variants, pENTR-Upd2 (Rajan et al., 2017) made for previous work in our lab was used. For site directed mutagenesis of putative AIM sites, pENTR-Upd2 was mutagenized to convert tryptophan and leucine encoding codons to alanine. For addition of a canonical NES+, sequence corresponding to amino acids LQELLELLRL (Verboon et al., 2015) was inserted after the start codon in either pENTER-Upd2-WT or p-ENTR-Upd2-AIM-. For site directed mutagenesis of Atg8 lipidation site,

pENTR-Atg8 was mutagenized to convert its penultimate Glycine to Alanine. All mutagenesis was done using the Q5® Site-Directed Mutagenesis Kit from NEB (Cat # E0554S). The sequence of oligonucleotides used for this mutagenesis reaction are available on request. The entry vectors were then moved using LR clonase reaction (Gateway® LR Clonase® II Enzyme mix, Cat#11791-020, Invitrogen) into destination vectors compatible with fly transformation, or cell culture and with the appropriate C-terminal tags for Upd2 and N-terminal tags for Atg8. Transgenic flies were generated by Bestgene.

**Generation of C-terminal tagged Upd2 CRISPR lines**

GFP or HA-tagged Upd2 CRISPR lines were developed in collaboration with WellGenetics Inc. using modified methods of Kondo and Ueda (Kondo and Ueda, 2013). In brief, for HA lines, following gRNA sequence were cloned into U6 promoter plasmids: TCCAATGAGTCTTGAGCCCT[CGG]/GCCGAGGGCTCAAGACTCAT[TGG]. Cassette 3xHA RFP containing 3xHA and 3xP3 RFP and two homology arms were cloned into pUC57 Kan as donor template for repair. upd2/CG5988 targeting gRNAs and hs-Cas9 were supplied in DNA plasmids, together with donor plasmid for microinjection into embryos of control strain $w^{1118}$. F1 flies carrying selection marker of 3xP3 RFP were further validated by genomic PCR and sequencing. CRISPR generates a break in upd2/CG5988 and is replaced by cassette 3xHA RFP. 3XP3 RFP, which facilitates the genetic screening, was flipped out by Cre recombinase. RE loxP RE (46 bp) remains after excision between Stop codon and 3'UTR. For GFP lines, gRNA sequence TCCAATGAGTCTTGAGCCCT[CGG] was used.

**Tissue culture:**

The day before transfection, cells were passaged to 60-80% confluency. For transfections related to ELISA experiments, cells were cultured in 96 well plates, and for co-immunoprecipitations in 6-well plates. For ELISAs, cells were transfected with 20ng/well of *pAc-upd2::GFP* (Hombria et al., 2005) or indicated Upd2 variants, 10ng/well *pACRenilla::Luciferase*, and 150ng of dsRNA/well for knockdown experiments. For coimmunoprecipitations, cells were transfected with 200ng/well of indicated plasmid.

For imaging experiments, cells were seeded on poly-D-lysine coated 8-well chambered culture slides for fixed imaging (MatTek CCS-8) and glass bottom FluoroDish (World Precision I: FD3510-100) for live imaging. The T7 flasks which were 100% confluent were used for seeing cells at 1:10 dilution at 400µl per well of the 8-well chamber dish or 1:20 dilution at 200µl per

dish for FluoroDish. Transfections were done with plasmids indicated. For 8-chamber slides 100ng/well and for FluoroDish 10ng/dish of each plasmid was transfected.

Transfections were done using the Effectene kit (Cat# 301427, QIAGEN) as per the manufacturer's instructions.

**dsRNA production and cell treatments:**

Amplicons for dsRNAs were designed using the SnapDragon dsRNA design tool (https://www.flyrnai.org/snapdragon) and in vitro transcribed (IVT) using MEGAscript® T7 Transcription Kit (Cat# AMB1334-5, ThermoFisher). IVT reactions were carried out as per the protocol provided by the DRSC (available at: http://www.flyrnai.org/DRSC-PRS.html). Sequence of amplicons used in this study can be found in the table below. *LacZ* dsRNA was used as controls. All dsRNA knockdown experiments were carried out using 2 independent dsRNAs per gene. We found that this produced a knockdown efficiency of >85% (based on qPCR analysis) in S2R+ cells. S2R+ transfected with dsRNAs were incubated for 4 days to allow for gene knockdown. On the 4$^{th}$ day, media was changed, and the ELISA assay was carried out on the 5$^{th}$ day. Note the data is represented as percent change in Upd2/Leptin secretion normalized to transfection efficiency with 0% change indicating baseline level of secretion. See ELISA assay procedure below.

Primer sequences used for dsRNA production.

| Target | Primer name | Sequence 5' → 3' |
|---|---|---|
| *LacZ* | LacZ F1 | TTTCCAGTTCCGTTTATCCG |
| | LacZ R1 | CAAAAATCCATTTCGCTGGT |
| *Atg8a* | Atg8a F1 | GTACAGGGAGCCCATGGTA |
| | Atg8a R1 | CGAGAAGGCTCCCAAGG |
| *Atg8a* | Atg8a F2 | GCCCTGCGTATCAGATCAAT |
| | Atg8a R2 | CGATGAGAATGTTTACGGCA |
| *Emb* | Emb F1 | AGAGGTACATGCAACTGCCC |
| | Emb R1 | GTTGGAACGAGACACCCACT |

| | | |
|---|---|---|
| *Emb* | Emb F2 | ACTAAGGCCAAGCACCTGAA |
| | Emb R2 | TGAACCATCGTGTCCTTGAA |

**Treatment of cells with drugs:**

For drug treatment experiments, the media was replaced with media containing the drug on day 3 after transfection with *upd2::GFP*. 4 hours later the conditioned media was used for ELISA or imaging. Drugs used in this study include Torin1 (Cat# ab218606, Abcam) and Importazole (Cat# CAYM-21491-5, Neta Scientific). Stocks solutions of the drugs were made in DMSO as per the manufacturer's instructions and used at a working concentration indicated in the figure legends of each experiment. DMSO treated replicates were used as controls. Note that for ELISAs, the data is represented as percent change in Upd2 secretion normalized to transfection efficiency, with 0% change indicating baseline level of secretion.

**ELISA assays:**

GFP sandwich ELISA assay was used for detecting Upd2::GFP. On day 1, 96 well medium bind polystyrene plates (Cat#CLS3368-100EA, Sigma) were incubated overnight at 4C with coating antibody (Cat# ACT-CM-GFPTRAP, Allele Biotechnology) diluted in 0.01M pH8.0 bicarbonate buffer at a concentration of 1µg/ml. On day 2, plates were washed briefly with PBS, blocked for 30 minutes with 1% BSA block in PBS, and coated with conditioned media and incubated overnight at 4C. Recombinant GFP protein (Cat# MB-0752, Vector labs), diluted in S2R+ cell growth media (64ng/µl to 4 ng/µl), was used in every ELISA plate as positive control to ensure linearity of GFP readings. On day 3, the plates were washed with PBS+0.05% Tween-20 (PBS-T), blocked with 1% BSA in PBS for 30 minutes at RT. GFP detection antibody (Cat# 600-401-215, Rockland) was added to the diluted 1:1000 in 0.1% BSA in PBS-T. Plates were washed with PBS-T and incubated with secondary HRP conjugated anti Rabbit secondary antibodies (Cat# ab136636, Abcam) diluted at 1:5000 in 1% BSA block. Plates were washed in PBS-T with a final wash in PBS. For detection, each well was incubated 100µl 1-step Ultra-TMB ELISA substrate (Cat# 34028, Pierce), which was previously equilibrated to RT, for approximately 5-15 minutes until detectable blue colorimetric reaction occurred. Reaction was stopped with 2N sulphuric acid and absorbance was measured at 450nm. The TMB readings were normalized to transfection efficiency as measured from Renilla Luciferase assays (see below).

**Renilla Luciferase assay:**

On day 2 of the ELISA assay, after the conditioned medium was transferred for use in ELISA assays, cells were re-suspended in 50µl of PBS, and incubated with 50µl/well Renilla-Glo® Luciferase reagent (Cat# E2710, Promega) for 10 minutes and read using a multiwell luminometer.

**Immunoprecipitation and Western blots:**

For Immunoprecipitation (IP) from S2R+ cells, protein for each condition was prepared by lysing 1 well of a 6-well dish, 4 days after transfection. 2mg/ml was used per IP experiments performed with camelid antibodies GFP-Trap Magnetic Agarose (Cat# gtma-20, Chromotek); RFP-Trap Magnetic Agarose (Cat# rtma-20, Chromotek); Myc-Trap magnetic agarose (Cat# ytma-20; ChromoTek); as per the manufacturer's protocol.

Western blots were performed detailed in our prior publication (Rajan et al., 2017). Antibodies used include Chicken anti-GFP (Cat#ab13970, abcam) 1:2000 in TBS-0.05% tween-20 (TBS-T), Rabbit- anti Upd2 [custom antibody AR4398 generated at YenZym Inc., to Upd2 peptide 318-334: RRPRRNSAERRHLAAIHC; antibody was verified by its recognition of GFP tagged Upd2 pull down in western blots] 1:2000 in TBS-T 0.05%; Rabbit- anti-GRASP (Cat# ab 30315, Abcam) 1:10000 in 1% BSA TBS-T 0.1%; Rabbit-anti RFP (Cat# 600-401-379, Rockland) 1:2500 in0.1% TBS-T ; Mouse-anti-Myc (abcam 9E10) 1:5000 in 0.1% TBS-T; mouse-Anti-Tubulin 1:5000 in 0.05% TBS-T(Cat# T5168, Sigma). The secondary antibodies used were HRP conjugated Goat antibodies directed to appropriate species and the western blot was developed using Amersham ECL kit Start or Prime (Cat# RPN3243 or # RPN2232 , GE life sciences).

**Tissue preparation for fixed immunostaining:**

For fat body preparation, incisions, using dissection scissors (Cat# 500086, World Precision Instruments Inc), were made to release the ventral abdomen from the rest of the fly body. Flies used for dissection were adult males, 7-10 days old. Dissections were done in Ringer's medium (1.8 mM $CaCl_2$, 2mM Kcl, 128mM Nacl, 4mM $MgCl_2$. 35mM sucrose, 5mM HEPES). Tissue was fixed in 4% formaldehyde for 20 minutes and rinsed with PBS. For immunohistochemistry the fixed fat tissue was permeabilized in PBS+ 1.0% Triton-X-100 for 3X washes 5 minutes, subsequently washed with PBS+0.3% Triton-X-100 (Fat wash). Blocked for 30 minutes at room temperature (RT) with gentle agitation in Fat wash+ 5% Normal donkey serum (Block). Primary antibodies, diluted in block, included Rabbit-anti-RFP (1:500, Rockland, #600-401-379);

Chicken-anti-GFP (1:2000, Abcam, #ab13970); Mouse-anti-HA (1:200; Abcam, #ab18181); mouse-anti-Lamin (1:100; ADL67.10 DSHB); Rabbit-anti-GABARAP (Atg8) (1:500; Abcam, # ab109364); and incubated overnight at 4C. Washed multiple times following day in fat wash at (RT) incubated with appropriate secondary antibody (from Jackson Immunoresearch) in block for 2-4 hours at RT. Washed 3X-5X for 5-15 minutes in fat wash, mounted in SlowFade Gold antifade reagent with DAPI (Cat# S36938, Invitrogen).

Dissection and immunostaining of adult brains was performed as previously described (Rajan et al., 2017). In brief: Adult brains were dissected in PBS, then fixed overnight in cold 0.8% Para-formaldehyde (PFA) in PBS at 4$^{o}$C. The following day, tissues were washed multiple times in 0.5% BSA and 0.5% Triton X-100 in PBS (PAT). Tissues were pre-blocked in PAT+ 5% NDS for 2 hours at RT, then incubated overnight with primary antibodies chicken anti-Dilp2 (1:250; (Brent and Rajan, 2020)) and rabbit anti-Dilp5 (1:500; (Brent and Rajan, 2020)) at 4$^{o}$C. The following day, tissues were washed multiple times in PAT, re-blocked for 30 minutes in PAT+ 5% NDS, then incubated in secondary antibody in block (final concentration of 1:500, from Jackson Immunoresearch) for 4 hours at RT. Samples were washed 3X-5X, 15 minutes per wash, in PAT, then mounted on slides with one layer of Scotch Tape spacers in Slowfade gold antifade. Images were captured with Zeiss LSM 800 confocal system and analyzed with Zeiss ZenLite or ImageJ.

**Cell staining:**

For immunohistochemistry, cells were fixed for 20 minutes in 4% formaldehyde, washed in PBS for 5 quick changes, permeabilized in PBS+ 0.1% Triton-X-100 for 3X washes 5 minutes, subsequently washed with PBS+0.1% Triton-X-100 (Cell wash). Blocked for 30 minutes at room temperature (RT) with gentle agitation in Cell wash+ 5% Normal donkey serum (Block). Primary antibodies--Rabbit-anti-RFP (1:500, Rockland, #600-401-379); Chicken-anti-GFP (1:2000, Abcam, #ab13970); mouse-anti-Lamin (1:100; ADL67.10 DSHB)--were diluted in block incubated overnight at 4$^{o}$C. Washed multiple times following day in fat wash at (RT) incubated with appropriate secondary antibody (from Jackson Immunoresearch) in block for 2-4 hours at RT. Washed 3X-5X for 5-15 minutes in cell wash, mounted with SlowFade Gold antifade reagent with DAPI (Cat# S36938, Invitrogen). Images were captured with Zeiss LSM 800 or Zeiss Elyra 7 with Lattice SIM confocal systems, and analyzed with Zeiss ZenLite or ImageJ (Schindelin et al., 2012).

For live imaging, cells were incubated with ProLong Live antifade reagent (Cat# P36974, ThermoFisher), LysoView™ -633 (Cat# 70058, Biotium), and NucBlue (Cat# R37605, Thermofisher) as per manufacturer's instructions, prior to imaging in appropriate media condition. Images were captured in time lapse mode on Zeiss LSM800 in the sequential scan setting.

**FLIC assay:**

The Fly Liquid Interaction Counter (FLIC) assay was performed as detailed previously in Ro et al., (Ro et al., 2014) and provides a measure of continuous feeding behavior and motivation. The Digital feeding monitor (DFM) used to run FLIC assays was purchased from Sable System Inc. and instructions provided in the manufacturers model were followed for set up. Flies used in experiment were aged 7 days and un-sedated flies were loaded into each DFM chamber using mouth pipettes as sedation affected the assay. For recording basal feeding behavior well-fed flies (6 replicates per condition) on standard lab-food were recorded in individual chambers for their interactions and feeding events for 3 hours. For recording hunger-driven feeding behavior flies were fasted for 16hrs at 29$^{o}$C on 0% sucrose, 1% agar and then loaded into chambers. The feeding behaviors of fed versus fasted (6-replicates per condition) loaded onto the same DFM were used for analysis. Analysis was performed using R. Macros used for R analysis were kindly provided by Scott Pletcher via a github open source code and are available upon request.

**qPCR analysis**

qPCR Total RNA prepared from 12-15 fat bodies per genotype, using the Direct-zol RNA miniprep kit (Zymo Research, cat#R2071). cDNA prepared with iScript cDNA Synthesis (Bio-Rad, cat#1708891), and 1mg RNA applied per reaction. qPCR performed with iQ SYBR Green Supermix (Bio-Rad, cat#1708882). rpl13A and robl employed to normalize RNA levels. Relative quantification of mRNA levels calculated with comparative CT method. Primers used in this study can be found in the table below.

Primer sequences used in this study.

| Target | Primer name | Sequence 5' → 3' |
|---|---|---|
| *rpl13A* | rpl13A F1 | AGCTGAACCTCTCGGGACAC |

| | | |
|---|---|---|
| | rpl13A R1 | TGCCTCGGACTGCCTTGTAG |
| *Robl* | robl F1 | AGCGGTAGTGTCTGCCGTGT |
| | robl R1 | CCAGCGTGGATTTGACCGGA |
| *SREBP* | SREBP F1 | AGTCGCCGCTTCTCGTCTA |
| | SREBP R1 | TGTATGGTGGCTGTTGGTTGG |
| *FASN1* | FASN1 F1 | TGACCAACAGTTCTTCGGTGT |
| | FASN1 R1 | GCGTCAATAATAGCTTCATGGGT |
| *Apolpp* | Apolpp F1 | TTGGAATCCTAGCTTCTGTGCT |
| | Apolpp R1 | AGTCATAGTAGTTGCCGGGTAT |
| *Mtp* | Mtp F1 | GTTTGGAGTGGAGATGAGGACC |
| | Mtp R1 | GGGTATCCGGGTAATTGAGCG |
| *InR* | InR F1 | AAGCGTGGGAAAATTAAGATGGA |
| | InR R1 | GGCTGTCAACTGCTTCTACTG |
| *Bmm* | Bmm F1 | TTTTGCAGTTGAACCACGCC |
| | Bmm R1 | CACGGGGTCCATATAAGCGG |
| *4ebp* | 4ebp F1 | GAAGGGAGTACGCGGAGTG |
| | 4ebp R1 | TCCCCATTGAGCCAAACTC |

**Triglyceride Measurements**

TAG assays were carried out as previously described (Rajan et al., 2017). In brief: Flies were homogenized in PBST (PBS + 0.1% Triton X-100) using 1mm zirconium beads (Cat#ZROB10, Next Advance) in a Bullet Blender® Tissue homogenizer (Model BBX24, Next Advance). Samples were heated to 70$^{o}$C for 10 minutes, then centrifuged at 14,000 rpm (in refrigerated tabletop centrifuge). 10.0 µl of the supernatant was applied to determine level of TAG in sample,

using the following reagents obtained from Sigma: Free glycerol (cat # F6428-40ML), Triglyceride reagent (cat# T2449-10ML), and Glycerol standard (cat# G7793-5ML).Three adult males employed per biological replicate. Note: For adult TAG assays, the most consistent results, with lowest standard deviations, were obtained with 10 day old males. TAG readings from whole fly lysate (n=4 replicates of 3 flies each) were normalized to number of flies per experiment. Normalized ratio from the control served as baseline, and data is represented as fold change of experimental genotypes with respect to the control.

**Starvation Survival Assays**

Survival curves were done using flies that were harvested in a 24hour time frame and aged for 7 days. 10 males per vial were flipped onto 1% sucrose and 1% agar starvation food. The number of dead flies were recorded each day until every fly had died. Flies were kept in a 25$^{o}$C incubator with a 12 hour light dark cycle for the entirety of the experiment. Survival analysis was performed using the Survival Curve module of GraphPad Prism. A Mantel-cox test was the test used to determine statistical significance. Greater than 90 flies were used per genotype per curve.

**QUANTIFICATION AND STATISTICAL ANALYSIS**

Excel or GraphPad Prism 7 software was used for data quantification and generation of graphs. Quantification of nuclear localization in S2R+ was performed as follows: Using Zeiss ZenLite, each cell exhibiting transfected expression was visualized in LUT Rainbow2 mode. Whole Cell fraction (WC) was generated from subsets of z-stacks covering an entire cell (using DIC as reference). For nuclear fraction (Nuc), DAPI or Lamin was used as a reference to generate a subset of the WC z-stack representing the nucleus. Maximum Intensity Projections (MIPs) were generated for both WC and Nuc stacks, and ImageJ was used to measure the Integrated Density of protein being quantified in compartment. The fraction of protein in the nucleus was determined as Nuc Integrated Density/WC Integrated Density. An average was calculated and 2-tailed t-test performed between control and experimental groups. Error bars represent %SD (Standard Deviation). For quantification of nuclear localization in fat tissue, Integrated Density was measured in ImageJ from MIPs of z-stacks covering the fat cell nucleus (based on DAPI or Lamin staining). An average was calculated and 2-tailed t-test performed between control and experimental groups.

To measure intensity of Dilp expression, ImageJ-calculated mean gray values were averaged from maximum intensity projections (MIPs) of a similar number of confocal stacks. Average values were normalized to control and t-test performed between control and experimental groups. Error bars represent %SD (Standard Deviation). Manders coefficients were calculated using the JACoP plugin for ImageJ on z-stacks through entire cells. Significance was calculated by 2-tailed t-test. Error bars represent %SD (Standard Deviation). For ELISA assays, the ELISA signal readings are normalized to transfection efficiency; the data is represented as percent fold change from control used as baseline. Specifically, the ratio of TMB readings to Renilla Luciferase readings is calculated. This ratio from the control is used as a baseline and the data is represented as percent fold change of experimental conditions with respect to the control. Statistical significance quantified by 2-tailed t-test on 6 biological replicates per condition. Error bars represent %SD (Standard Deviation). For TAG analysis, statistical significance was quantified by 2-tailed t-test on 3-6 biological replicates per condition. Error bars indicate %SD (Standard Deviation). For qPCR analysis, normalized levels of gene expression were analyzed using one-way ANOVA. Error bars represent standard error of the mean (SEM).

We determined that our data-points were normally distributed, based on two measures: i) A GraphPad outlier test did not identify any outliers in our data; and ii) the majority of our data points for a particular condition were relatively similar to one other, with only a small standard error of mean or standard deviation.

References

Ahima, R.S., Prabakaran, D., Mantzoros, C., Qu, D., Lowell, B., Maratos-Flier, E., and Flier, J.S. (1996). Role of leptin in the neuroendocrine response to fasting. Nature *382*, 250-252.

Anding, A.L., and Baehrecke, E.H. (2015). Vps15 is required for stress induced and developmentally triggered autophagy and salivary gland protein secretion in Drosophila. Cell Death Differ *22*, 457-464.

Baggio, L.L., and Drucker, D.J. (2020). Glucagon-like peptide-1 receptor co-agonists for treating metabolic disease. Mol Metab, 101090.

Baker, K.D., and Thummel, C.S. (2007). Diabetic larvae and obese flies-emerging studies of metabolism in Drosophila. Cell Metab *6*, 257-266.

Bard, F., Casano, L., Mallabiabarrena, A., Wallace, E., Saito, K., Kitayama, H., Guizzunti, G., Hu, Y., Wendler, F., Dasgupta, R.*, et al.* (2006). Functional genomics reveals genes involved in protein secretion and Golgi organization. Nature *439*, 604-607.

Brankatschk, M., and Eaton, S. (2010). Lipoprotein particles cross the blood-brain barrier in Drosophila. J Neurosci *30*, 10441-10447.

Brent, A.E., and Rajan, A. (2020). Insulin and Leptin/Upd2 Exert Opposing Influences on Synapse Number in Fat-Sensing Neurons. Cell Metab *32*, 786-800 e787.

Bruns, C., McCaffery, J.M., Curwin, A.J., Duran, J.M., and Malhotra, V. (2011). Biogenesis of a novel compartment for autophagosome-mediated unconventional protein secretion. J Cell Biol *195*, 979-992.

Cadwell, K., and Debnath, J. (2018). Beyond self-eating: The control of nonautophagic functions and signaling pathways by autophagy-related proteins. J Cell Biol *217*, 813-822.

Cunha, L.D., Yang, M., Carter, R., Guy, C., Harris, L., Crawford, J.C., Quarato, G., Boada-Romero, E., Kalkavan, H., Johnson, M.D.L.*, et al.* (2018). LC3-Associated Phagocytosis in Myeloid Cells Promotes Tumor Immune Tolerance. Cell *175*, 429-441 e416.

Davis, L.I. (1995). The nuclear pore complex. Annu Rev Biochem *64*, 865-896.

Deshpande, S.A., Carvalho, G.B., Amador, A., Phillips, A.M., Hoxha, S., Lizotte, K.J., and Ja, W.W. (2014). Quantifying Drosophila food intake: comparative analysis of current methodology. Nat Methods *11*, 535-540.

DiAngelo, J.R., and Birnbaum, M.J. (2009). Regulation of fat cell mass by insulin in Drosophila melanogaster. Mol Cell Biol *29*, 6341-6352.

Dou, Z., Xu, C., Donahue, G., Shimi, T., Pan, J.A., Zhu, J., Ivanov, A., Capell, B.C., Drake, A.M., Shah, P.P.*, et al.* (2015). Autophagy mediates degradation of nuclear lamina. Nature *527*, 105-109.

Drake, K.R., Kang, M., and Kenworthy, A.K. (2010). Nucleocytoplasmic distribution and dynamics of the autophagosome marker EGFP-LC3. PLoS One *5*, e9806.

Dupont, N., Jiang, S., Pilli, M., Ornatowski, W., Bhattacharya, D., and Deretic, V. (2011). Autophagy-based unconventional secretory pathway for extracellular delivery of IL-1beta. Embo J *30*, 4701-4711.

Duran, J.M., Anjard, C., Stefan, C., Loomis, W.F., and Malhotra, V. (2010). Unconventional secretion of Acb1 is mediated by autophagosomes. J Cell Biol *188*, 527-536.

Eijkelenboom, A., and Burgering, B.M. (2013). FOXOs: signalling integrators for homeostasis maintenance. Nat Rev Mol Cell Biol *14*, 83-97.

Farooqi, I.S., and O'Rahilly, S. (2009). Leptin: a pivotal regulator of human energy homeostasis. The American journal of clinical nutrition *89*, 980S-984S.

Fasken, M.B., Saunders, R., Rosenberg, M., and Brighty, D.W. (2000). A leptomycin B-sensitive homologue of human CRM1 promotes nuclear export of nuclear export sequence-containing proteins in Drosophila cells. J Biol Chem *275*, 1878-1886.

Flier, J.S. (2019). Starvation in the Midst of Plenty: Reflections on the History and Biology of Insulin and Leptin. Endocr Rev *40*, 1-16.

Flier, J.S., and Maratos-Flier, E. (2017). Leptin's Physiologic Role: Does the Emperor of Energy Balance Have No Clothes? Cell Metab *26*, 24-26.

Fukuda, M., Asano, S., Nakamura, T., Adachi, M., Yoshida, M., Yanagida, M., and Nishida, E. (1997). CRM1 is responsible for intracellular transport mediated by the nuclear export signal. Nature *390*, 308-311.

Galluzzi, L., Bravo-San Pedro, J.M., Levine, B., Green, D.R., and Kroemer, G. (2017). Pharmacological modulation of autophagy: therapeutic potential and persisting obstacles. Nat Rev Drug Discov *16*, 487-511.

Galluzzi, L., and Green, D.R. (2019). Autophagy-Independent Functions of the Autophagy Machinery. Cell *177*, 1682-1699.

Garrido, D., Rubin, T., Poidevin, M., Maroni, B., Le Rouzic, A., Parvy, J.P., and Montagne, J. (2015). Fatty acid synthase cooperates with glyoxalase 1 to protect against sugar toxicity. PLoS Genet *11*, e1004995.

Geminard, C., Rulifson, E.J., and Leopold, P. (2009). Remote control of insulin secretion by fat cells in Drosophila. Cell Metab *10*, 199-207.

Geng, J., and Klionsky, D.J. (2008). The Atg8 and Atg12 ubiquitin-like conjugation systems in macroautophagy. 'Protein modifications: beyond the usual suspects' review series. EMBO Rep *9*, 859-864.

Goldstein, I., and Hager, G.L. (2015). Transcriptional and Chromatin Regulation during Fasting - The Genomic Era. Trends Endocrinol Metab *26*, 699-710.

Gorlich, D., and Kutay, U. (1999). Transport between the cell nucleus and the cytoplasm. Annu Rev Cell Dev Biol *15*, 607-660.

Gronke, S., Mildner, A., Fellert, S., Tennagels, N., Petry, S., Muller, G., Jackle, H., and Kuhnlein, R.P. (2005). Brummer lipase is an evolutionary conserved fat storage regulator in Drosophila. Cell Metab *1*, 323-330.

Heckmann, B.L., Teubner, B.J.W., Tummers, B., Boada-Romero, E., Harris, L., Yang, M., Guy, C.S., Zakharenko, S.S., and Green, D.R. (2019). LC3-Associated Endocytosis Facilitates beta-Amyloid Clearance and Mitigates Neurodegeneration in Murine Alzheimer's Disease. Cell *178*, 536-551 e514.

Hickey, M.S., Considine, R.V., Israel, R.G., Mahar, T.L., McCammon, M.R., Tyndall, G.L., Houmard, J.A., and Caro, J.F. (1996). Leptin is related to body fat content in male distance runners. Am J Physiol *271*, E938-940.

Hombria, J.C., Brown, S., Hader, S., and Zeidler, M.P. (2005). Characterisation of Upd2, a Drosophila JAK/STAT pathway ligand. Dev Biol *288*, 420-433.

Huang, R., and Liu, W. (2015). Identifying an essential role of nuclear LC3 for autophagy. Autophagy *11*, 852-853.

Huang, R., Xu, Y., Wan, W., Shou, X., Qian, J., You, Z., Liu, B., Chang, C., Zhou, T., Lippincott-Schwartz, J.*, et al.* (2015). Deacetylation of nuclear LC3 drives autophagy initiation under starvation. Mol Cell *57*, 456-466.

Ichimura, Y., Kirisako, T., Takao, T., Satomi, Y., Shimonishi, Y., Ishihara, N., Mizushima, N., Tanida, I., Kominami, E., Ohsumi, M.*, et al.* (2000). A ubiquitin-like system mediates protein lipidation. Nature *408*, 488-492.

Jacomin, A.-C., Petridi, S., Di Monaco, M., Bhujabal, Z., Jain, A., Mulakkal, N.C., Palara, A., Powell, E.L., Chung, B., Zampronio, C.*, et al.* (2020). Regulation of Expression of Autophagy Genes by Atg8a-Interacting Partners Sequoia, YL-1, and Sir2 in Drosophila. Cell Rep *31*, 107695-107695.

Jura, N., Scotto-Lavino, E., Sobczyk, A., and Bar-Sagi, D. (2006). Differential modification of Ras proteins by ubiquitination. Molecular Cell *21*, 679-687.

Kaffman, A., and O'Shea, E.K. (1999). Regulation of nuclear localization: a key to a door. Annu Rev Cell Dev Biol *15*, 291-339.

Kaushik, S., Singh, R., and Cuervo, A.M. (2010). Autophagic pathways and metabolic stress. Diabetes Obes Metab *12 Suppl 2*, 4-14.

King-Jones, K., and Thummel, C.S. (2005). Nuclear receptors--a perspective from Drosophila. Nat Rev Genet *6*, 311-323.

Kirisako, T., Baba, M., Ishihara, N., Miyazawa, K., Ohsumi, M., Yoshimori, T., Noda, T., and Ohsumi, Y. (1999). Formation process of autophagosome is traced with Apg8/Aut7p in yeast. J Cell Biol *147*, 435-446.

Knight, Z.A., Hannan, K.S., Greenberg, M.L., and Friedman, J.M. (2010). Hyperleptinemia is required for the development of leptin resistance. PloS one *5*, e11376.

Kolaczynski, J.W., Considine, R.V., Ohannesian, J., Marco, C., Opentanova, I., Nyce, M.R., Myint, M., and Caro, J.F. (1996a). Responses of leptin to short-term fasting and refeeding in humans: a link with ketogenesis but not ketones themselves. Diabetes *45*, 1511-1515.

Kolaczynski, J.W., Ohannesian, J.P., Considine, R.V., Marco, C.C., and Caro, J.F. (1996b). Response of leptin to short-term and prolonged overfeeding in humans. J Clin Endocrinol Metab *81*, 4162-4165.

Kondo, S., and Ueda, R. (2013). Highly improved gene targeting by germline-specific Cas9 expression in Drosophila. Genetics *195*, 715-721.

Kosugi, S., Hasebe, M., Entani, T., Takayama, S., Tomita, M., and Yanagawa, H. (2008). Design of peptide inhibitors for the importin alpha/beta nuclear import pathway by activity-based profiling. Chem Biol *15*, 940-949.

Kosugi, S., Hasebe, M., Matsumura, N., Takashima, H., Miyamoto-Sato, E., Tomita, M., and Yanagawa, H. (2009a). Six classes of nuclear localization signals specific to different binding grooves of importin alpha. J Biol Chem *284*, 478-485.

Kosugi, S., Hasebe, M., Tomita, M., and Yanagawa, H. (2009b). Systematic identification of cell cycle-dependent yeast nucleocytoplasmic shuttling proteins by prediction of composite motifs. Proc Natl Acad Sci U S A *106*, 10171-10176.

Kunte, A.S., Matthews, K.A., and Rawson, R.B. (2006). Fatty acid auxotrophy in Drosophila larvae lacking SREBP. Cell Metab *3*, 439-448.

Kutay, U., Bischoff, F.R., Kostka, S., Kraft, R., and Gorlich, D. (1997). Export of importin alpha from the nucleus is mediated by a specific nuclear transport factor. Cell *90*, 1061-1071.

la Cour, T., Kiemer, L., Molgaard, A., Gupta, R., Skriver, K., and Brunak, S. (2004). Analysis and prediction of leucine-rich nuclear export signals. Protein Eng Des Sel *17*, 527-536.

Lee, P.T., Zirin, J., Kanca, O., Lin, W.W., Schulze, K.L., Li-Kroeger, D., Tao, R., Devereaux, C., Hu, Y., Chung, V.*, et al.* (2018). A gene-specific T2A-GAL4 library for Drosophila. Elife *7*.

Leidal, A.M., and Debnath, J. (2020a). LC3-dependent extracellular vesicle loading and secretion (LDELS). Autophagy *16*, 1162-1163.

Leidal, A.M., and Debnath, J. (2020b). Unraveling the mechanisms that specify molecules for secretion in extracellular vesicles. Methods *177*, 15-26.

Leidal, A.M., Huang, H.H., Marsh, T., Solvik, T., Zhang, D., Ye, J., Kai, F., Goldsmith, J., Liu, J.Y., Huang, Y.H.*, et al.* (2020). The LC3-conjugation machinery specifies the loading of RNA-binding proteins into extracellular vesicles. Nat Cell Biol *22*, 187-199.

Lin, L., Rodrigues, F., Kary, C., Contet, A., Logan, M., Baxter, R.H.G., Wood, W., and Baehrecke, E.H. (2017). Complement-Related Regulates Autophagy in Neighboring Cells. Cell *170*, 158-171 e158.

Mahajan, R., Delphin, C., Guan, T., Gerace, L., and Melchior, F. (1997). A small ubiquitin-related polypeptide involved in targeting RanGAP1 to nuclear pore complex protein RanBP2. Cell *88*, 97-107.

Mason, D.A., and Goldfarb, D.S. (2009). The nuclear transport machinery as a regulator of Drosophila development. Semin Cell Dev Biol *20*, 582-589.

Mattaj, I.W., and Englmeier, L. (1998). Nucleocytoplasmic transport: the soluble phase. Annu Rev Biochem *67*, 265-306.

Melchior, F. (2000). SUMO--nonclassical ubiquitin. Annu Rev Cell Dev Biol *16*, 591-626.

Mizushima, N., and Yoshimori, T. (2007). How to interpret LC3 immunoblotting. Autophagy *3*, 542-545.

Mortimore, G.E., Hutson, N.J., and Surmacz, C.A. (1983). Quantitative correlation between proteolysis and macro- and microautophagy in mouse hepatocytes during starvation and refeeding. Proc Natl Acad Sci U S A *80*, 2179-2183.

Musselman, L.P., and Kuhnlein, R.P. (2018). Drosophila as a model to study obesity and metabolic disease. J Exp Biol *221*.

Nakagawa, T., and Nakayama, K. (2015). Protein monoubiquitylation: targets and diverse functions. Genes Cells *20*, 543-562.

Nakatogawa, H., Ichimura, Y., and Ohsumi, Y. (2007). Atg8, a ubiquitin-like protein required for autophagosome formation, mediates membrane tethering and hemifusion. Cell *130*, 165-178.

Nassel, D.R., Kubrak, O.I., Liu, Y., Luo, J., and Lushchak, O.V. (2013). Factors that regulate insulin producing cells and their output in Drosophila. Front Physiol *4*, 252.

Neufeld, T.P., and Baehrecke, E.H. (2008). Eating on the fly: function and regulation of autophagy during cell growth, survival and death in Drosophila. Autophagy *4*, 557-562.

Noda, N.N., Kumeta, H., Nakatogawa, H., Satoo, K., Adachi, W., Ishii, J., Fujioka, Y., Ohsumi, Y., and Inagaki, F. (2008). Structural basis of target recognition by Atg8/LC3 during selective autophagy. Genes Cells *13*, 1211-1218.

Noda, N.N., Ohsumi, Y., and Inagaki, F. (2010). Atg8-family interacting motif crucial for selective autophagy. FEBS letters *584*, 1379-1385.

Palm, W., Sampaio, J.L., Brankatschk, M., Carvalho, M., Mahmoud, A., Shevchenko, A., and Eaton, S. (2012). Lipoproteins in Drosophila melanogaster--assembly, function, and influence on tissue lipid composition. PLoS Genet *8*, e1002828.

Parvy, J.P., Napal, L., Rubin, T., Poidevin, M., Perrin, L., Wicker-Thomas, C., and Montagne, J. (2012). Drosophila melanogaster Acetyl-CoA-carboxylase sustains a fatty acid-dependent remote signal to waterproof the respiratory system. PLoS Genet *8*, e1002925.

Porstmann, T., Santos, C.R., Griffiths, B., Cully, M., Wu, M., Leevers, S., Griffiths, J.R., Chung, Y.L., and Schulze, A. (2008). SREBP activity is regulated by mTORC1 and contributes to Akt-dependent cell growth. Cell Metab *8*, 224-236.

Puddington, L., Lively, M.O., and Lyles, D.S. (1985). Role of the nuclear envelope in synthesis, processing, and transport of membrane glycoproteins. J Biol Chem *260*, 5641-5647.

Rajan, A., Housden, B.E., Wirtz-Peitz, F., Holderbaum, L., and Perrimon, N. (2017). A Mechanism Coupling Systemic Energy Sensing to Adipokine Secretion. Dev Cell *43*, 83-98 e86.

Rajan, A., and Perrimon, N. (2012). *Drosophila* Cytokine Unpaired 2 Regulates Physiological Homeostasis by Remotely Controlling Insulin Secretion. Cell *151*, 123-137.

Rapoport, T.A., Jungnickel, B., and Kutay, U. (1996). Protein transport across the eukaryotic endoplasmic reticulum and bacterial inner membranes. Annu Rev Biochem *65*, 271-303.

Reggiori, F., Monastyrska, I., Verheije, M.H., Cali, T., Ulasli, M., Bianchi, S., Bernasconi, R., de Haan, C.A., and Molinari, M. (2010). Coronaviruses Hijack the LC3-I-positive EDEMosomes, ER-derived vesicles exporting short-lived ERAD regulators, for replication. Cell Host Microbe *7*, 500-508.

Ro, J., Harvanek, Z.M., and Pletcher, S.D. (2014). FLIC: high-throughput, continuous analysis of feeding behaviors in Drosophila. PLoS One *9*, e101107.

Schindelin, J., Arganda-Carreras, I., Frise, E., Kaynig, V., Longair, M., Pietzsch, T., Preibisch, S., Rueden, C., Saalfeld, S., Schmid, B*., et al.* (2012). Fiji: an open-source platform for biological-image analysis. Nat Methods *9*, 676-682.

Shpilka, T., Weidberg, H., Pietrokovski, S., and Elazar, Z. (2011). Atg8: an autophagy-related ubiquitin-like protein family. Genome Biol *12*, 226.

Shravage, B.V., Hill, J.H., Powers, C.M., Wu, L., and Baehrecke, E.H. (2013). Atg6 is required for multiple vesicle trafficking pathways and hematopoiesis in Drosophila. Development *140*, 1321-1329.

Shu, X.E., Swanda, R.V., and Qian, S.B. (2020). Nutrient Control of mRNA Translation. Annu Rev Nutr *40*, 51-75.

Singh, R., and Cuervo, A.M. (2011). Autophagy in the cellular energetic balance. Cell Metab *13*, 495-504.

Singh, R., Kaushik, S., Wang, Y., Xiang, Y., Novak, I., Komatsu, M., Tanaka, K., Cuervo, A.M., and Czaja, M.J. (2009a). Autophagy regulates lipid metabolism. Nature *458*, 1131-1135.

Singh, R., Xiang, Y., Wang, Y., Baikati, K., Cuervo, A.M., Luu, Y.K., Tang, Y., Pessin, J.E., Schwartz, G.J., and Czaja, M.J. (2009b). Autophagy regulates adipose mass and differentiation in mice. J Clin Invest *119*, 3329-3339.

Soderholm, J.F., Bird, S.L., Kalab, P., Sampathkumar, Y., Hasegawa, K., Uehara-Bingen, M., Weis, K., and Heald, R. (2011). Importazole, a small molecule inhibitor of the transport receptor importin-beta. ACS Chem Biol *6*, 700-708.

Speese, S.D., Ashley, J., Jokhi, V., Nunnari, J., Barria, R., Li, Y., Ataman, B., Koon, A., Chang, Y.T., Li, Q*., et al.* (2012). Nuclear envelope budding enables large ribonucleoprotein particle export during synaptic Wnt signaling. Cell *149*, 832-846.

Stolz, A., Putyrski, M., Kutle, I., Huber, J., Wang, C., Major, V., Sidhu, S.S., Youle, R.J., Rogov, V.V., Dotsch, V*., et al.* (2017). Fluorescence-based ATG8 sensors monitor localization and function of LC3/GABARAP proteins. EMBO J *36*, 549-564.

Teleman, A.A., Chen, Y.W., and Cohen, S.M. (2005). 4E-BP functions as a metabolic brake used under stress conditions but not during normal growth. Genes & development *19*, 1844-1848.

Teleman, A.A., Ratzenbock, I., and Oldham, S. (2012). Drosophila: a model for understanding obesity and diabetic complications. Exp Clin Endocrinol Diabetes *120*, 184-185.

Tennessen, J.M., Barry, W.E., Cox, J., and Thummel, C.S. (2014). Methods for studying metabolism in Drosophila. Methods *68*, 105-115.

Thoreen, C.C., Kang, S.A., Chang, J.W., Liu, Q., Zhang, J., Gao, Y., Reichling, L.J., Sim, T., Sabatini, D.M., and Gray, N.S. (2009). An ATP-competitive mammalian target of rapamycin inhibitor reveals rapamycin-resistant functions of mTORC1. J Biol Chem *284*, 8023-8032.

Verboon, J.M., Rincon-Arano, H., Werwie, T.R., Delrow, J.J., Scalzo, D., Nandakumar, V., Groudine, M., and Parkhurst, S.M. (2015). Wash interacts with lamin and affects global nuclear organization. Curr Biol *25*, 804-810.

Welte, M.A., and Gould, A.P. (2017). Lipid droplet functions beyond energy storage. Biochim Biophys Acta Mol Cell Biol Lipids *1862*, 1260-1272.

Xu, L., Lubkov, V., Taylor, L.J., and Bar-Sagi, D. (2010). Feedback regulation of Ras signaling by Rabex-5-mediated ubiquitination. Curr Biol *20*, 1372-1377.

Zhang, M., Kenny, S., Ge, L., Xu, K., and Schekman, R. (2015). Translocation of interleukin-1beta into a vesicle intermediate in autophagy-mediated secretion. Elife *4*.

Zirin, J., and Perrimon, N. (2010). Drosophila as a model system to study autophagy. Semin Immunopathol *32*, 363-372.

# Figure 1

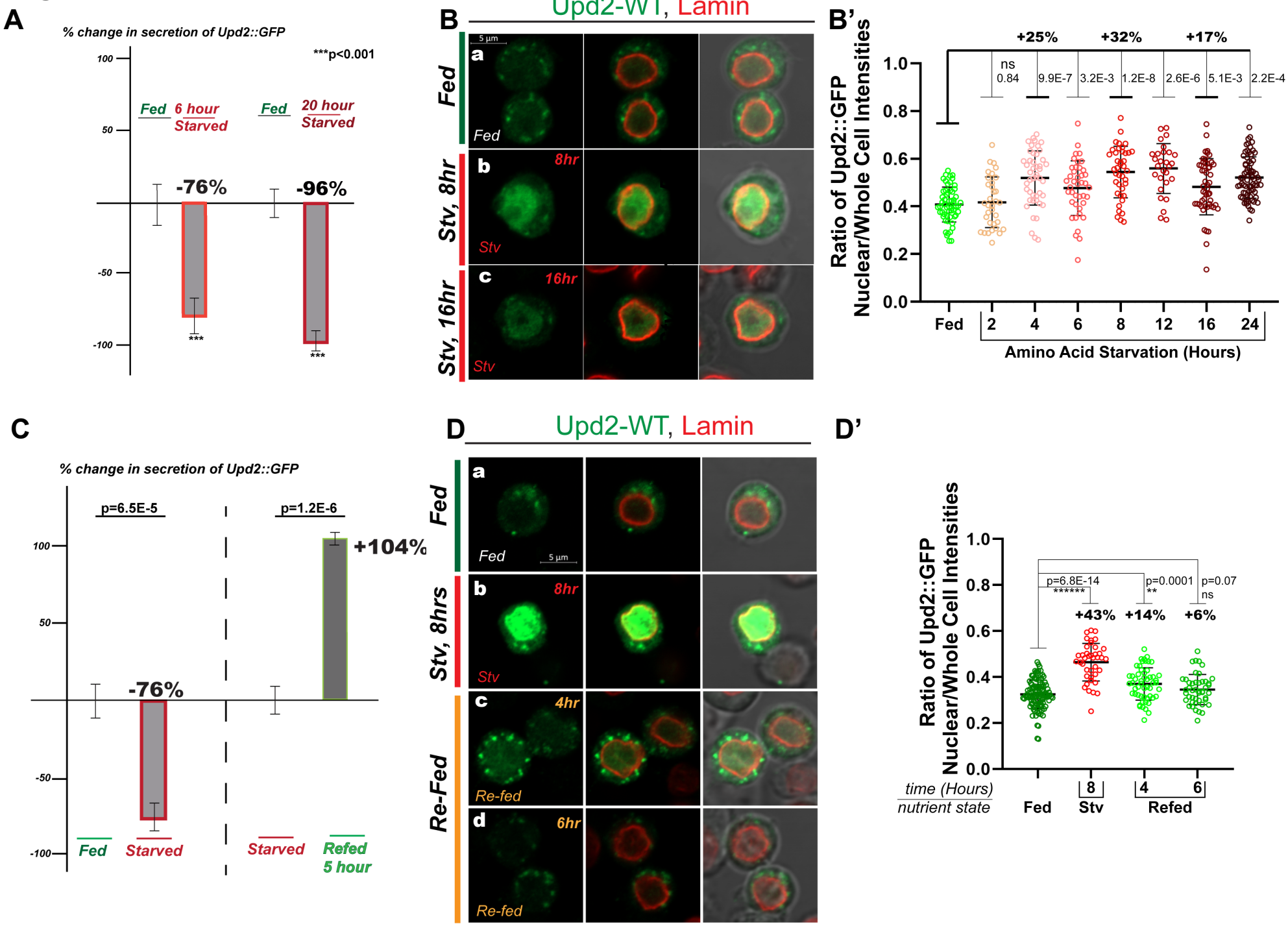
A
% change in secretion of Upd2::GFP
***p<0.001
100
50
-50
-100
Fed
6 hour Starved
Fed
20 hour Starved
-76%
-96%
***
***
B
Upd2-WT, Lamin
Fed
Stv, 8hr
Stv, 16hr
5 µm
a
Fed
b
8hr
Stv
c
16hr
Stv
B'
Ratio of Upd2::GFP Nuclear/Whole Cell Intensities
+25%
+32%
+17%
ns 0.84
9.9E-7
3.2E-3
1.2E-8
2.6E-6
5.1E-3
2.2E-4
1.0
0.8
0.6
0.4
0.2
0.0
Fed
2
4
6
8
12
16
24
Amino Acid Starvation (Hours)
C
% change in secretion of Upd2::GFP
p=6.5E-5
p=1.2E-6
100
50
-50
-100
-76%
+104%
Fed
Starved
Starved
Refed 5 hour
D
Upd2-WT, Lamin
Fed
Stv, 8hrs
Re-Fed
a
Fed
5 µm
b
8hr
Stv
c
4hr
Re-fed
d
6hr
Re-fed
D'
Ratio of Upd2::GFP Nuclear/Whole Cell Intensities
p=6.8E-14
******
p=0.0001
**
p=0.07
ns
+43%
+14%
+6%
1.0
0.8
0.6
0.4
0.2
0.0
time (Hours)
nutrient state
Fed
8
Stv
4
6
Refed

## Figure Legends

### Figure 1: Fasting induces Upd2 nuclear accumulation.

**(A)** Effect of amino acid starvation on Upd2's release into media. Normalized percent fold change in secreted GFP signal detected by GFP sandwich ELISA assay performed on conditioned media of S2R+ cells transiently transfected with *Upd2-WT::GFP*. Cells were incubated either with complete media (control) or Amino-Acid (AA) free media for the indicated times. Statistical significance is quantified by unpaired two-tailed t-test on 6 biological replicates per condition.

**(B)** Effect of amino acid starvation on Upd2's nuclear accumulation. Confocal micrographs of single optical-slices of *Drosophila* S2R+ cells transiently transfected with *Upd2-WT::GFP* (green) stained with Lamin (red). **(a)** In fed state, Upd2-WT::GFP is localizes to cytosolic puncta and its nuclear localization is not obvious. **(b, c)** In AA starved cells (8 and 16 hours post-starvation) Upd2 is visible both as cytosolic puncta and shows nuclear enrichment. Scale bar is 5um and right most panel shows DIC image merge. In **B'**, the ratio of Upd2::GFP nuclear/whole cell intensity is plotted. Each dot represents a cell, 50-100 cells were counted per time point. Statistical significance is quantified by unpaired two-tailed t-test.

**(C)** Effect of re-feeding on Upd2's release into media. Normalized percent fold change in secreted GFP signal detected by GFP sandwich ELISA assay performed on conditioned media of S2R+ cells transiently transfected with *Upd2-WT::GFP*. Cells were incubated either with complete media (control) or Amino-Acid (AA) free media for the indicated times. Statistical significance is quantified by unpaired two-tailed t-test on 6 biological replicates per condition.

**(D)** Effect of re-feeding on Upd2's nuclear accumulation. Confocal micrographs of single optical-slices of *Drosophila* S2R+ cells transiently transfected with *Upd2-WT::GFP* (green) stained with Lamin (red). **(a)** In fed state, *Upd2-WT::GFP* is localized to cytosolic puncta and nuclear localization is not obvious. **(b)** In AA starved cells (8 hours post-starvation) Upd2 is visible both as cytosolic puncta and shows nuclear enrichment. (**c, d**) On re-feeding with complete media, by 4 hours **(c)** Upd2's starvation-induced accumulation begins to reduce and is restored to pre-fasting levels by 6 hours **(d)**. Scale bar is 5um and right most panel shows DIC image merge. In **D',** the ratio of Upd2::GFP nuclear/whole cell intensity is plotted. Each dot represents a cell, 50-100 cells were counted per time point. Statistical significance is quantified by unpaired two-tailed t-test.

# Figure 2

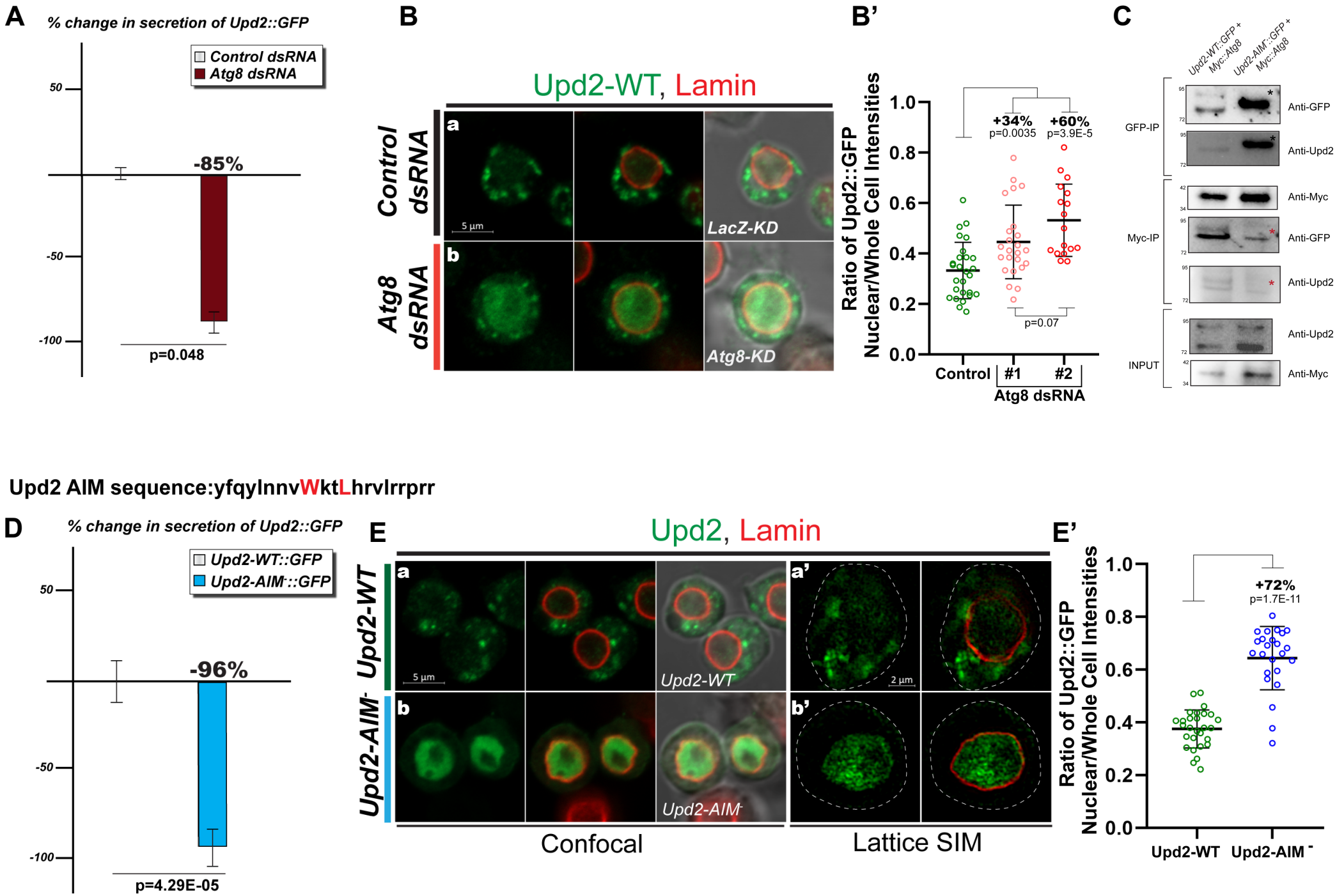
A
% change in secretion of Upd2::GFP
Control dsRNA
Atg8 dsRNA
50
-50
-100
-85%
p=0.048
B
Upd2-WT, Lamin
Control dsRNA
Atg8 dsRNA
a
b
5 µm
LacZ-KD
Atg8-KD
B'
Ratio of Upd2::GFP Nuclear/Whole Cell Intensities
1.0
0.8
0.6
0.4
0.2
0.0
+34%
p=0.0035
+60%
p=3.9E-5
p=0.07
Control
#1
#2
Atg8 dsRNA
C
Upd2-WT::GFP+ Myc::Atg8
Upd2-AIM-::GFP+ Myc::Atg8
GFP-IP
Myc-IP
INPUT
Anti-GFP
Anti-Upd2
Anti-Myc
Anti-GFP
Anti-Upd2
Anti-Upd2
Anti-Myc
Upd2 AIM sequence:yfqylnnvWktLhrvlrrprr
D
% change in secretion of Upd2::GFP
Upd2-WT::GFP
Upd2-AIM-::GFP
50
-50
-100
-96%
p=4.29E-05
E
Upd2, Lamin
Upd2-WT
Upd2-AIM-
a
a'
b
b'
5 µm
2 µm
Upd2-WT
Upd2-AIM-
Confocal
Lattice SIM
E'
Ratio of Upd2::GFP Nuclear/Whole Cell Intensities
1.0
0.8
0.6
0.4
0.2
0.0
+72%
p=1.7E-11
Upd2-WT
Upd2-AIM -

**Figure 2: Atg8 regulates nucleocytoplasmic localization of Upd2.**

**(A)** Effect of Atg8 knockdown on Upd2's release into media in fed cells. Normalized percent fold change in secreted GFP signal detected by GFP sandwich ELISA assay performed on conditioned media of S2R+ cells transiently transfected with *Upd2-WT::GFP* dsRNA for control (*LacZ*) or *Atg8* dsRNA. ELISA for *Upd2-WT::GFP* was performed after 5 days of knockdown, and the amount of Upd2-WT::GFP in a 24-hour period (Day 5) was assessed. Statistical significance is quantified by unpaired two-tailed t-test on 6 biological replicates per condition.

**(B)** Effect of Atg8 knockdown on Upd2's nuclear accumulation. Confocal micrographs of single optical-slices of *Drosophila* S2R+ cells transiently co-transfected with *Upd2-WT::GFP* (green) stained with Lamin (red). **(a)** In fed state, in cells co-transfected with *LacZ-dsRNA* (control) Upd2-WT::GFP is localized to cytosolic puncta and nuclear localization is not obvious. **(b)** In fed state, Atg8-KD (*Atg8 dsRNA*) significant increase in Upd2-WT::GFP nuclear accumulation is observed. Scale bar is 5um and right most panel shows DIC image merge. In **B'**, the ratio of Upd2::GFP nuclear/whole cell intensity is plotted. Each dot represents a cell, 20-40 cells were counted per dsRNA condition. Two independent *Atg8-dsRNAs* were used. Statistical significance is quantified by unpaired two-tailed t-test.

**(C)** Upd2-WT coimmunoprecipitates with Atg8 and this interaction relies on Upd2's AIM. GFP- and Myc-IPs were prepared from S2R+ cells transiently transfected with the indicated cDNAs. GFP, Myc IPs and 2% of the input were analyzed by immunoblotting for the indicated proteins. Note Upd2-AIM$^-$ always runs slightly higher than Upd2 (see asterisk) and is always more abundant in the lysate as the Upd2-AIM$^-$ is not secreted (see D below), but Upd2-AIM- it is not readily detectable in the Myc-IPs (see red asterisk), despite being more abundant in input. Atg8-Myc is always more abundant in Upd2-AIM- input than in Upd2 WT input, despite loading same amount of protein in input.

**(D)** Effect of point mutations to Upd2's AIM (*Upd2-AIM$^-$::GFP*) on its release into media in fed cells. Normalized percent fold change in secreted GFP signal detected by GFP sandwich ELISA assay performed on conditioned media of S2R+ cells transiently transfected with *Upd2-WT::GFP* or *Upd2-AIM$^-$::GFP*. Mutated residues in Upd2's AIM is shown in red. Statistical significance is quantified by unpaired two-tailed t-test on 6 biological replicates per condition.

**(E)** Effect of point mutations to Upd2's AIM (*Upd2-AIM$^-$::GFP*) on its nuclear accumulation. Confocal micrographs (**a, b**) and Lattice SIM images (**a', b'**) of single optical-slices of *Drosophila* S2R+ cells transiently co-transfected with (a, a') *Upd2-WT::GFP* or ( b, b') *Upd2-AIM$^-$::GFP* (green) stained with Lamin (red) in a fed state. Scale bars are 5um for a, b and 2um for a', b'; right most panel of a, b shows DIC image merge. In **E'**, the ratio of Upd2::GFP nuclear/whole cell intensity is plotted. Each dot represents a cell, 20-40 cells were counted per dsRNA condition. Statistical significance is quantified by unpaired two-tailed t-test.

# Figure 3

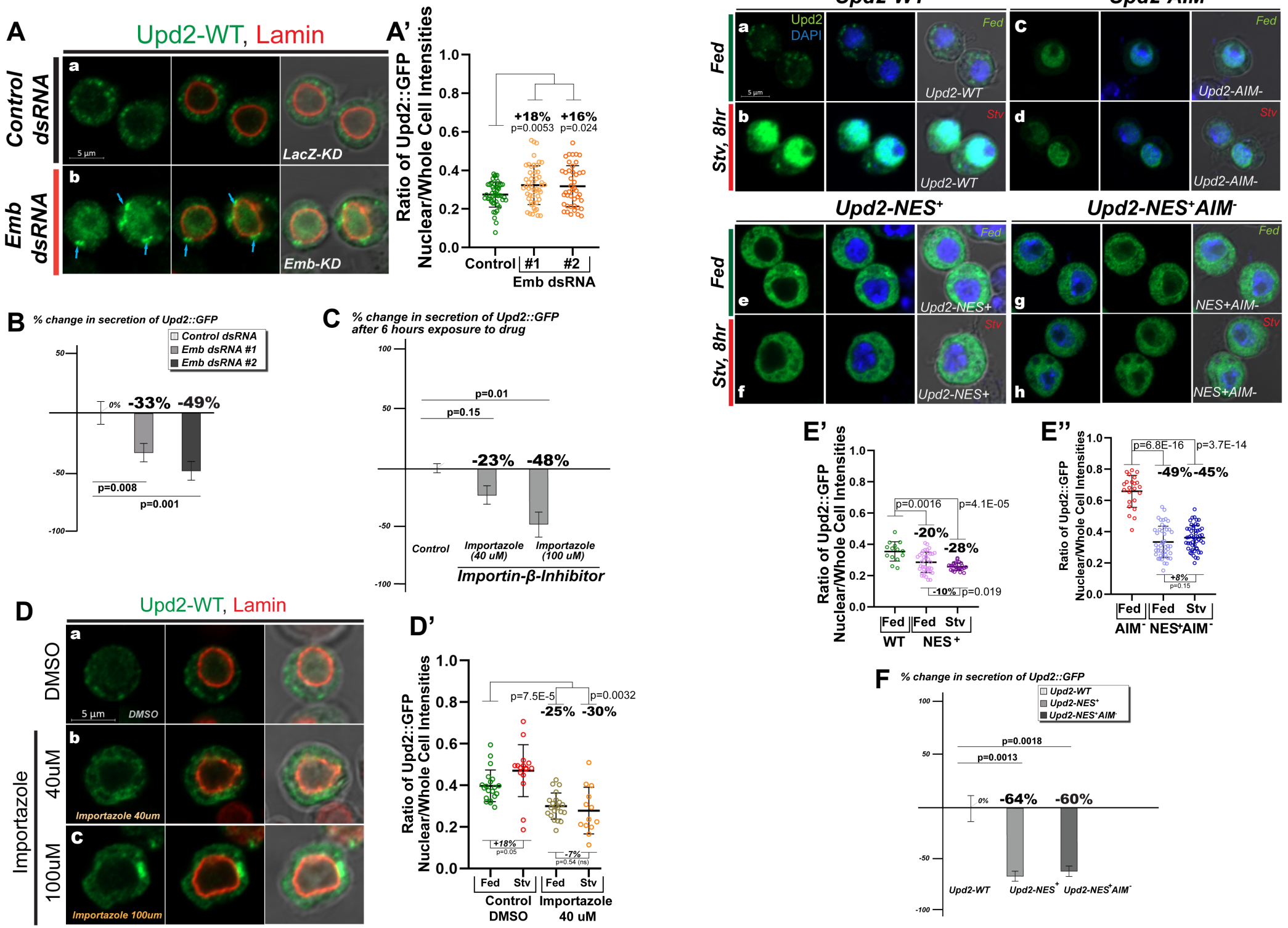
A
Upd2-WT, Lamin
Control dsRNA
Emb dsRNA
a
b
5 µm
LacZ-KD
Emb-KD
A'
Ratio of Upd2::GFP Nuclear/Whole Cell Intensities
+18%
p=0.0053
+16%
p=0.024
Control
#1
#2
Emb dsRNA
B
% change in secretion of Upd2::GFP
Control dsRNA
Emb dsRNA #1
Emb dsRNA #2
0%
-33%
-49%
p=0.008
p=0.001
C
% change in secretion of Upd2::GFP after 6 hours exposure to drug
p=0.01
p=0.15
-23%
-48%
Control
Importazole (40 uM)
Importazole (100 uM)
Importin-β-Inhibitor
D
Upd2-WT, Lamin
DMSO
Importazole
40uM
100uM
Importazole 40um
Importazole 100um
D'
p=7.5E-5
p=0.0032
-25%
-30%
+18%
p=0.05
-7%
p=0.54 (ns)
Fed
Stv
Control DMSO
Importazole 40 uM
E
Upd2-WT
Upd2-AIM-
Upd2-NES+
Upd2-NES+AIM-
Fed
Stv, 8hr
Upd2
DAPI
Upd2-AIM-
Upd2-NES+
NES+AIM-
E'
p=0.0016
p=4.1E-05
-20%
-28%
-10%
p=0.019
WT
NES+
E''
p=6.8E-16
p=3.7E-14
-49%
-45%
+8%
p=0.15
AIM-
NES+AIM-
F
% change in secretion of Upd2::GFP
Upd2-WT
Upd2-NES+
Upd2-NES+AIM-
p=0.0018
p=0.0013
0%
-64%
-60%

**Figure 3: Nucleocytoplasmic shuttling of Upd2 is required for its subsequent release.**

**(A, A')** Effect of Embargoed (Emb)/ CRM1 exportin knockdown on Upd2's nuclear accumulation. Confocal micrographs of single optical-slices of *Drosophila* S2R+ cells transiently co-transfected with *Upd2-WT::GFP* (green) stained with Lamin (red). In fed state, cells are co-transfected with **(a)** *LacZ-dsRNA* (control), or **(b)** Emb-KD (*Emb dsRNA*). *Emb-KD* increases Upd2-WT::GFP nuclear accumulation and shows an enrichment of Upd2-WT::GFP at the interface of nuclear lamina and cytoplasm (see blue arrows). Scale bar is 5um and right most panel shows DIC image merge. In **A'**, the ratio of Upd2::GFP nuclear/whole cell intensity is plotted. Each dot represents a cell, 50-80 cells were counted per dsRNA condition. Two independent *Emb-dsRNAs* (#1 and #2) were used. Statistical significance is quantified by unpaired two-tailed t-test.

**(B)** Effect of Embargoed (Emb) exportin knockdown on Upd2's release in fed cells. Normalized percent fold change in secreted GFP signal detected by GFP sandwich ELISA assay performed on conditioned media of S2R+ cells transiently transfected with *Upd2-WT::GFP* dsRNA for control (*LacZ*) or two independent *Emb* dsRNAs. ELISA for *Upd2-WT::GFP* was performed after 5 days of knockdown, and the amount of Upd2-WT::GFP in a 24-hour period (Day 5) was assessed. Statistical significance is quantified by unpaired two-tailed t-test on 6 biological replicates per condition.

**(C)** Effect of pharmacological inhibition of nuclear import on Upd2's release in fed cells. Quantification of relative normalized secreted GFP signal detected by GFP sandwich ELISA assay performed on conditioned media of S2R+ cells transfected with *Upd2-WT::GFP* and treated with drug Importazole, an Importin-beta inhibitor for 6 hours. Percent change in Upd2::GFP secretion relative to DMSO is depicted. Error bars represent %SD. Statistical significance quantified by t-test on 6 biological replicates per condition.

**(D)** Effect of pharmacological inhibition of nuclear import on Upd2's nuclear localization in fed cells. Confocal micrographs of single optical-slices of *Drosophila* S2R+ cells transiently transfected with *Upd2-WT::GFP* (green) stained with Lamin (red) and treated with DMSO **(a)** or indicated concentrations of importazole **(b, c)**. Scale bar is 5um and right most panel shows DIC image merge. In **D'**, the ratio of Upd2::GFP nuclear/whole cell intensity is plotted. Note that in starved state Upd2 nuclear accumulation does not significantly increase when treated with 40uM Importazole. Each dot represents a cell, 15-30 cells were counted per condition. Statistical significance is quantified by unpaired two-tailed t-test.

**(E)** Effect of nuclear export signal (NES) addition to Upd2-WT or -AIM$^-$ (*Upd2-NES$^+$::GFP or Upd2-NES$^+$AIM$^-$::GFP* ) on its nuclear accumulation. Confocal micrographs of single optical-slices of *Drosophila* S2R+ cells transiently co-transfected with *Upd2::GFP* variants (a, b) WT; (c, d) AIM$^-$; (e, f) NES$^+$; (g, h) NES$^+$AIM$^-$ Upd2::GFP (green) stained with DAPI (blue) in a fed state (a ,c, e, g) or AA-starved for 8 hours (b, d, f, h). Scale bars are 5um right most panel shows DIC image merge. In **E' and E''**, the ratio of Upd2::GFP

nuclear/whole cell intensity is plotted. Note that an NES$^{+}$ addition prevents Upd2 from accumulating in the nucleus even on starvation (E') and is epistatic to the AIM$^{-}$ mutation (E''). Each dot represents a cell, 15-80 cells were counted per condition. Statistical significance is quantified by unpaired two-tailed t-test.

**(F)** Effect of nuclear export signal (NES) addition to Upd2-WT or AIM$^{-}$ (*Upd2-NES$^{+}$::GFP or Upd2-NES$^{+}$AIM$^{-}$::GFP* ) on its release. Normalized percent fold change in secreted GFP signal detected by GFP sandwich ELISA assay performed on conditioned media of S2R+ cells transiently transfected with *Upd2::GFP* variants: WT; NES$^{+}$; NES$^{+}$AIM$^{-}$ the amount of Upd2-WT::GFP in a 24-hour period was assessed. Statistical significance is quantified by unpaired two-tailed t-test on 6 biological replicates per condition.

# Figure 4

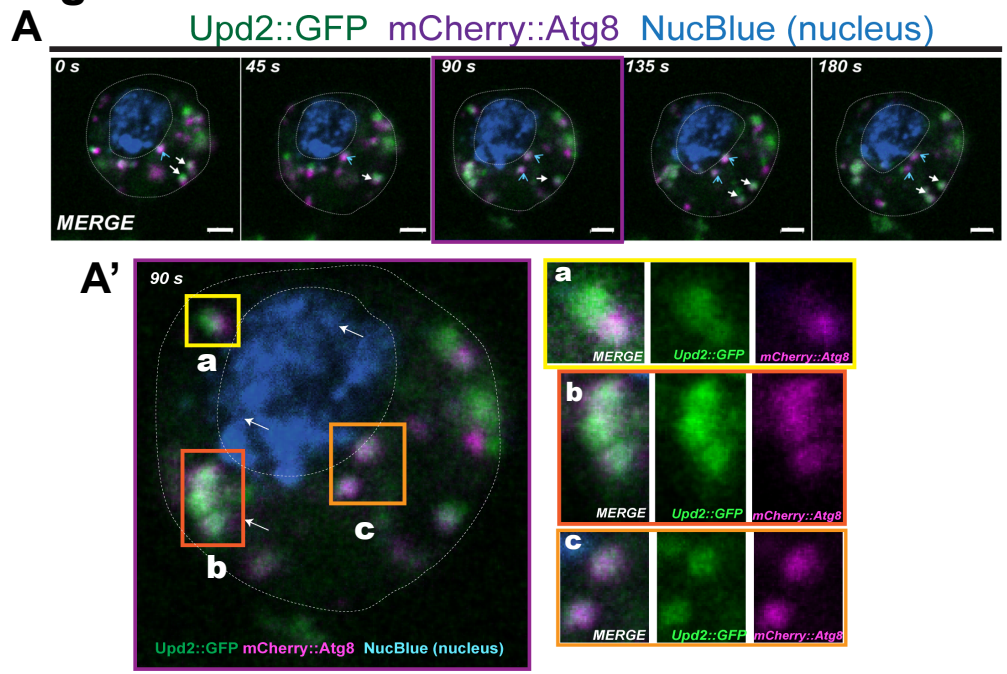
A
Upd2::GFP mCherry::Atg8 NucBlue (nucleus)
0 s
45 s
90 s
135 s
180 s
MERGE
A'
90 s
a
b
c
Upd2::GFP mCherry::Atg8 NucBlue (nucleus)
MERGE
Upd2::GFP
mCherry::Atg8

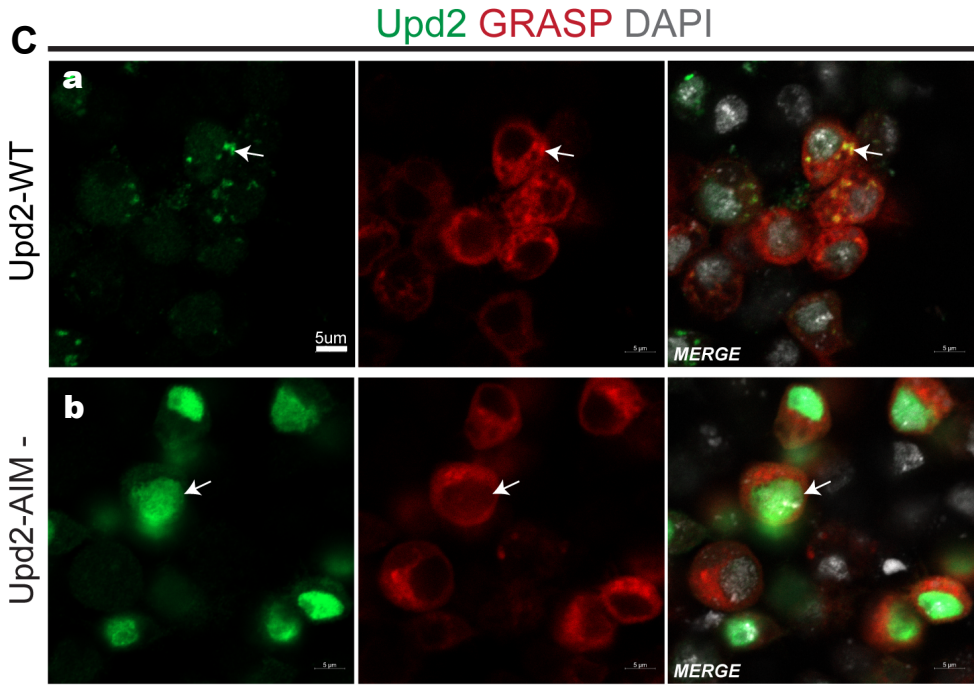
C
Upd2 GRASP DAPI
Upd2-WT
Upd2-AIM -
a
b
5um
MERGE

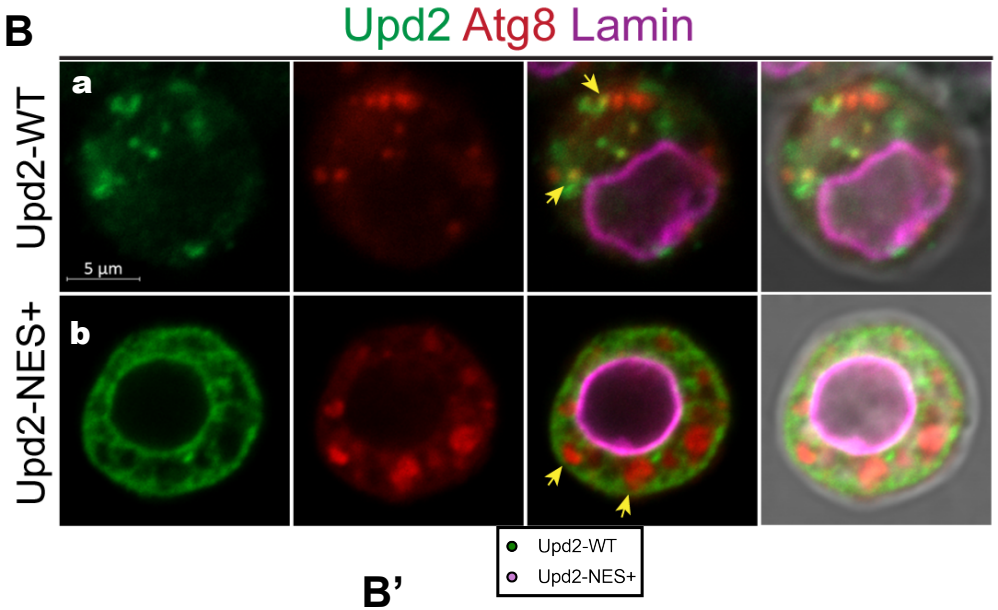
B
Upd2 Atg8 Lamin
Upd2-WT
Upd2-NES+
a
b
5 µm
Upd2-WT
Upd2-NES+

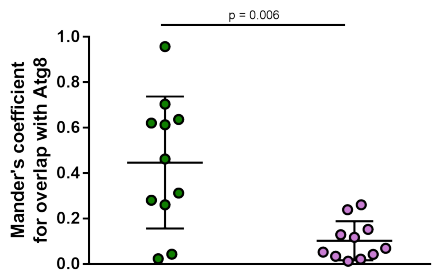
B'
p = 0.006
Mander's coefficient for overlap with Atg8
1.0
0.8
0.6
0.4
0.2
0.0

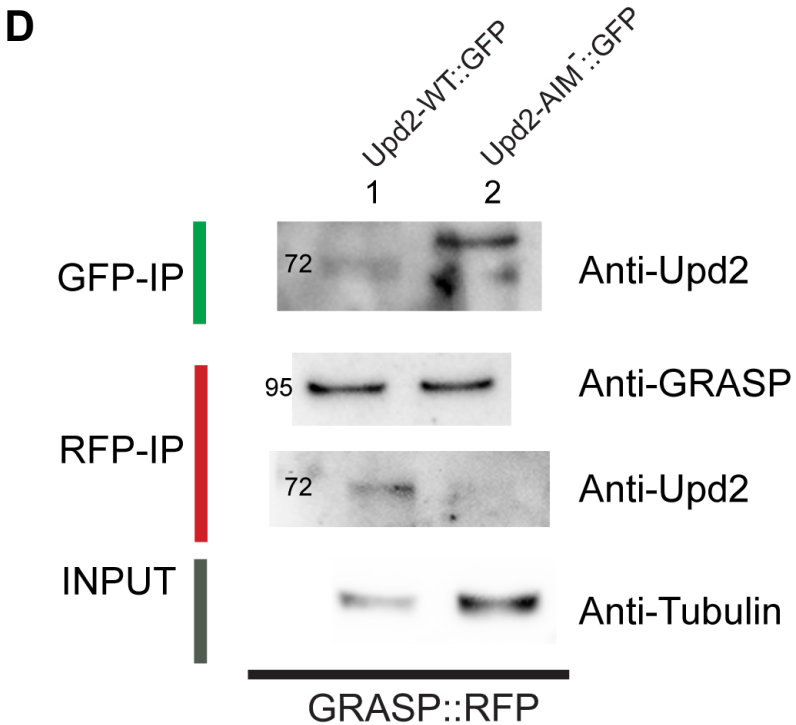
D
Upd2-WT::GFP
Upd2-AIM-::GFP
1
2
GFP-IP
RFP-IP
INPUT
72
95
72
Anti-Upd2
Anti-GRASP
Anti-Upd2
Anti-Tubulin
GRASP::RFP

**Figure 4: Upd2 nucleocytoplasmic shuttling licenses its release via Atg8-GRASP pathway.**

**(A)** Live dynamics of Upd2 and Atg8 in S2R+ cells. Confocal micrographs of live time lapse shots acquired every 45 seconds(s), of *Drosophila* S2R+ cells cultured in a fed state. Cells are transiently transfected with cDNAs for tagged Upd2::GFP (green) and mCherry::Atg8 (magenta); live cell dyes mark nucleus (NucBlue™ -dark blue). Atg8 and Upd2 exhibit discrete punctate localization. The Atg8 and Upd2 puncta show dynamics of both colocalization as well as association in: i) nuclear periphery (blue arrows), ii) cell periphery (white arrows). (**A'**) 90 second snapshot is enlarged for clarity, along with magnified insets. Inset **(a)** Upd2 and Atg8 shows association, not complete colocalization; **(b, c)** Upd2 and Atg8 show significant overlap. Cell outlines and nuclear outlines are marked for clarity and based on DIC images of the cells in Supplementary Figure S1. See also Movie S1. Scale bars, 2μM.

**(B)** Effect of nuclear export signal (NES) addition to Upd2-WT's colocalization with Atg8. Confocal micrographs of single optical-slices of fed *Drosophila* S2R+ cells transiently transfected with *Upd2-WT::GFP* (green), mCherry-Atg8-WT (red) stained with Lamin (magenta). In WT state, Upd2 shows partial co-localization with Atg8. Addition of NES alters Upd2's punctate distribution in the cytoplasm and its co-localization with Atg8 is significantly diminished as quantified in B' using the Mander's coefficient. Statistical significance is quantified by unpaired two-tailed t-test

**(C)** Effect of mutating Upd2's AIM on its colocalization with GRASP. Confocal micrographs of single optical-slices of *Drosophila* S2R+ cells transiently transfected with cDNAs expressing *Upd2-WT::GFP* or *Upd2-AIM$^-$::GFP* (green) and *GRASP::RFP* (red) stained with DAPI (white). In fed state, *Upd2-WT::GFP* is localized to cytosolic puncta enriched for GRASP (white arrows). When Upd2's AIM is mutated (*Upd2-AIM$^-$::GFP*) Upd2 is nuclear (white arrows), and the cytosolic puncta are not readily detectable. GRASP is exclusively cytosolic. Scale bars are 5μM.

**(D)** Effect of mutating Upd2's AIM on its interaction with GRASP. GFP- and RFP-IPs were prepared from S2R+ cells transiently co-transfected with GRASP-RFP and Upd2-WT::GFP or Upd2-AIM-::GFP. GFP, RFP IPs and 2% of the input were analyzed by immunoblotting for the indicated proteins. Note Upd2-AIM$^-$ always runs slightly higher than Upd2 and is always more abundant in the lysate as the Upd2-AIM$^-$ is not secreted, but it is not readily detectable in the RFP-IPs, despite loading more input.

# Figure 5

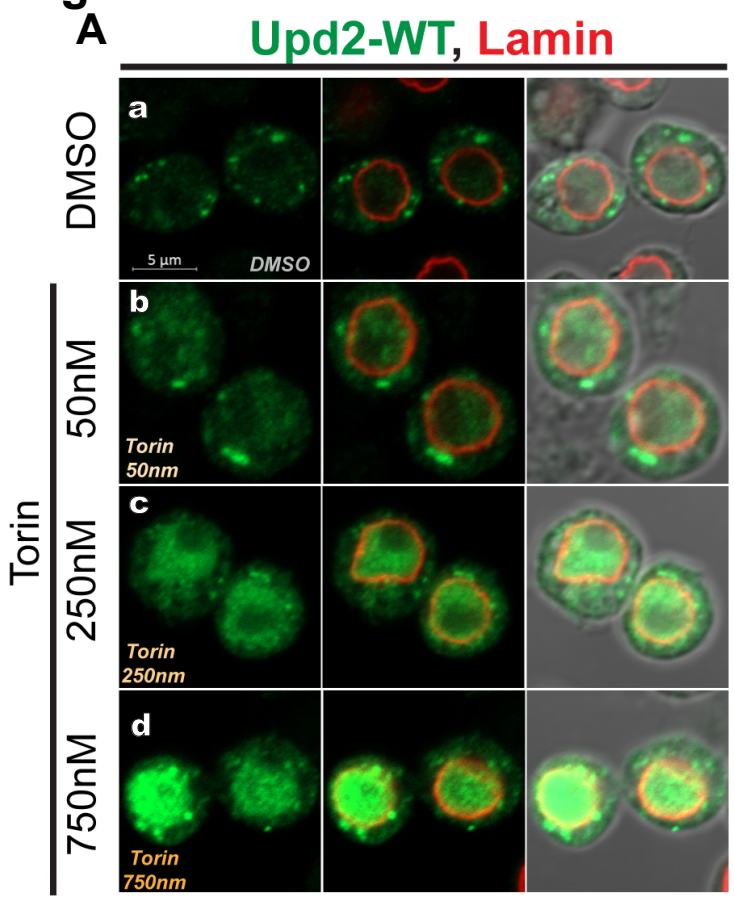
A
Upd2-WT, Lamin
DMSO
Torin
50nM
250nM
750nM
a
b
c
d
5 µm
DMSO
Torin 50nm
Torin 250nm
Torin 750nm

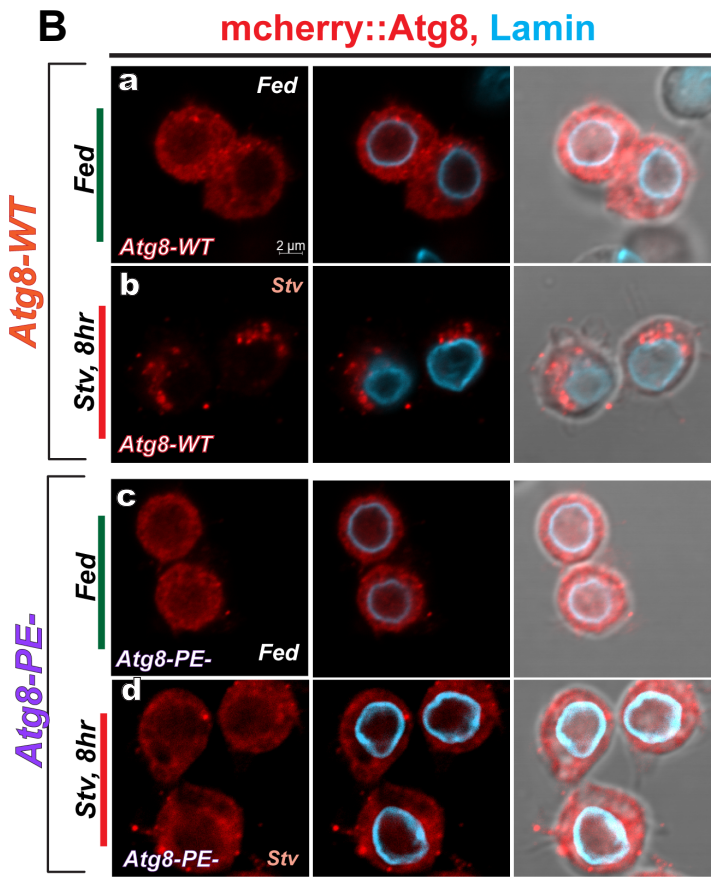
B
mcherry::Atg8, Lamin
Atg8-WT
Atg8-PE-
Fed
Stv, 8hr
a
b
c
d
Fed
Stv
Atg8-WT
Atg8-PE-
2 µm

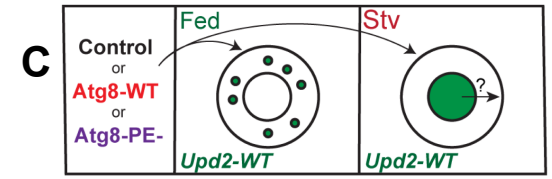
C
Control
or
Atg8-WT
or
Atg8-PE-
Fed
Stv
Upd2-WT
Upd2-WT
?

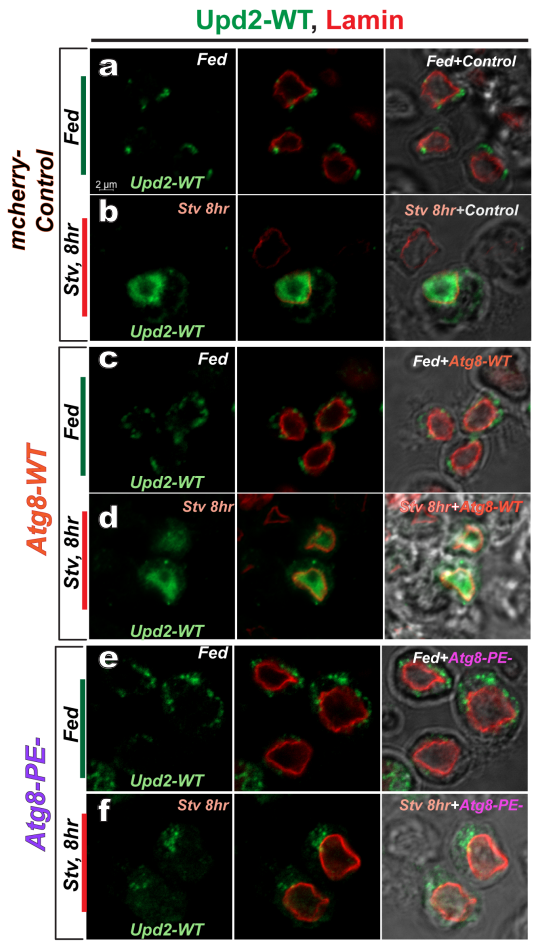
Upd2-WT, Lamin
mcherry-Control
Atg8-WT
Atg8-PE-
Fed
Stv, 8hr
a
b
c
d
e
f
Fed
Stv 8hr
Fed+Control
Stv 8hr+Control
Fed+Atg8-WT
Stv 8hr+Atg8-WT
Fed+Atg8-PE-
Stv 8hr+Atg8-PE-
Upd2-WT
2 µm

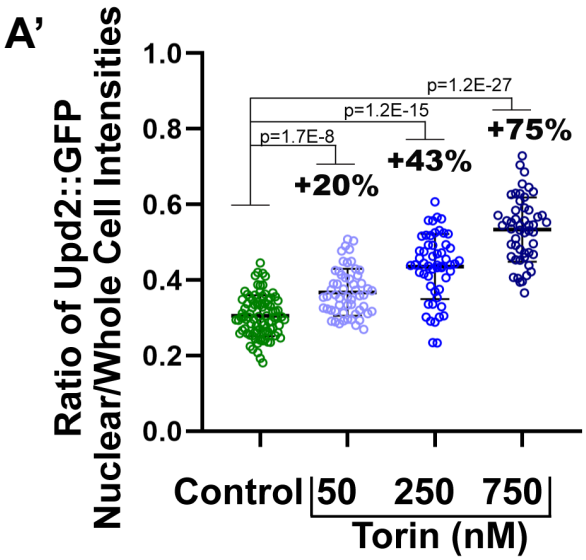
A'
Ratio of Upd2::GFP Nuclear/Whole Cell Intensities
1.0
0.8
0.6
0.4
0.2
0.0
p=1.2E-27
p=1.2E-15
p=1.7E-8
+20%
+43%
+75%
Control
50
250
750
Torin (nM)

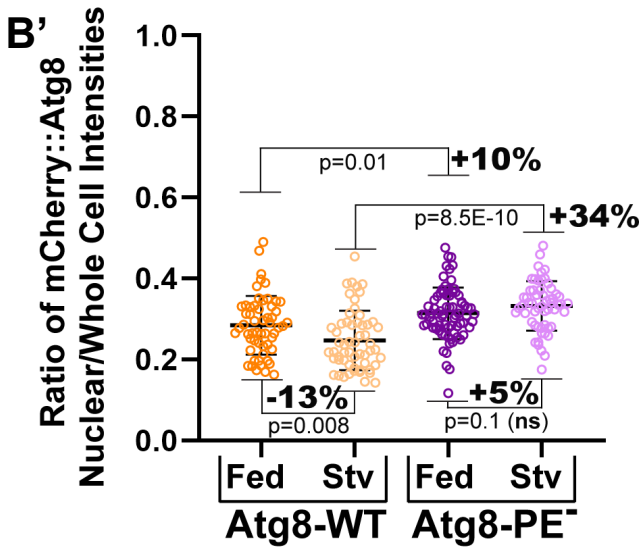
B'
Ratio of mCherry::Atg8 Nuclear/Whole Cell Intensities
1.0
0.8
0.6
0.4
0.2
0.0
p=0.01
+10%
p=8.5E-10
+34%
-13%
p=0.008
+5%
p=0.1 (ns)
Fed
Stv
Fed
Stv
Atg8-WT
Atg8-PE-

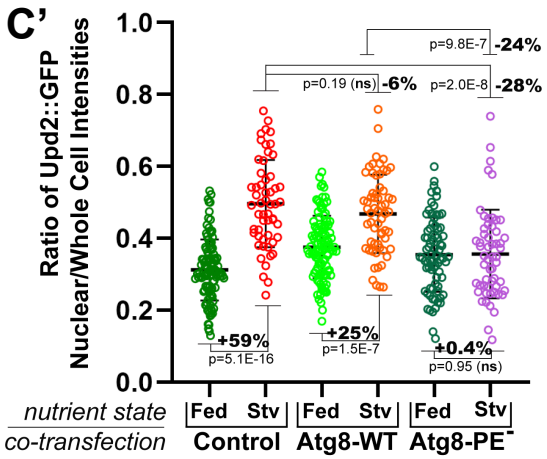
C'
Ratio of Upd2::GFP Nuclear/Whole Cell Intensities
1.0
0.8
0.6
0.4
0.2
0.0
p=9.8E-7
-24%
p=0.19 (ns)
-6%
p=2.0E-8
-28%
+59%
p=5.1E-16
+25%
p=1.5E-7
+0.4%
p=0.95 (ns)
nutrient state
co-transfection
Fed
Stv
Fed
Stv
Fed
Stv
Control
Atg8-WT
Atg8-PE-

**Figure 5: Atg8 lipidation induces Upd2 nuclear accumulation.**

**(A)** Effect of pharmacological autophagy activation on Upd2 nuclear accumulation. Confocal micrographs of single optical-slices of *Drosophila* S2R+ cells transiently transfected with *Upd2-WT::GFP* (green) stained with Lamin (red) and treated with DMSO **(a)** or indicated concentrations of autophagy activator Torin1 **(b, c, d)**. Scale bar is 5um and right most panel shows DIC image merge. In B**'**, the ratio of Upd2::GFP nuclear/whole cell intensity is plotted. Each dot represents a cell, 50-100 cells were counted per condition. Statistical significance is quantified by unpaired two-tailed t-test.

**(B)** Effect of starvation induced changes in the nuclear pool of mCherry-tagged Atg8 wild-type (*Atg8-WT*) versus lipidation-defective Atg8 (*Atg8-PE-*). Confocal micrographs of single optical-slices of *Drosophila* S2R+ cells transiently transfected with (**a, b**) *mCherry::Atg8-WT* (red) or (**c, d**) *mCherry::Atg8-PE-* (red) stained with Lamin (blue) in either well-fed state (a, c) or AA-starved (b, d). Scale bar is 2um and right most panel shows DIC image merge. In **C'**, the ratio of mCherry::Atg8 nuclear/whole cell intensity is plotted. While Atg8-WT pool in the nucleus is reduced on starvation, lipidation-defective pool of Atg8 is similar between fed and starved states. Each dot represents a cell, 50-80 cells were counted per condition. Statistical significance is quantified by unpaired two-tailed t-test.

**(C)** Effect of providing exogenous mCherry-tagged Atg8 wild-type (*Atg8-WT*) versus lipidation-defective Atg8 (*Atg8-PE-*) on Upd2 nuclear localization during starvation: Schematic, in the top panel, shows experimental design; an assay for the effect of increasing the dose of lipidation-defective Atg8 on Upd2 nuclear accumulation. Below, confocal micrographs of representative single optical-slices of *Drosophila* S2R+ cells transiently co-transfected with *Upd2-WT::GFP* and (**a, b**) *mCherry* or (**c, d**) *mCherry::Atg8-WT* or (**e, f**) *mCherry::Atg8-PE-* stained with GFP (green) and Lamin (red) in either well-fed state (a, c, e) or AA-starved (b, d, f). Scale bar is 2um and right most panel shows DIC image merge. In **D'**, the ratio of Upd2::GFP nuclear/whole cell intensity is plotted. While Atg8-WT and control show that Upd2 nuclear accumulation increases on starvation, cells co-transfected with lipidation-defective Atg8-PE-, do not show Upd2 nuclear accumulation increase on starvation. Each dot represents a cell, 80-130 cells were counted per condition. Statistical significance is quantified by unpaired two-tailed t-test.

Also see companion Figure S2, that assays Upd2's ability to immunoprecipitate with lipidation-defective Atg8-PE-.

# Figure 6

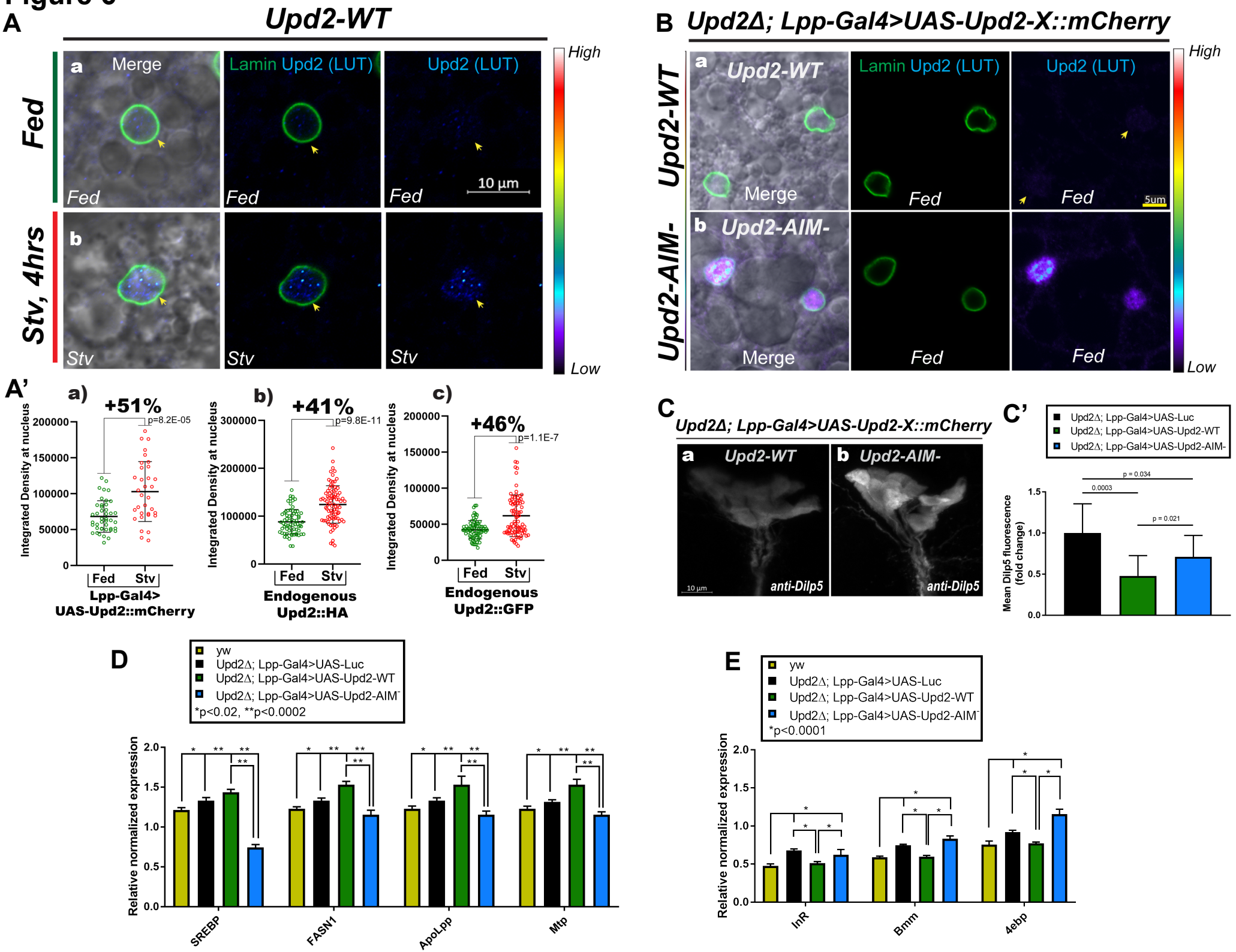
A
Upd2-WT
Fed
Stv, 4hrs
a Merge
Lamin Upd2 (LUT)
Upd2 (LUT)
Fed
Stv
10 µm
High
Low
B Upd2Δ; Lpp-Gal4>UAS-Upd2-X::mCherry
Upd2-WT
Upd2-AIM-
a Upd2-WT
b Upd2-AIM-
Merge
Fed
5um
A'
a)
+51%
p=8.2E-05
Integrated Density at nucleus
Fed
Stv
Lpp-Gal4>
UAS-Upd2::mCherry
b)
+41%
p=9.8E-11
Endogenous
Upd2::HA
c)
+46%
p=1.1E-7
Endogenous
Upd2::GFP
C
Upd2Δ; Lpp-Gal4>UAS-Upd2-X::mCherry
anti-Dilp5
10 µm
C'
Upd2Δ; Lpp-Gal4>UAS-Luc
Upd2Δ; Lpp-Gal4>UAS-Upd2-WT
Upd2Δ; Lpp-Gal4>UAS-Upd2-AIM-
p = 0.034
0.0003
p = 0.021
Mean Dilp5 fluorescence
(fold change)
D
yw
Upd2Δ; Lpp-Gal4>UAS-Luc
Upd2Δ; Lpp-Gal4>UAS-Upd2-WT
Upd2Δ; Lpp-Gal4>UAS-Upd2-AIM-
*p<0.02, **p<0.0002
Relative normalized expression
SREBP
FASN1
ApoLpp
Mtp
E
yw
Upd2Δ; Lpp-Gal4>UAS-Luc
Upd2Δ; Lpp-Gal4>UAS-Upd2-WT
Upd2Δ; Lpp-Gal4>UAS-Upd2-AIM-
*p<0.0001
Relative normalized expression
InR
Bmm
4ebp

**Figure 6: On fasting Upd2 accumulates in fly fat and Upd2-AIM- systemically signals a state of chronic starvation.**

**(A)** Effect of starvation on Upd2 nuclear accumulation in adult fly fat tissue: Confocal micrographs of fixed and immunostained adult fly fat from flies CRISPR engineered (see methods) with HA and GFP tag in the endogenous Upd2 locus (that rescues the upd2Δ mutant- see Figure S3). Fat is stained with RFP antibody (in a, b) in well-fed flies, or flies starved on agarose for 4 hours. Upd2-WT in fed state is detectable in very low levels in the nucleus (see look up table (LUT)) and yellow arrows in a. Upd2 shows increased nuclear accumulation on starvation. Scale bar is 10um and left post panel shows merges DIC image. (A') Upd2 nuclear accumulation is quantified three different Upd2 tagged genotypes: (a) mCherry tagged Upd2 (*UAS-X*) under the control of a fat-cell specific promoter (*Lpp-Gal4*); (b) Upd2-HA endogenous tag and ; (c) Upd2-GFP endogenous tag. Each dot represents a fat cell nucleus, 30-100 fat nuclei were counted per condition per genotype. Statistical significance is quantified by unpaired two-tailed t-test.

**(B)** Effect of point mutations to Upd2's AIM (*Upd2-AIM*$^{-}$) on its nuclear accumulation in adult fly fat: Confocal micrographs of single optical sections of fixed and immunostained adult fly fat from transgenic flies expressing mCherry tagged Upd2-cDNAs for (a) Upd2-WT (*UAS-Upd2-WT*) or (b) Upd2's AIM mutated (*UAS-Upd2-AIM*$^{-}$) under the control of a fat-cell specific promoter (*Lpp-Gal4*) in a *upd2-deletion* background (*upd2Δ; Lpp-Gal4*). In Upd2-WT in fed state is detectable in very low levels in the nucleus (see look up table (LUT)) and yellow arrows in a. Upd2-AIM- shows significantly nuclear accumulation even in a fed state.

**(C)** Effect of point mutations to Upd2's AIM (*Upd2-AIM*$^{-}$) on its ability to rescue the insulin accumulation defect in the IPCs of Upd2 deletion mutants (Insulin producing cells): Confocal micrographs of fixed and immunostained adult brain of well-fed transgenic flies expressing mCherry tagged Upd2-cDNAs for (a) Upd2-WT (*UAS-Upd2-WT*) or (b) Upd2's AIM mutated (*UAS-Upd2-AIM*$^{-}$) under the control of a fat-cell specific promoter (*Lpp-Gal4*) in a *upd2-deletion* background (*upd2Δ; Lpp-Gal4*). Scale bar is 10um. While *Upd2-WT* transgene rescue insulin accumulation defect of *upd2Δ*, the *Upd2-AIM*$^{-}$ as quantified in C'. Statistical significance is quantified by unpaired two-tailed t-test and 11-12 brains were used per genotype. Also see companion supplementary figure S4.

(**D, E**) Effect of point mutations to Upd2's AIM (*Upd2-AIM*$^{-}$) on gene expression profiles relevant for fat storage and starvation response: Relative normalized expression, of steady-state mRNA levels, assayed by qPCR on adult fat tissue (see methods) from *Upd2Δ* mutants in which either Upd2-WT or Upd2-AIM- was over-expressed in fat. *yw and updΔ* flies with control transgene serves as baseline (*Upd2Δ; Lpp-Gal4>UAS-Luc*). **In D**, expression of genes involved in either de-novo lipid synthesis or LPP production are examined. **In E**, expression of FOXO target genes- *InR*, *brummer* (*Bmm*), and *4ebp/Thor*- provide a readout of Insulin signaling. One-way ANOVA followed by Turkey's multiple comparisons test. Error bars represent standard error of the mean (SEM). N = 3 replicates per primer pair. See companion Figure S5.

# Figure 7

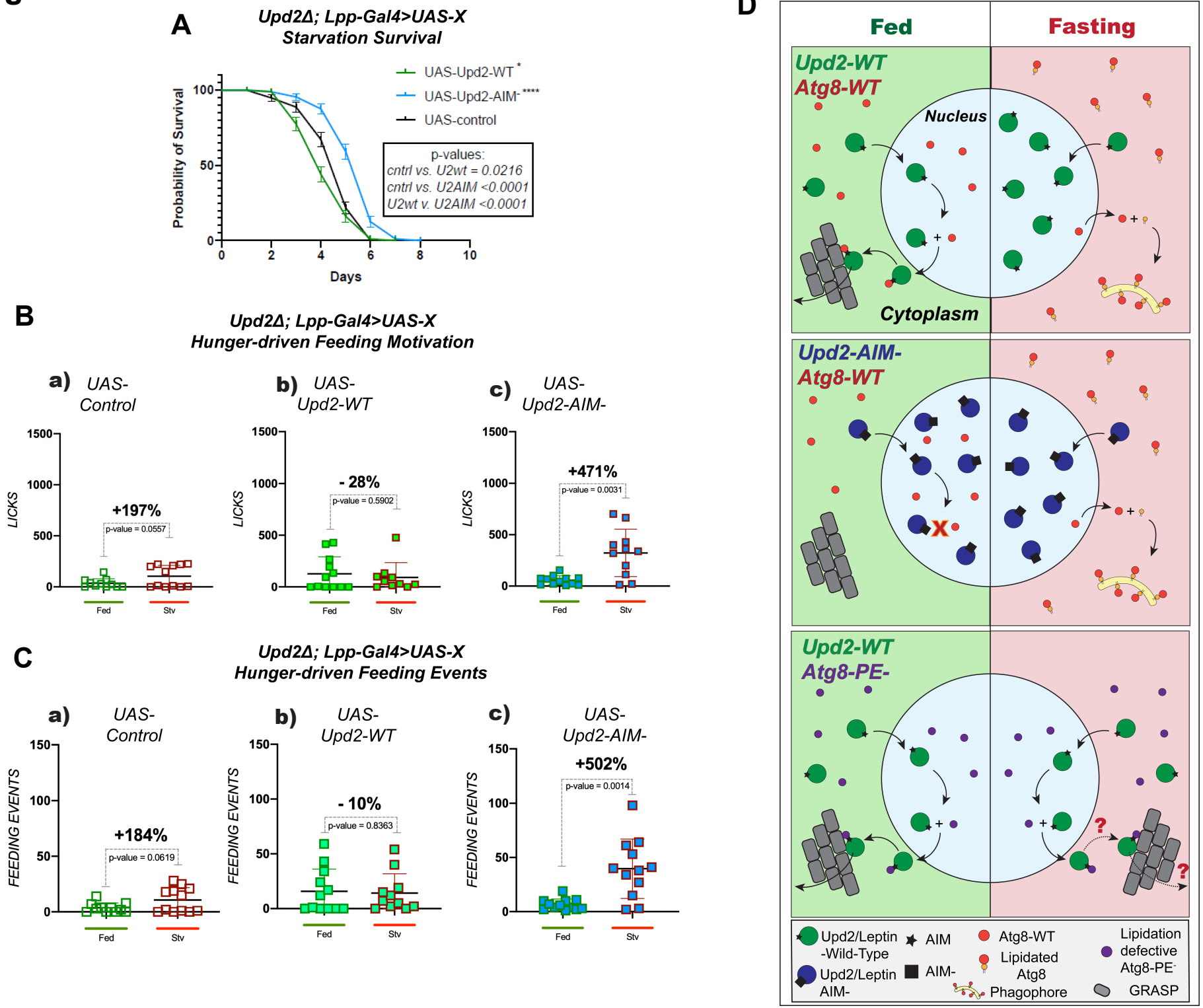
A
Upd2Δ; Lpp-Gal4>UAS-X
Starvation Survival
UAS-Upd2-WT *
UAS-Upd2-AIM- ****
UAS-control
p-values:
cntrl vs. U2wt = 0.0216
cntrl vs. U2AIM <0.0001
U2wt v. U2AIM <0.0001
Probability of Survival
Days
B
Upd2Δ; Lpp-Gal4>UAS-X
Hunger-driven Feeding Motivation
a) UAS-Control
b) UAS-Upd2-WT
c) UAS-Upd2-AIM-
LICKS
+197%
p-value = 0.0557
- 28%
p-value = 0.5902
+471%
p-value = 0.0031
Fed
Stv
C
Upd2Δ; Lpp-Gal4>UAS-X
Hunger-driven Feeding Events
FEEDING EVENTS
+184%
p-value = 0.0619
- 10%
p-value = 0.8363
+502%
p-value = 0.0014
D
Fed
Fasting
Upd2-WT
Atg8-WT
Nucleus
Cytoplasm
Upd2-AIM-
Atg8-WT
Upd2-WT
Atg8-PE-
Upd2/Leptin -Wild-Type
Upd2/Leptin AIM-
AIM
AIM-
Atg8-WT
Lipidated Atg8
Phagophore
Lipidation defective Atg8-PE-
GRASP

**Figure 7: Atg8-controlled Upd2 retention in nucleus is a mechanism to resist starvation and increase post-fasting hunger response.**

**(A)** Effect of fat-specific expression of Upd2-AIM- on starvation survival: Flies expressing cDNAs (*UAS-X*) for *Upd2-WT*, *Upd2-AIM*$^{-}$ and control (*UAS-Luciferase)* specifically in fly fat (*Upd2Δ; Lpp-Gal4>UAS-X*). Transgenic flies with fat-specific overexpression of *Upd2-AIM*$^{-}$ are starvation-resistant, whereas overexpression of normal Upd2 (*Upd2-WT*) results in starvation-sensitivity with a median life span of 4 days compared to 6 days *for Upd2-AIM-* that lives significantly longer than the control as assessed by the Log-rank (Mantel-Cox) test. See companion supplementary figure S6A.

**(B, C)** Effect of fat-specific expression of Upd2-AIM- on post-fasting hunger driven feeding: Quantification of feeding behavior in transgenic flies, expressing indicated cDNAs (*UAS-X*) specifically in fat-tissue (*Upd2Δ; Lpp-Gal4>UAS-X*), measured using the Fly Liquid Interaction Counter (FLIC-see methods). Each dot represents a fly. 10-12 flies were used per experiment per genotype. The flies were starved for 16 hours prior to testing. The difference between fed and starved flies of the same genotype were assayed as licks i.e., interactions with food, which is a measure of feeding motivation (B) and feeding events (C). Error bars represent percent standard deviation and statistical significance was calculated using 2-tailed unpaired t-test. See companion supplementary figure S6 B, C.

**(D)** Working model: Atg8 mediates adipokine nuclear exit and its subsequent release: In a fed state, the ortholog of human Leptin in flies, Upd2, enters the nucleus; via its Atg8-interaction motif (AIM) Upd2 complexes with Atg8. Atg8 then enables Upd2 nuclear exit via an Exportin/CRM1 based mechanism. Atg8 subsequently targets Upd2 to the GRASP secretory pathway. On fasting, Atg8 lipidation and recruitment to autophagy decreases the Atg8 nuclear pool. In turn, this increases Upd2 nuclear accumulation and causes cells to retain the adipokine on fasting. When Upd2's interaction with Atg8 is disrupted (AIM-), Upd2 localizes to the nucleus even in a fed state and is not secreted. In flies, constitutive expression of Upd2-AIM- in fat cells, results in a chronic starvation phenotype. Upd2-AIM- flies are starvation resistant and exhibit higher hunger-driven feeding motivation. Altogether, this suggests that fasting-induced Upd2 accumulation facilitates organismal adaptation to nutrient deprivation and drives post-fasting hunger response. When cells are dosed with lipidation-defective nuclear Atg8, Upd2 export from the nucleus occurs even on fasting. Future studies, indicated by question marks, are required to evaluate whether Upd2 which is exported from the nucleus by lipidation-defective Atg8 can be targeted to the appropriate secretory compartment. If indeed Upd2 can be subsequently released via a lipidation-defective route, then ensuing investigations should explore whether such a lipidation-defective Atg8 mediated secretion allows Upd2 to reach its appropriate neuronal target.

# Figure S1

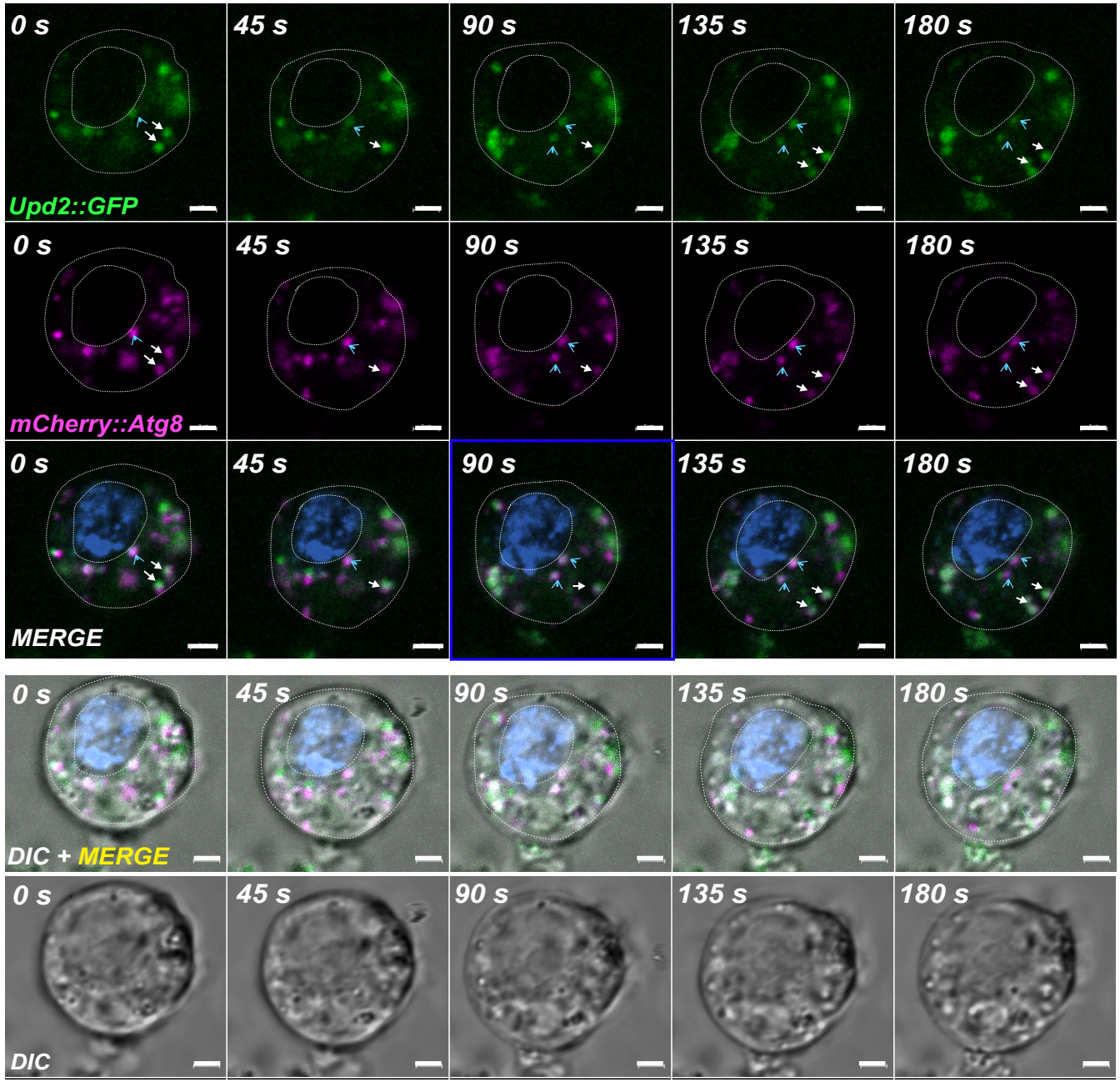
Drosophila S2R+ cells- Complete Medium
Upd2::GFP mCherry::Atg8 NucBlue (nucleus)
0 s
45 s
90 s
135 s
180 s
Upd2::GFP
mCherry::Atg8
MERGE
DIC + MERGE
DIC

**Supplementary: Figure S1** ***(companion to Figure 4A)***
**See also Movie S1.**

Confocal micrographs of time-lapse shots, acquired every 45 seconds(s), of *Drosophila* S2R+ cells cultured in complete media and transiently transfected with cDNAs for tagged Upd2::GFP (green) and mCherry::Atg8 (magenta); live cell dyes mark nucleus (NucBlue™ -dark blue). Atg8 and Upd2 exhibit discrete punctate localization. The Atg8 and Upd2 puncta show dynamics of both colocalization as well as association in: i) nuclear periphery (blue arrows), ii) cell periphery (white arrows). Cell outlines and nuclear outlines are marked for clarity and based on DIC images of the cells. Also see Movie S1. Scale bars, 2μM.

# Figure S2

## A

a) Atg8-Trojan-Gal4 / FM7a ;; + / + ♀ X w1118 / Y ;; UAS-Atg8-WT / UAS-Atg8-WT *or* UAS-Atg8-PE⁻ / UAS-Atg8-PE⁻ ♂

b)

| X chromosome genotype | Transgene on chromosome III | | | |
|---|---|---|---|---|
| | UAS-Atg8-WT | | UAS-Atg8-PE⁻ | |
| | # males | % males | # males | % males |
| Atg8-Trojan-Gal4 | 36 | 46.8 | 0 | 0 |
| FM7a | 41 | 53.2 | 36 | 100 |

c)

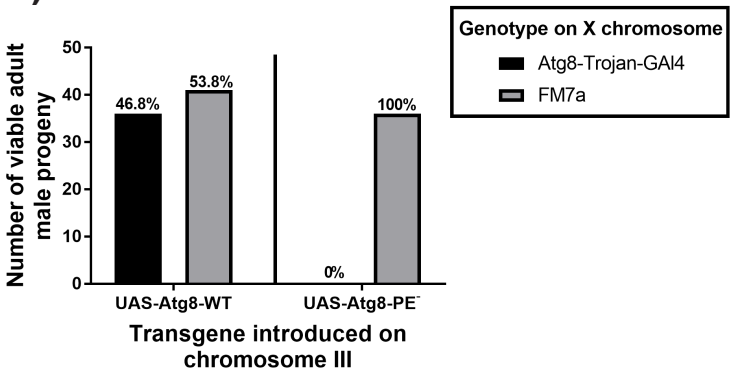


## B

***Fat depots from adult flies starved for 4-6 hours***

**GFP-tagged Atg8 transgene, anti-Atg8 (antibody), Lamin**

***Lpp-Gal4> UAS-GFP::Atg8-WT***

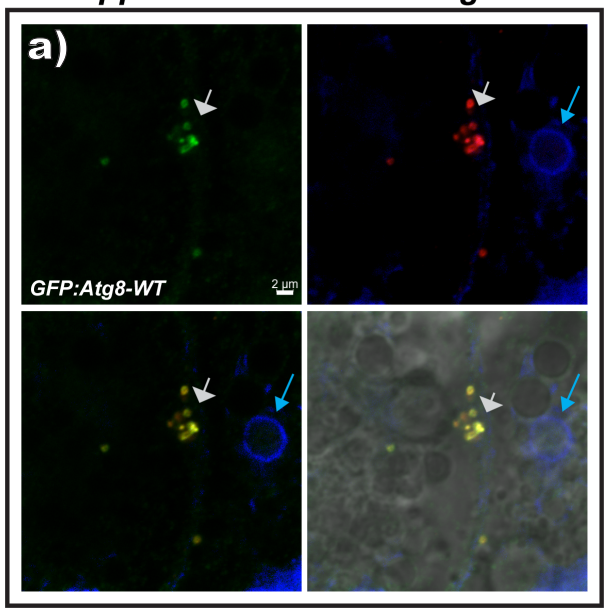


***Lpp-Gal4> UAS-GFP::Atg8-PE-***

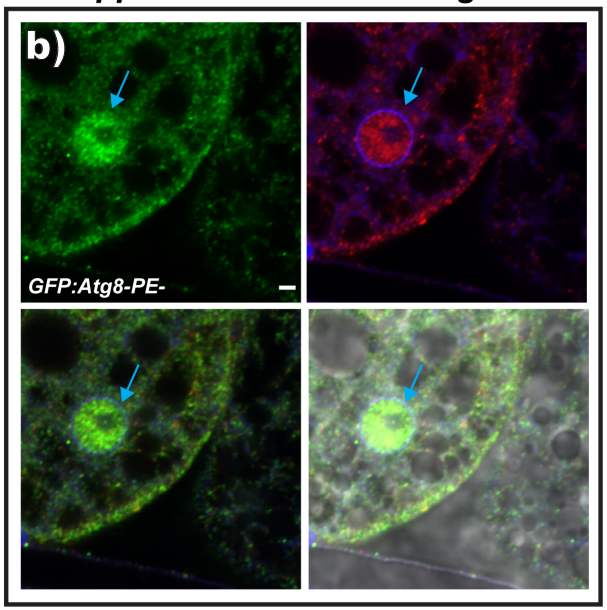


## C

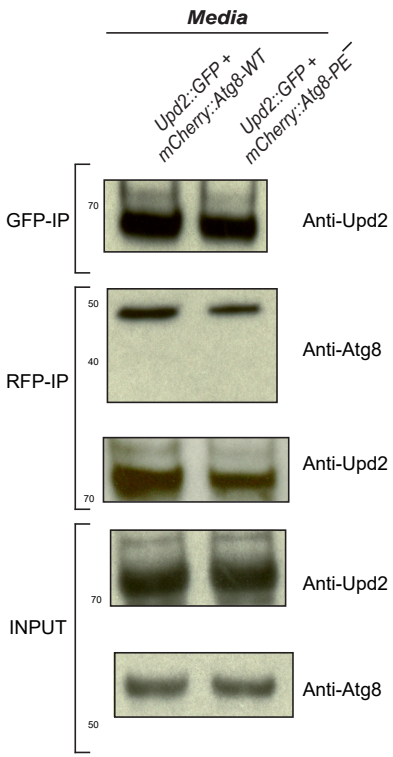

**Supplementary: Figure S2** ***(companion to Figure 5)***

**A)** Rescue of an Atg8 knock out allele- *Atg8-Trojan-Gal4* (see methods), which is lethal. **a)** The crossing scheme depicting the *Atg8-Trojan-Gal4* allele rescue with wild-type Atg8 transgene (*UAS-GFP::Atg8-WT*) or the lipidation-defective Atg8 transgene (*UAS-GFP::Atg8-PE-*). b,c) Outcome of cross to rescue lethality. In b) table shows the number of progenies counted from the cross and the % of transgenic rescue. C) graph of the %progeny of each genotype. While the expected percentage of flies with UAS-GFP-Atg8-WT, as expected the UAS-Atg8-PE- (lipidation-defective version) does not rescue the Atg8 knockout allele.

**B)** Confocal micrographs of single optical sections of fixed and immunostained [anti-GFP(green); anti-Atg8 (red); anti-Lamin (blue)] adult fly fat from transgenic flies- starved for 4 hours- expressing GFP-tagged Atg8-cDNAs for (a) Atg8-WT (*UAS-GFP::Atg8-WT*) or (b) lipidation-defective Atg8 (*UAS-GFP::Atg8-PE*$^{-}$) under the control of a fat-cell specific promoter (*Lpp-Gal4*) in an *Atg8-WT* background. Within 4 hours of starvation in adult fly fat: (a) GFP::Atg8-WT (green) is localized to punctate structures (white arrows) in the cytoplasm, that also co-stain with an Atg8 antibody. GFP::Atg8-WT is barely detectable in the nucleus (blue arrows). (b) In starved fat, lipidation-defective Atg8 continues to be enriched in the nucleus (blue arrows), it is present in the cytoplasm but in a diffuse pattern as opposed to being localized to distinct punctae.

**C)** Upd2 coimmunoprecipitates with Atg8-WT and lipidation-defective Atg8 (Atg8-PE$^{-}$) in the extracellular media fractions. GFP and mCherry immunoprecipitates (IPs) were prepared from cell lysates and conditioned media of *Drosophila* S2R+ cells transiently transfected with the indicated cDNAs. GFP-, mCherry- IPs and 2% of the input were analyzed by immunoblotting for the indicated proteins.

# Figure S3

## Rescue of Upd2-Deletion by Endogenous Upd2 tag knock-in

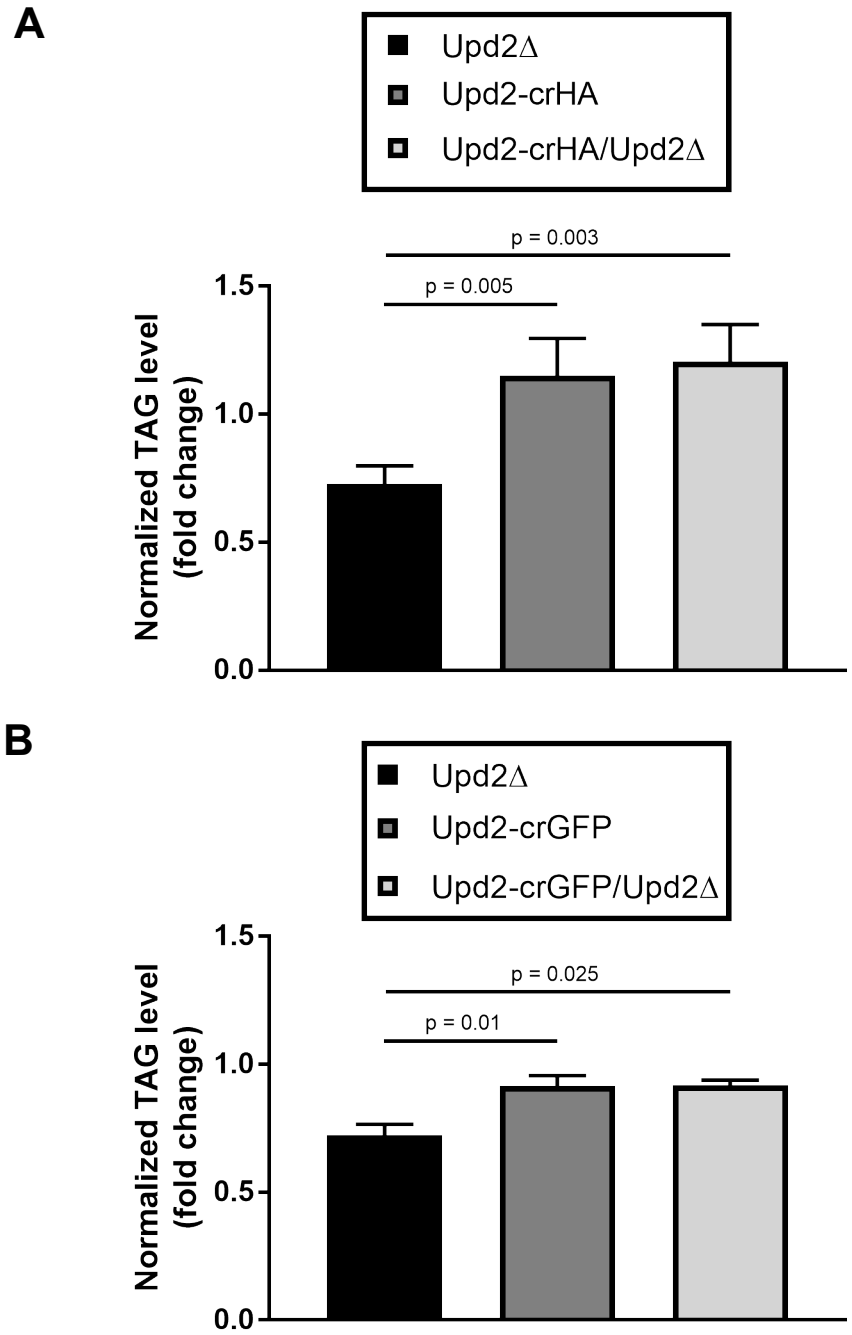

**Supplementary: Figure S3** ***(companion to Figure 6A)***

Rescue of *Upd2Δ* triglyceride (TAG) storage reduction phenotype by endogenous CRISPR tag knock-in of HA [*Upd2-crHA*] (A) and GFP [*Upd2-crGFP*] (B) in the Upd2 locus.

# Figure S4

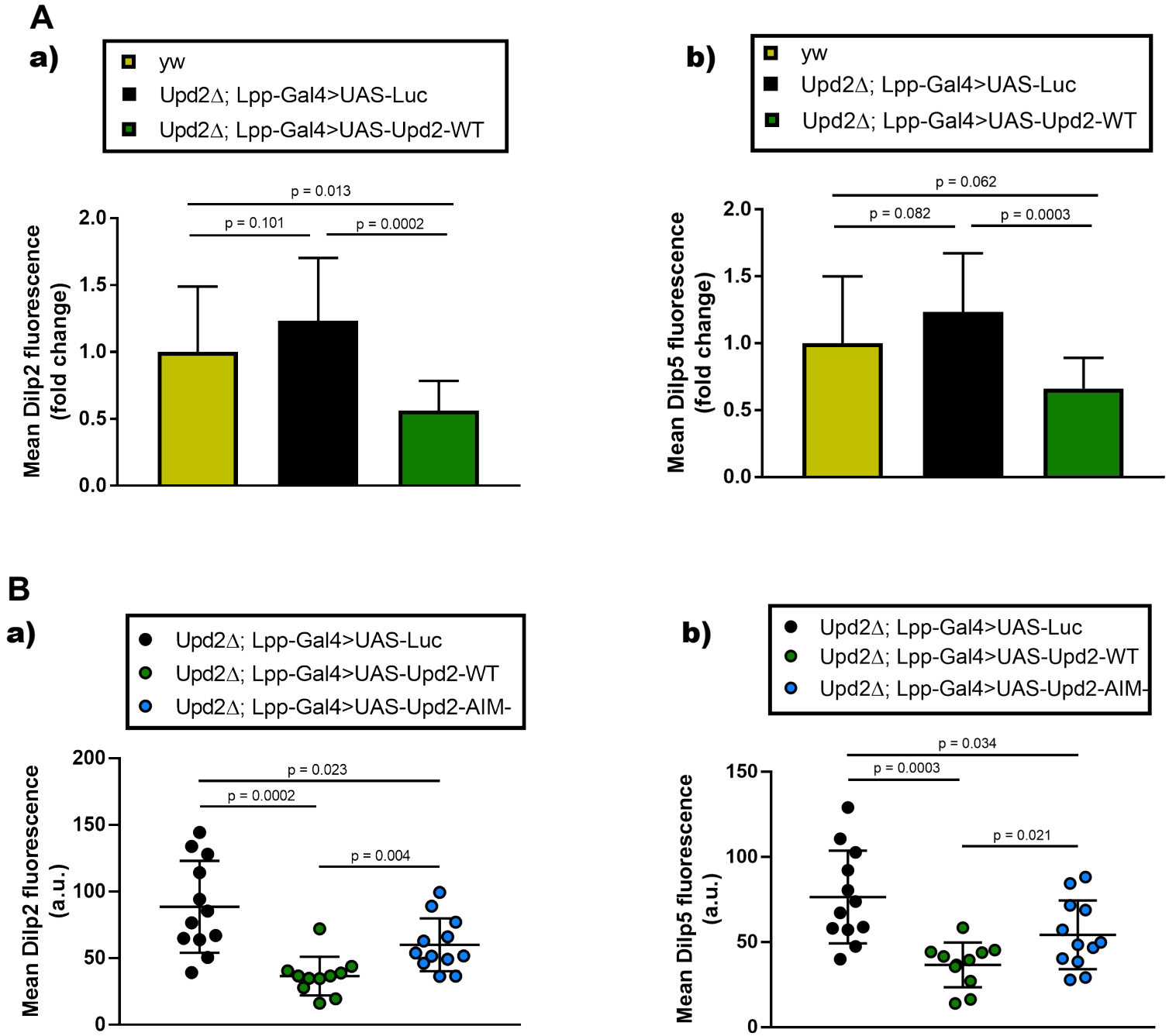
A
a)
yw
Upd2Δ; Lpp-Gal4>UAS-Luc
Upd2Δ; Lpp-Gal4>UAS-Upd2-WT
Mean Dilp2 fluorescence (fold change)
2.0
1.5
1.0
0.5
0.0
p = 0.013
p = 0.101
p = 0.0002
b)
yw
Upd2Δ; Lpp-Gal4>UAS-Luc
Upd2Δ; Lpp-Gal4>UAS-Upd2-WT
Mean Dilp5 fluorescence (fold change)
2.0
1.5
1.0
0.5
0.0
p = 0.062
p = 0.082
p = 0.0003
B
a)
Upd2Δ; Lpp-Gal4>UAS-Luc
Upd2Δ; Lpp-Gal4>UAS-Upd2-WT
Upd2Δ; Lpp-Gal4>UAS-Upd2-AIM-
Mean Dilp2 fluorescence (a.u.)
200
150
100
50
0
p = 0.023
p = 0.0002
p = 0.004
b)
Upd2Δ; Lpp-Gal4>UAS-Luc
Upd2Δ; Lpp-Gal4>UAS-Upd2-WT
Upd2Δ; Lpp-Gal4>UAS-Upd2-AIM-
Mean Dilp5 fluorescence (a.u.)
150
100
50
0
p = 0.034
p = 0.0003
p = 0.021

**Supplementary: Figure S4** ***(companion to Figure 6C, C')***

**(A)** Mean change in Dilp2 (a) or Dilp5 (b) accumulation in a *upd2Δ* mutant compared to background control (yw) that is rescued by the Upd2 transgene.

**(B)** Plot of Dilp2 (a) or Dilp5 (b) fluorescence intensity (see methods) calculated from maximum intensity projections of immunostaining of the insulin producing cells (IPCs) in adult brains of the indicated genotypes. Each dot represents an adult fly brain IPC and 10-12 brains we quantified per genotype.

# Figure S5

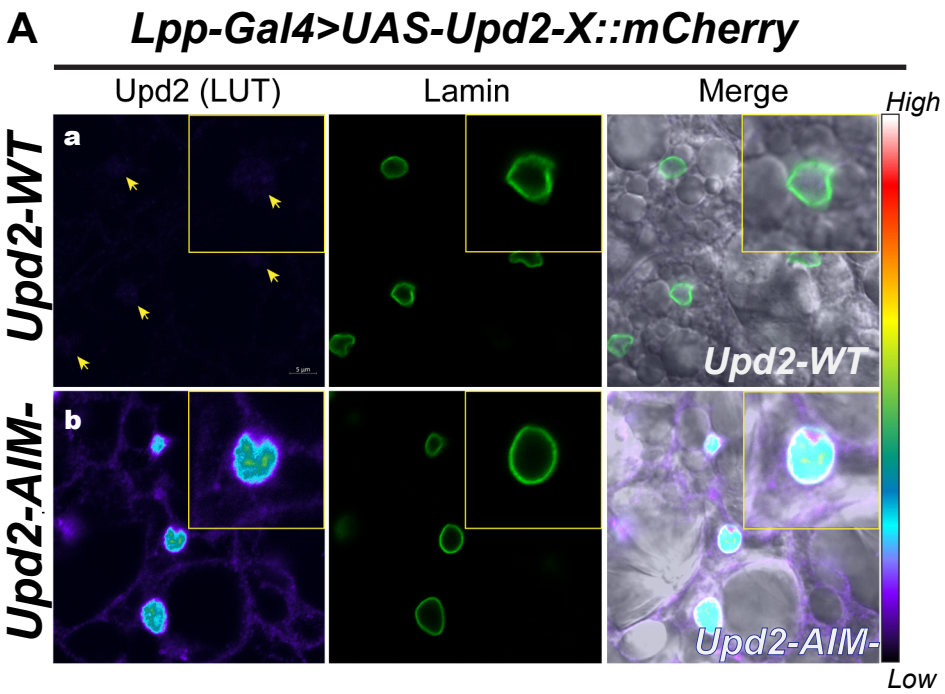
A
Lpp-Gal4>UAS-Upd2-X::mCherry
Upd2 (LUT)
Lamin
Merge
High
Low
Upd2-WT
Upd2-AIM-
a
b
Upd2-WT
Upd2-AIM-

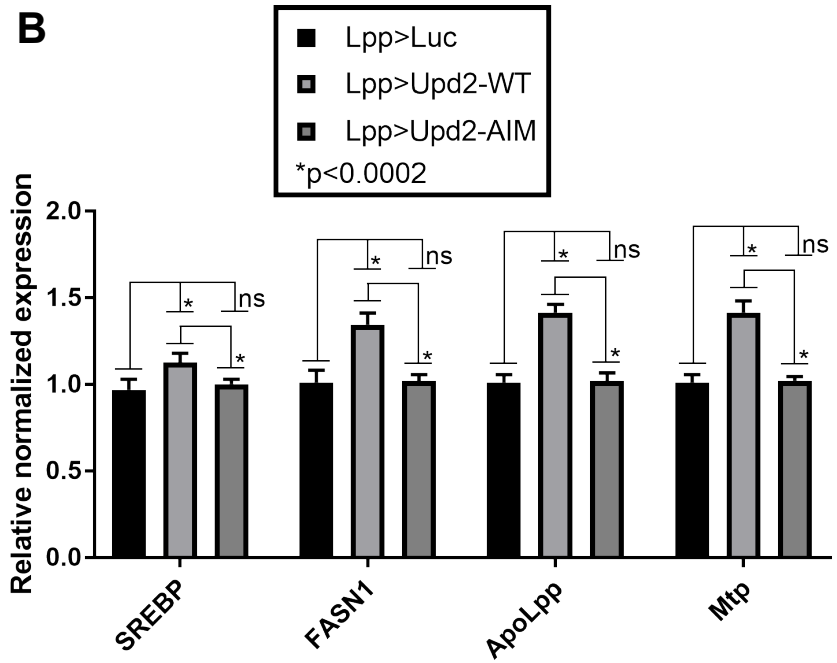
B
Lpp>Luc
Lpp>Upd2-WT
Lpp>Upd2-AIM
*p<0.0002
Relative normalized expression
2.0
1.5
1.0
0.5
0.0
ns
*
SREBP
FASN1
ApoLpp
Mtp

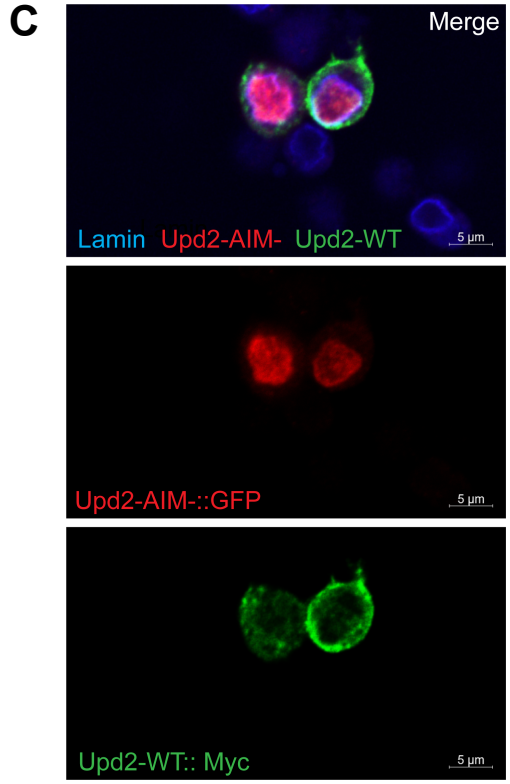
C
Merge
Lamin
Upd2-AIM-
Upd2-WT
5 µm
Upd2-AIM-::GFP
Upd2-WT:: Myc

**Supplementary: Figure S5** ***(companion to Figure 6A, D)***

**(A)** Confocal micrographs of single optical sections of fixed and immunostained adult fly fat of well-fed transgenic flies expressing mCherry tagged Upd2-cDNAs for (a) Upd2-WT (*UAS-Upd2-WT*) or (b) Upd2's AIM mutated (*UAS-Upd2-AIM*$^{-}$) under the control of a fat-cell specific promoter (*Lpp-Gal4*). In Upd2-WT in fed state is detectable in very low levels in the nucleus (see look up table (LUT)) and yellow arrows in a. Upd2-AIM- shows significantly nuclear accumulation even in a fed state.

**(B)** Relative normalized expression, of steady-state mRNA levels, assayed by qPCR on adult fat tissue in which either Upd2-WT or Upd2-AIM- was over-expressed in fat under the control of *Lpp-Gal4.* Flies expressing UAS-Luciferase control transgene serves as baseline (*Lpp-Gal4>UAS-Luc*). Expression of genes involved in either de-novo lipid synthesis or LPP production are examined. One-way ANOVA followed by Turkey's multiple comparisons test. Error bars represent standard error of the mean (SEM). N = 3 replicates per primer pair. Also see Figure 6D.

**(C)** Confocal micrographs of single optical-slices of complete media fed *Drosophila* S2R+ cells transiently transfected with *Upd2-WT::Myc* (green), *Upd2-AIM-::GFP* (red) stained with Lamin (blue). Note that while Upd2-AIM- is nuclear, the Upd2-WT is cytoplasmic.

# Figure S6

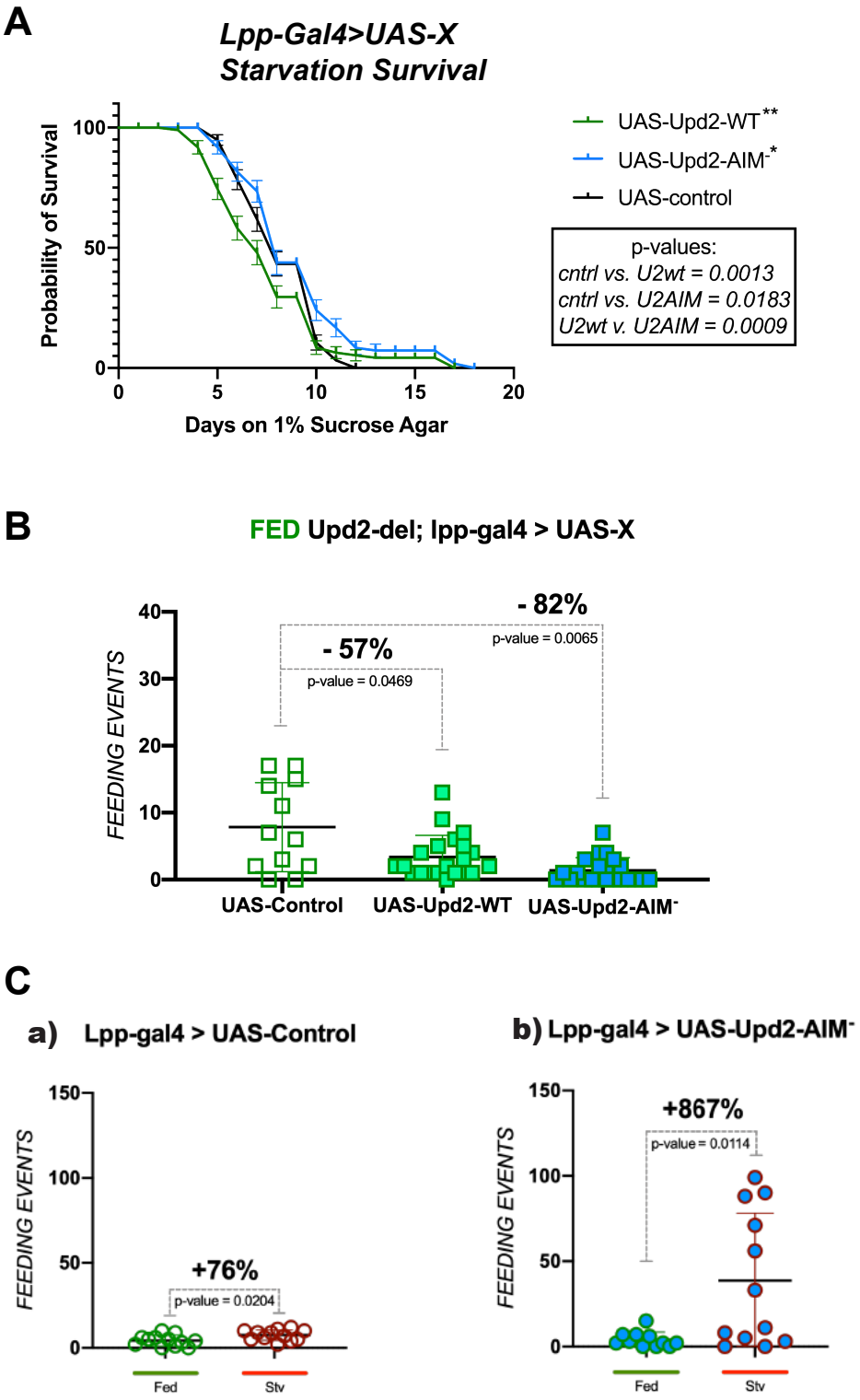
A
Lpp-Gal4>UAS-X
Starvation Survival
Probability of Survival
100
50
0
0
5
10
15
20
Days on 1% Sucrose Agar
UAS-Upd2-WT**
UAS-Upd2-AIM-*
UAS-control
p-values:
cntrl vs. U2wt = 0.0013
cntrl vs. U2AIM = 0.0183
U2wt v. U2AIM = 0.0009
B
FED Upd2-del; lpp-gal4 > UAS-X
FEEDING EVENTS
40
30
20
10
0
- 82%
p-value = 0.0065
- 57%
p-value = 0.0469
UAS-Control
UAS-Upd2-WT
UAS-Upd2-AIM-
C
a) Lpp-gal4 > UAS-Control
FEEDING EVENTS
150
100
50
0
+76%
p-value = 0.0204
Fed
Stv
b) Lpp-gal4 > UAS-Upd2-AIM-
FEEDING EVENTS
150
100
50
0
+867%
p-value = 0.0114
Fed
Stv

**Supplementary: Figure S6** ***(companion to Figure 7)***

**(A)** Flies expressing cDNAs (*UAS-X*) for *Upd2-WT*, *Upd2-AIM*$^{-}$ and control (*UAS-Luciferase)* specifically in fly fat (*Lpp-Gal4>UAS-X*) in a background with endogenous Upd2 intact. Transgenic flies with fat-specific overexpression of *Upd2-AIM*$^{-}$ are starvation-resistant, whereas overexpression of normal Upd2 (*Upd2-WT*) results in starvation-sensitivity. Statistical significance assessed by Log-rank (Mantel-Cox) test. Also see Figure 7A.

**(B)** Quantification of feeding behavior in transgenic flies, expressing indicated cDNAs (*UAS-X*) specifically in fat-tissue (*Upd2Δ; Lpp-Gal4>UAS-X*), measured using the Fly Liquid Interaction Counter (FLIC-see methods). Each dot represents a fly. 10-12 flies were used per experiment per genotype. The difference between Upd2-AIM- and Upd2-WT transgene expressing flies have reduced baseline feeding. Error bars represent percent standard deviation and statistical significance was calculated using 2-tailed unpaired t-test. Also see Figure 7B, C.

**(C)** Quantification of feeding behavior in transgenic flies, expressing indicated cDNAs (*UAS-X*) specifically in fat-tissue (*Upd2Δ; Lpp-Gal4>UAS-X*), measured using the Fly Liquid Interaction Counter (FLIC-see methods). Each dot represents a fly. 10-12 flies were used per experiment per genotype. The flies were starved for 16 hours prior to testing. The difference between fed and starved flies of the same genotype were assayed as feeding events. Also see Figure 7B, C.